DEVELOPMENT OF APPROXIMATIONS FOR HSCT WING BENDING MATERIAL WEIGHT USING RESPONSE SURFACE METHODOLOGY

By

Vladimir O. Balabanov

a dissertation submitted to the faculty of

virginia polytechnic institute and state university

in partial fulfillment of the requirements for the degree of

Doctor of Philosophy

in

Aerospace Engineering

Raphael T. Haftka, Co-Chairman	Bernard Grossman, Co-Chairman
Layne T. Watson	William H. Mason
Owen Hughes	Rakesh K. Kapania

September 1997

Blacksburg, Virginia

DEVELOPMENT OF APPROXIMATIONS FOR HSCT WING BENDING MATERIAL WEIGHT USING RESPONSE SURFACE METHODOLOGY

by

Vladimir O. Balabanov

Committee Chairs: Raphael T. Haftka and Bernard Grossman
Aerospace Engineering

(ABSTRACT)

A procedure for generating a customized weight function for wing bending material weight of a High Speed Civil Transport (HSCT) is described. The weight function is based on HSCT configuration parameters. A response surface methodology is used to fit a quadratic polynomial to data gathered from a large number of structural optimizations. To reduce the time of performing a large number of structural optimizations, coarse-grained parallelization with a *master-slave* processor assignment on an Intel *Paragon* computer is used. The results of the structural optimization are noisy. Noise reduction in the structural optimization results is discussed. It is shown that the response surface filters out this noise. A statistical design of experiments technique is used to minimize the number of required structural optimizations and to maintain accuracy. Simple analysis techniques are used to find regions of the design space where reasonable HSCT designs could occur, thus customizing the weight function to the design requirements of the HSCT, while the response surface itself is created employing detailed analysis methods. Analysis of variance is used to reduce the number of polynomial terms in the response surface model function. Linear and constant corrections based on a small number of high fidelity results are employed to improve the accuracy of the response surface model. Configuration optimization of the HSCT employing a customized weight function is compared to the configuration optimization of the HSCT with a general weight function.

Acknowledgements

During the last four years I was fortunate to work with the research group of professors and graduate students at the Aerospace and Ocean Engineering Department of Virginia Polytechnic Institute and State University. The unique environment of cooperation and support both in studies and in research encouraged and greatly contributed to my academic and professional growth.

In the very first lines of this work I would like to express my deep gratitude and thankfulness to my advisor and committee co-chair, Dr. Raphael T. Haftka. From my very first days at Virginia Tech he was a source of guidance and support to me. No matter what kind of problem was discussed, his advice and encouragement always provided new perspectives. The expertise that he shared with me remains a tremendous source for the professional growth to me. I am very thankful for everything he has done for me.

Also, I am deeply indebted to Dr. Bernard Grossman, my second advisor and committee co-chair. His help, advice and support could not be overestimated. I am grateful for all of his efforts.

I am most thankful to all the members of my committee: Dr. Layne. T. Watson, Dr. William H. Mason, Dr. Owen Hughes, Dr. Rakesh K. Kapania. On occasions too numerous to count their technical expertise and assistance played the key role in the progress of my research. All their extraordinary help is greatly appreciated.

The great contribution to everything I have done was made by my many friends – graduate students from Virginia Tech. It is impossible to list all of them over here, but particular thanks are addressed to Matt Kaufman, Tony Giunta, Oleg Golovidov, Duane Knill.

Financial support for this research project was provided through a grant from the High Performance Computing and Communications Program at the NASA Langley Research Center. I am thankful to our contract monitor, Dr. Perry Newman and other researches at Langley who assisted with this project.

I would like to thank my very first advisor, Dr. G. A. Amiryants from the Central Aerohydrodynamic Research institute (TsAGI), Russia. He and all the people with whom I worked in the Static Aeroelasticity Division introduced me to the "real world" research. They encouraged and supported my first steps as a research engineer. I am very thankful for everything they have done for me.

Foremost, I wish to thank my parents Nina and Oleg Balabanov, who always provide guidance and on whom I can rely upon in everything I do. They made me understand the great power of knowledge.

This work would not be written without two most precious persons in my life. Their everyday patience, love, and care is the driving force for all my accomplishments. Expressing my deepest love to my daughter Anna and my wife Yelena I dedicate this work to them.

Contents

List of Tables

List of Figures

Chapter 1

Introduction

1.1 Motivation

Multidisciplinary design optimization (MDO) has become increasingly important as more and more design problems, which have been traditionally solved one discipline at a time, are being analyzed from a multidisciplinary point of view. Numerous methods have emerged in recent years for the modeling of problems involving mutually interacting disciplines. A broad survey of these methods is presented in Ref. [1].

At Georgia Institute of Technology a multilevel decomposition approach was applied to the design of a High Speed Civil Transport (HSCT) wing [2]. In this method, separate system, discipline, and component level analysis tools of varying fidelity were used to estimate wing weight while considering stress, flutter, and buckling constraints. The HSCT was then sized based on this wing weight. The multilevel decomposition approach was complemented in Ref. [3] by bringing together design and manufacturing considerations early in the design process to reduce time and costs.

The robust design simulation approach was used by Mavris *et al.* [4] to find economically viable robust designs using the HSCT as a case study. This probabilistic approach views the chosen objective as a probabilistic distribution function determined by input variables which the designer cannot control, and seeks a solution that minimizes sensitivity to these variables.

The concurrent subspace optimization approach (developed by J. Sobieski [5])

has been used at the University of Notre Dame on a variety of optimization problems [6], [7]. In this approach sensitivity information is provided from the global sensitivity equations [8]. One application of this approach is focused on the design-for-manufacturability of integrated circuits [6] and results in a design tolerant to uncontrollable statistical fluctuations in the fabrication process, though simple counterexamples are known to the convergence of the overall optimization process.

The collaborative optimization strategy developed at Stanford University [9], [10] is a multidisciplinary design architecture that is well-suited to large scale multidisciplinary optimization problems. It preserves traditional disciplinary groupings by allowing parallel execution of disciplinary optimizations. In this method a system-level optimizer guides the progress of concurrently working discipline-specific optimizers, although convergence to an optimal system design may not occur.

At the Multidisciplinary Analysis and Design (MAD) Center of Virginia Tech a variable-complexity modeling approach has been developed. This approach involves use of different fidelity tools: refined and computationally expensive models together with simple and computationally inexpensive models. It could be used in conjunction with any other MDO method described above. Our design group previously applied this approach to the combined aerodynamic-structural optimization of subsonic transport aircraft wings [11] and the aerodynamic-structural optimization of the High Speed Civil Transport [12], [13].

Simultaneous aerodynamic and structural optimization is one of the most common MDO applications, particularly, for the design of aircraft wings or complete aircraft configurations. The tradeoff between aerodynamic and structural efficiency has always driven aircraft design: slender shapes have less drag but are heavier than stubby shapes. Thus two major aerodynamic-structural interactions could be identified. First, structural weight affects the required lift and, thus, drag. Second, structural deformations change the aerodynamic shape. The second effect is compensated for by building the structure so that it will deform to the desired shape. After this compensation is implemented, the interaction between the aerodynamic and structural designers becomes one sided. The aerodynamic design affects all aspects of the

structural design; the structural design affects the aerodynamic design through a single number — the structural weight. This asymmetry allows a two-level optimization formulation, with the aerodynamic design at the upper level and the structural design at the lower level. Additionally, the asymmetric interaction between structures and aerodynamics presents an enormous savings in computational resources because the large number of derivatives of aerodynamic quantities with respect to structural design variables do not need to be calculated.

The asymmetric interaction between aerodynamic and structural design permits the aerodynamic design to proceed first, starting with accurate estimates of structural weight. Weight equations (or weight functions) are usually used in the conceptual and preliminary design phases. Often, these weight equations are statistically-derived, experience-based algebraic models. (See Refs. [14], [15] for a survey of wing weight equations.) However, weight equations may not accurately predict weights of some components of relatively new conceptual designs, such as the High Speed Civil Transport. Huang *et al.* [16] compared the results of structural optimization with the weight equation from the Flight Optimization System (FLOPS) [17]. The weight function was found suitable for predicting general trends in structural weight, but unable to accurately model all effects of changing aircraft geometry.

It is possible to improve the accuracy of weight equations by performing periodic structural optimization during the design process as demonstrated by Dudley *et al.* [13], where the weight was adjusted by a constant factor to make the weight equation value equal to the result of the structural optimization. This procedure improved the accuracy of the weight function, but derivatives of the scale factor were not available to the configuration design optimizer, making optimal solutions difficult to find. In addition, the scale factor was only updated periodically during the design due to the computational cost associated with structural optimization.

A direct integration of the structural and configuration optimization was also considered as an alternative to the use of the weight equation. However, results from the structural optimization are not a smooth function of the configuration shape parameters. Because of that, a derivative-based optimization would have been difficult to perform. In addition, the configuration design process requires structural weight

information at a large number of design points, and structural optimization is computationally expensive to perform. Coupling unrelated optimization processes also introduces code integration problems where different optimization software packages utilize different design variables, input parameters, and output formats. These reasons made direct integration of the structural and configuration optimization infeasible for HSCT design, where multiple structural optimizations must be performed.

1.2 Objective

An alternative method for improving results of the weight equations is to perform many structural optimizations in a region around a nominal design point and create a customized weight function which is tailored to a particular set of design requirements (e.g., range, Mach number, number of passengers). Limiting the type of the aircraft to which the weight function is applicable can increase accuracy the of the results produced by this weight function. However, a large number of structural optimizations is still needed. We shall employ parallel computing to reduce the significant computational cost associated with performing structural optimization. Another approach to reduce the computational cost is to incorporate results from the structural optimization of different fidelity finite element models in the single weight function, with structural optimization of high-fidelity finite element models performed for only a relatively small number of geometric configurations.

The objective of the present work is to create a customized weight function for the HSCT configuration that must fly at the range of 5500 nautical miles at a cruise Mach number of 2.4, while carrying 251 passengers. The major challenge in this problem is that the number of design variables defining HSCT geometry configuration is relatively large. Our design group at Virginia Tech has developed a model that defines the HSCT geometry configuration and performance characteristics using 29 design variables [18].

We intend to construct a customized wing structural weight function based on the results of the structural optimization. However, the results of the structural optimization are a non-smooth function of the HSCT configuration parameters [19].

This noise could be caused by incomplete convergence of the optimization process, by changes in the set of active constraints, or by numerical noise in the calculated aerodynamic quantities. The accuracy of the weight function could be influenced significantly by this noise.

1.3 Methodology

One of the ways to construct a customized weight function is to employ statistical techniques based on design of experiments theory and response surface modeling methodology ([20], pp. 1–15). These techniques construct algebraic approximations, often quadratic polynomials, for an objective function and/or constraints, based on least square estimates of these functions at a set of sample sites carefully distributed throughout the design space. The optimization or analysis then proceeds on the basis of these approximations, which are often called *response surface* (RS) models.

The selection of the sample sites (*design of experiments*) where the objective function and/or constraints are calculated is a crucial part in creating response surface approximations. Standard statistical designs of experiments are typically oriented towards relatively small (up to 10–15) numbers of independent variables involved in the RS model: full factorial design, central composite design, Box-Behnken design, etc. ([21], pp. 288–290, 542–548). These standard statistical sample site patterns are successfully used in many complicated engineering design problems [22], [23]. However, when more than 10–15 variables are involved in the RS model, researchers often have to explore rarely used sample site patterns and invent their own [24], [25], [26].

Design of experiment techniques were originally created to construct RS approximations from experimental results having some random experimental error at each point where the objective function is sampled. In particular, repeated experiments at the same points would yield different results. Computer generated results, while still subject to numerical noise, give identical results for repeated application at the same point.

Alternative methods of computing response surface approximations to the data based on interpolation and Bayesian statistics are sometimes referred to as *design and*

analysis of computer experiments (DACE) methods [27], [28]. In the DACE approach the output of the computer code is treated as a realization of a stochastic process and Bayesian analysis is used to estimate correlation coefficients and conditional probabilities. The DACE approach also allows convenient integration of results of different fidelity into the same RS model [29]. However, when RS models in the form of quadratic polynomials are constructed using the method of least squares, it is also possible to account for results of different fidelity. One of the possible ways is to use a weighted least squares method to construct the RS polynomial model. This approach was successfully applied to engineering problems [30].

RS modeling methods are a perfect tool to filter out numerical noise [23], [31]. The optimization process becomes much more efficient when RS models (which are smooth algebraic functions) are used to evaluate the objective function and/or constraints. Elimination of numerical noise also increases the chances that an optimizer will not be trapped in a local optima and a global optimum will be found [32].

The RS model construction requires many evaluations of an objective function and/or constraints at selected sample sites. These evaluations could be very costly. However, the sample site pattern where the objective function and/or constraints should be evaluated is known beforehand. This makes the evaluations completely independent and easily amenable to parallel computing. Indeed, coarse grained parallel computing has been effectively used in a number of engineering problems to reduce the computational time of creating RS models [33], [34].

1.4 Overview

The design group at the MAD Center of Virginia Tech has been working for a long time on the different aspects of combined aerodynamic-structural optimization of the HSCT. The present work is part of that joint effort. Hence HSCT configuration optimization is the test case for the approaches developed in the present work. A general description of the HSCT configuration optimization problem is given in Chapter 2

Chapter 3 provides details on structural modeling, methods, and codes used to conduct structural analysis and optimization of the HSCT structural model. HSCT

configuration optimization is a very complicated problem and the present work will concentrate mostly on structural aspects of this problem.

It is computationally costly to perform structural optimization for many HSCT configurations. In Chapter 4 there is a description of how parallel computing was used in our particular case to reduce the computing time for many independent structural optimizations.

Issues related to numerical noise in the results of the structural optimizations are presented in Chapter 5. We describe ways of detecting the amount of noise and the main source of the noise. Reduction of the amount of noise is discussed.

The work presented in Chapter 6 was done in collaboration with D. L. Knill. In this chapter we analyze how the results of structural analysis are influenced by the method of aerodynamic loads calculation.

We are constructing a customized weight function for a particular HSCT configuration and response surface methodology is one of the main tools. A general description of response surface methodology and design of experiments technique, along with specifics of the application of this methodology to our particular problem, are given in Chapter 7.

After the customized weight function is constructed, it is incorporated into the global HSCT configuration optimization to compare the new weight function to the traditionally used weight function. The global HSCT configuration optimization procedure is described in Chapters 8 and 9. Results from using several different customized weight functions in the global HSCT configuration optimization are also discussed in the same chapters.

In Chapter 10 we discuss the linear and constant correction to the response surface model from lower fidelity results. These corrections are introduced based on relatively small number of high fidelity results. Concluding remarks are given in Chapter 11.

Chapter 2

HSCT Configuration Optimization Problem

2.1 Formulation of the Problem

In research conducted by members of the Multidisciplinary Analysis and Design (MAD) Center for Advanced Vehicles at Virginia Tech, the design problem is the optimization of a High Speed Civil Transport (HSCT) configuration to minimize takeoff gross weight (TOGW) for a range of 5,500 nautical miles and a cruise Mach number of 2.4, while carrying 251 passengers. The choice of gross weight as the objective function directly incorporates both aerodynamic and structural considerations, in that the structural design directly affects aircraft empty weight and drag, while aerodynamic performance dictates the drag and thus the required fuel weight. Trim and control requirements are also explicitly treated.

For this HSCT configuration optimization problem the area-ruled fuselage has a fixed length of 300 ft and an internal volume of 23,720 ft^3. The HSCT configuration and mission are defined using 29 variables (Table 2.1).

Twenty-five of these variables describe the geometric layout of the HSCT, three variables describe the mission profile, and one variable refers to engine thrust. Variables describing wing geometry of the HSCT are shown in Figure 2.1.

Sixty eight geometric, performance, and aerodynamic constraints are included in

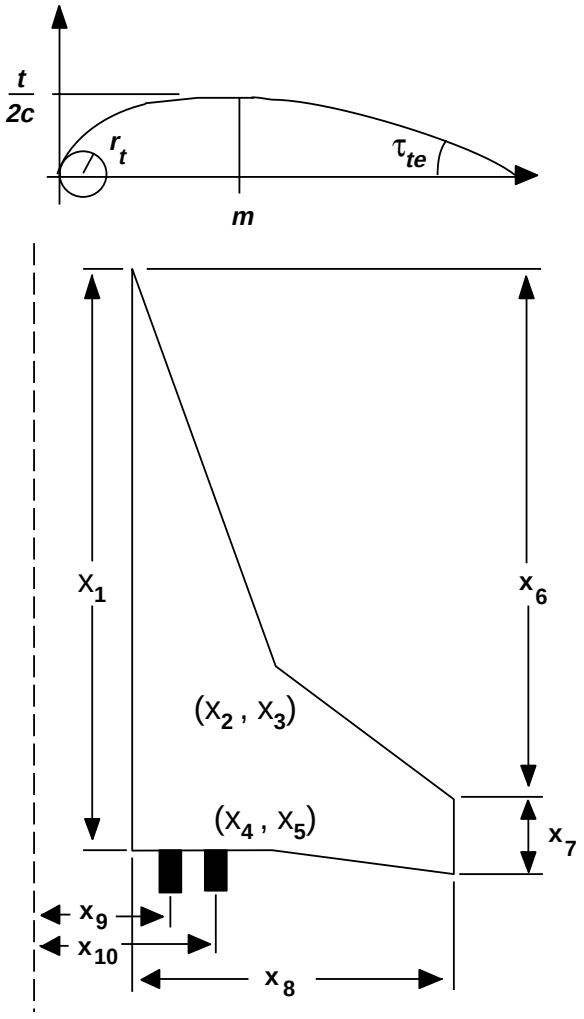

Figure 2.1: HSCT wing planform and airfoil parameters.

the configuration optimization process (Table 2.2). They are necessary to prevent the optimizer from creating physically meaningless HSCT configurations.

Aerodynamic and performance constraints can only be assessed after a complete analysis of the HSCT configuration is performed; however, the geometric constraints can be evaluated using algebraic relations based on 29 design variables. Thus we have the opportunity to efficiently identify reasonable designs from the point of view of planform geometry, eliminating nonsensical designs where, for example, the tip chord of the wing is greater than the root chord.

Table 2.1: HSCT configuration variables and their baseline values.

Number	Typical Value	Description
1	178.15	Wing root chord (ft)
2	114.1	LE break point, x (ft)
3	40.7	LE break point, y (ft)
4	173.4	TE break point, x (ft)
5	12.2	TE break point, y (ft)
6	146.4	LE wing tip, x (ft)
7	9.20	Wing tip chord (ft)
8	82.6	Wing semi-span (ft)
9	0.51	Chordwise max. t/c location
10	2.53	LE radius parameter
11	2.82	Airfoil t/c at root (%)
12	1.90	Airfoil t/c at LE break (%)
13	1.70	Airfoil t/c at tip (%)
14	2.61	Fuselage restraint 1, x (ft)
15	0.47	Fuselage restraint 1, r (ft)
16	13.24	Fuselage restraint 2, x (ft)
17	2.49	Fuselage restraint 2, r (ft)
18	111.68	Fuselage restraint 3, x (ft)
19	5.32	Fuselage restraint 3, r (ft)
20	186.91	Fuselage restraint 4, x (ft)
21	5.34	Fuselage restraint 4, r (ft)
22	11.50	Nacelle 1, y (ft)
23	28.37	Nacelle 2, y (ft)
24	464,743	Mission fuel (lbs)
25	58,403	Starting cruise altitude (ft)
26	37.97	Cruise climb rate (ft/min)
27	921.2	Vertical tail area (ft^2)
28	986.6	Horizontal tail area (ft^2)
29	57,271	Max. sea level thrust/engine, (lb)

Table 2.2: Constraints for HSCT configuration optimization.

Number	Description
1	Range $\geq$ 5,500 *n.mi.*
2	Required C_L at landing speed ≤ 1
3-20	Section $C_\ell \leq 2$
21	Landing angle of attack $\leq 12^\circ$
22	Fuel volume $\leq$ half of wing volume
23	Spike prevention
24-41	Wing chord ≥ 7.0 *ft.*
42-43	No engine scrape at landing angle-of-attack
44-45	No engine scrape at landing angle-of-attack, with 5° roll
46	No wing tip scrape at landing
47	Rudder deflection for crosswind landing $\leq 22.5^\circ$
48	Bank angle for crosswind landing $\leq 5^\circ$
49	Takeoff rotation to occur ≤ 5 *sec*
50	Tail deflection for approach trim $\leq 22.5^\circ$
51	Wing root T.E. $\leq$ horiz. tail L.E.
52	Balanced field length $\leq 10,500$ *ft* (11,000 in 29 DV problem)
53	T.E. break scrape at landing with 5° roll
54	L.E. break $\leq$ semispan
55	T.E. break $\leq$ semispan
56-58	Root, break, tip $t/c \geq 1.5\%$
59	Fuselage: $x_{rest_1} \geq 5ft$
60	Fuselage: $x_{rest_1} + 10\text{ft} \leq x_{rest_2}$
61	Fuselage: $x_{rest_2} + 10\text{ft} \leq x_{rest_3}$
62	Fuselage: $x_{rest_3} + 10\text{ft} \leq x_{rest_4}$
63	Fuselage: $x_{rest_4} + 10\text{ft} \leq 300\text{ft}$
64	Nacelle 1, $y \geq$ side-of-body
65	Nacelle 1, $y \leq$ nacelle 2, y
66	Engine-out limit with vertical tail design; otherwise 50%
67-68	Maximum thrust required $\leq$ available thrust

2.2 Analysis Methods and Tools

In the conceptual and preliminary phases of the aircraft design statistically-derived, experience-based algebraic models, known as weight functions or weight equations, are often used to estimate weight of the aircraft. For the conceptual level analysis of the aircraft we use the weight functions from the Flight Optimization System (FLOPS) [17]. In the preliminary level aerodynamic analyses we use the vortex lattice method (VLM) ([35], pp. 261–282) for low-speed conditions, the Mach box method [36],[37], and the Harris wave drag code [38] for supersonic conditions. A simple strip boundary layer is implemented to compute friction drag [12].

We use two techniques to estimate the stability and control derivatives: empirical algebraic relations from the U.S.A.F. Stability and Control DATCOM [39], as interpreted by J. Roskam [40], and a VLM code developed by J. Kay *et al.* [41]. The DATCOM methods rely on simple theories and some experimental data, and do not handle unusual aircraft configurations well. The VLM code is better able to handle different configurations, but is more expensive computationally. A more detailed description of these techniques is given in Ref. [18].

The global HSCT configuration optimization is conducted using a penalty function method implemented in the program NEWSUMT-A [42]. We have also employed the method of feasible directions and the sequential quadratic programming method as implemented in the optimization program DOT [43].

Previous studies showed a good correlation between the FLOPS weight function and structural optimization for structural weight prediction [16]. However, work by Huang *et al.* [16] also indicated that the FLOPS weight function may not be accurate enough in estimating the dependence of the wing bending material weight on planform shape changes for HSCT-type configuration. Consequently, we have been working on the use of finite element structural optimization to estimate structural bending material weight. Some details on calculating wing bending material weight in FLOPS are given in Appendix A. The results from the structural optimization are then used in HSCT configuration optimization via response surface methods. A finite-element-based structural optimization code, GENESIS [44], was used to conduct structural

optimization studies of selected HSCT configurations. More details on structural modeling and codes used will be given in Chapter 3.

Chapter 3

Structural Modeling

The goal of performing structural optimization is to provide wing bending material weight which is later used in the HSCT configuration optimization process. Due to the large number of structural optimizations that must be performed to create a response surface, a relatively simple structural finite element (FE) model is used. We employ a FE model of the HSCT with a fixed arrangement of spars, ribs, and skin panels. The wing and fuselage skin are modeled by membrane elements. Spar and rib caps are modeled by rod elements. Vertical rods and shear panels are used to model spar and rib webs. The typical wing box cell used in the FE model is shown in Figure 3.1.

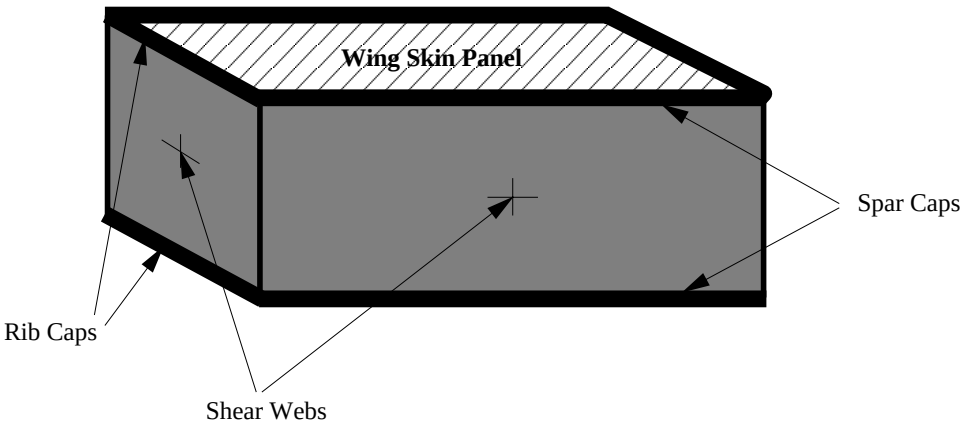

Figure 3.1: Close-up view of the typical wing box cell.

Because of symmetry, we only generate a finite element model of half the aircraft. The boundary conditions specify symmetry of the displacements about the centerline. To remove the singularity of the stiffness matrix, displacements and rotations of two nodes on the centerline in all directions are constrained. These two nodes are located near the center of gravity, but due to the fact that loads used are self-balanced the reactions in the supports are small. The initial thicknesses and areas of the elements are chosen to match the estimated structural weight. The aircraft is assumed to be built of titanium. Material properties are given in Table 3.1.

Table 3.1: Material properties used in FE analysis and optimization.

Property	Value
E	16.0 x 10^6 (psi)
G	6.0 x 10^6 (psi)
ν	0.332
ρ	0.163 (lb/in^3)
$\sigma_{x_{yield}} = \sigma_{y_{yield}}$	91.8 x 10^3 (psi)
$\sigma_{xy_{yield}}$	53.0 x 10^3 (psi)
$\sigma_{x_{fatigue}} = \sigma_{y_{fatigue}}$	25.0 x 10^3 (psi)
$\sigma_{xy_{fatigue}}$	14.4 x 10^3 (psi)

Two types of FE models are used in our studies. Material properties and types of elements used for modeling the same parts of the aircraft are the same for these two types of models. The typical wing box cell (Figure 3.1) is also the same. One type of model consists of a smaller number of elements than the other. Models of this type are referred to as *coarse FE models*. The other type of model employs a larger number of elements and accounts for the landing gear. In this study such models are called *refined FE models*.

3.1 Coarse Structural Finite Element Model

The typical coarse FE model of the HSCT that we use consists of 1,127 elements joined together at 226 nodes with a total number of 1,242 degrees of freedom (Figure 3.2). To perform structural optimization, two categories of structural design variables are

defined in the coarse and in the refined FE models: those that define the wing panel thicknesses and the ones defining spar and rib cap areas. Forty design variables are used in the coarse FE model (Figure 3.2), including 26 to define skin panel thicknesses, 12 for spar cap areas, and two design variables for the rib cap areas. Within each group a uniform thickness or area distribution is assumed.

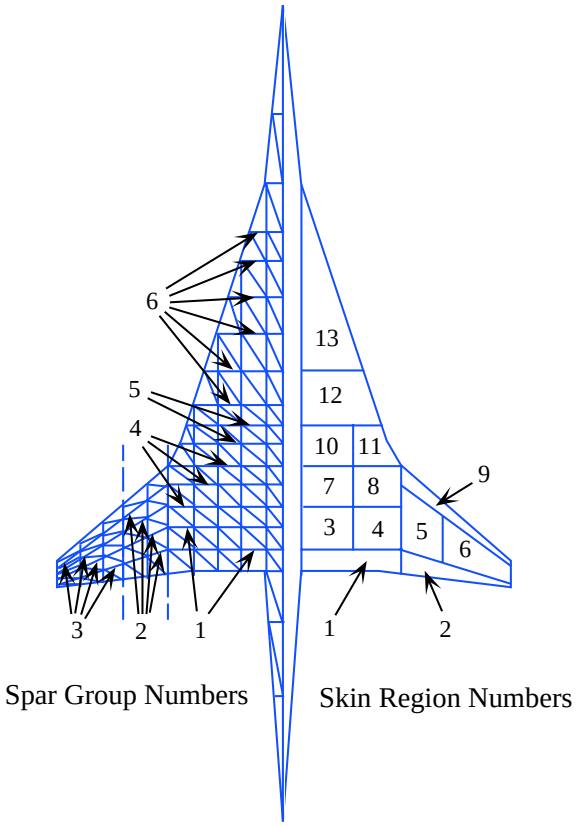

Figure 3.2: Coarse HSCT FE model and structural design variables.

3.2 Refined Structural Finite Element Model

The FE model described above is still rather coarse and does not account for a lot of details. In order to improve the wing bending material weight estimates given by the coarse FE model, we decided to create a more refined FE model. The refined FE model has a larger number of elements in the regions that contribute the most to the

wing bending material weight, with respect to the number of elements in the coarse FE model. The refined FE model has a larger number of design variables than the coarse FE model — 74. Figure 3.3 shows an example of such a FE model. It has 2, 214 elements, 555 nodes, and 3,216 degrees of freedom.

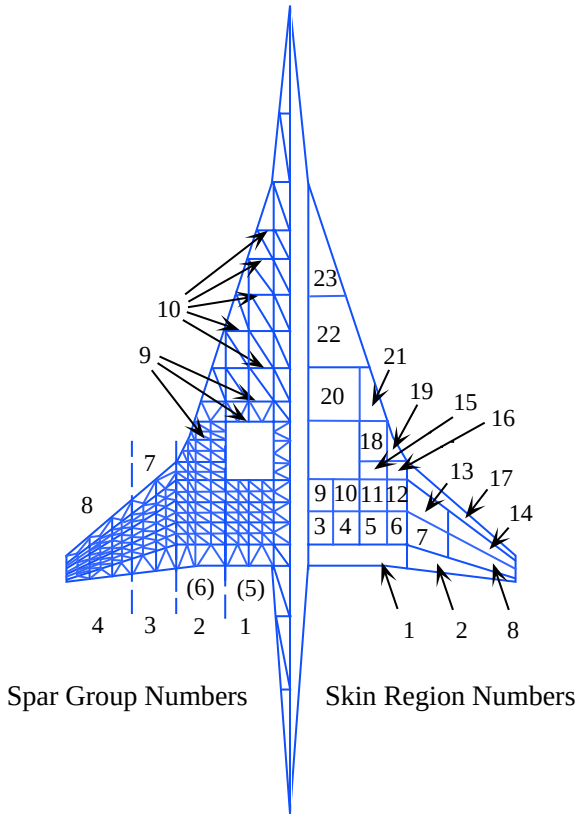

Figure 3.3: Refined HSCT FE model and structural design variables.

Besides increasing the number of elements, simplified accommodations for the landing gear were also taken into account in the refined FE model. In Figure 3.3 the landing gear accommodation is shown as a cutout. A close-up view of this cutout along with adjacent portions of the wing and the fuselage are shown in Figure 3.4.

However, the time required to perform structural optimization for the refined FE model is an order of magnitude larger than the time required to perform structural optimization for the coarse FE model. That is why the refined FE model is used

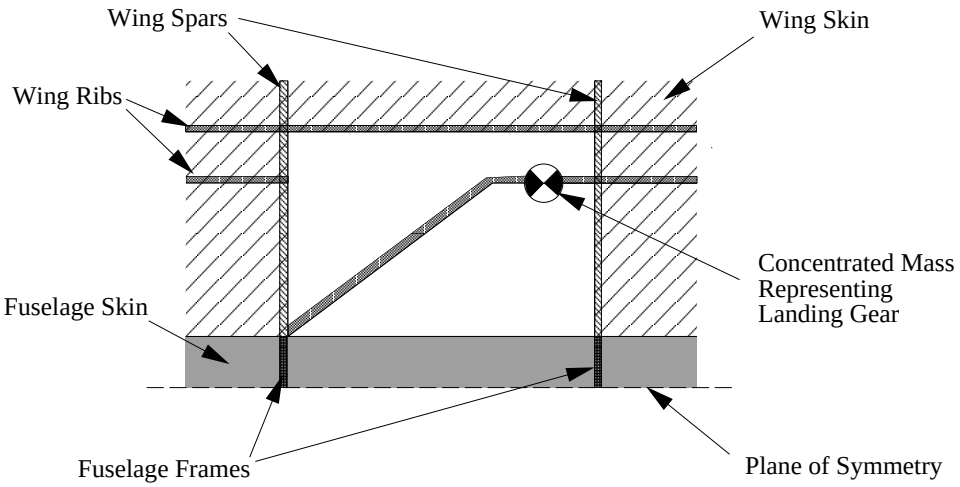

Figure 3.4: Close-up view of the simplified accommodation for the landing gear.

sparingly and the majority of the results that follow are obtained using the coarse FE model.

3.3 Structural Optimization Formulation

The weight obtained from any of the finite element models that we use is incomplete in itself for predicting the weight of the complex wing structure. It does not account for such items as joints, rivets, local reinforcements, etc. We only employ FE models to estimate the bending material weight of the structure, because wing bending material weight is the most significant part of the load carrying structural weight and using structural optimization we can estimate well only the load carrying part of the structural weight. In addition, in previous work [16] it was found that it is this particular portion of the weight that is not predicted well enough by FLOPS to account for the changes in the configuration parameters of the HSCT. The description of the procedure used in FLOPS to calculate wing weight is given in Appendix A. We continue to use FLOPS weight equations to estimate other parts of the structural and nonstructural weight. Following the FLOPS weight equation breakdown, the

bending material weight is defined to consist mostly of the weight of the spar caps and skin panels. It accounts for about 4.5% of the gross takeoff weight. However, the entire wing structural weight is the objective function of the structural optimization. After optimization is performed, wing bending material weight is calculated based on thickness of specific portions of the wing, excluding minimum gage and control surface areas. The minimum gage of the wing skin is taken to be 0.004 ft, and the minimum spar and rib cap area is 0.005 ft^2. Some technical details about the program that calculates the wing bending material weight are given in Appendix F.

The formal structural optimization problem is stated as follows: minimize the weight of the structure, when all the wing skin panels, spar, and rib elements are subjected to Von Mises stress constraints and local buckling constraints.

All the structural constraints are normalized to a range of -1 to 1. Constraints with a value of 1 or close to 1 are considered active. As the constraints are evaluated they are screened by choosing a threshold value so that the number of constraints above or equal to this value equals the number defined by the user (200 in our case). Only structural constraints which are above or equal to threshold value are used in the structural optimization process. All the other structural constraints are discarded from consideration within one structural optimization cycle. The screening procedure is applied individually to each load case. This procedure considerably reduces the computational cost of the structural optimization.

Following Ref. [45], five load cases are considered for the structural optimization (Table 3.2).

Table 3.2: Load cases for the structural optimization.

Load case	Mach number	Load factor	Altitude (ft)	fuel
1 - High-speed cruise	2.4	1.0	63,175	50 %
2 - Transonic climb	1.2	1.0	29,670	90 %
3 - Low-speed pull-up	0.6	2.5	10,000	95 %
4 - High-speed pull-up	2.4	2.5	56,949	80 %
5 - Taxiing	0.0	1.5	0	100 %

The loads applied to the structural FE model are composed of the aerodynamic and inertia forces. Inertia loads represent the combined effects of non-structural

items, fuel weight, and the distributed weight of the structure. Aerodynamic loads for supersonic flight conditions are determined using a supersonic panel method, and loads for subsonic flight conditions are calculated from a vortex-lattice method. The same aerodynamic model is used to determine aerodynamic loads both for coarse and refined FE models. A surface spline interpolation method [46] is used to translate forces from aerodynamic nodes to structural nodes. The structure is assumed to be rigid for the determination of aerodynamic forces. Previous studies indicated that structural flexibility did not have a large effect on the wing bending material weight for this particular type of the aircraft configuration [16], [45]. Particularly, in the work by Huang *et. al.* ([16]) the largest difference in the wing bending material weight between a rigid and flexible wing was found to be about 7%. In addition, because five load cases is a small number, the flexible wing results may be unconservative. It was shown in Ref. [16] that using structural optimization with a rigid wing model for determination of aerodynamic forces gives a conservative estimate of the effect of the geometric changes on the structural weight.

3.4 Finite Element Mesh and Load Generator

Rather than manually construct a FE model for each HSCT configuration, a special mesh generator was developed to automate this procedure (see also [16]). The aircraft geometry is stored as a discrete numerical description in the Craidon format [47], which is used in the aerodynamic analysis. This geometry description is used as the basis for creating the FE model of the aircraft. Besides the Craidon geometry, the user specifies the number of frames in the fuselage, the numbers of spars and ribs in the wing, and the fractions of the chord taken by the leading and trailing-edge control surfaces. Instead of dealing with the three dimensional problem, the automatic mesh generator treats the whole aircraft as a two dimensional middle plane. At first this middle plane is divided into several regions such as fuselage, inboard part of the wing, outboard part of the wing,and control surfaces. Then the regions are further subdivided into finite elements according to the given number of frames, ribs, spars, and configuration requirements. Finally, a surface interpolation subroutine is used to

split the middle plane into upper and lower surfaces according to Craidon geometry description of the surface of the wing and fuselage.

Besides the FE nodal coordinates and FE topology, the mesh generator also estimates the locations of all nonstructural items and fuel tanks. Thirty one tanks are located throughout the aircraft. The fuel at a given flight condition is distributed between the tanks to trim the aircraft. Since there are many ways to distribute the fuel, we define the optimization problem that seeks the fuel distribution closest to the one when the fuel occupies the same percentage of volume in all the fuel tanks:

Minimize:

$$\sum_{i=1}^{n_t} (W_i - W_{i0})^2 \tag{3.1}$$

Subject to:

$$\sum_{i=1}^{n_t} (W_i - W_{i0}) = 0\,, \tag{3.2}$$

$$x_{CG} = x_{CP}\,, \tag{3.3}$$

$$0 \leq W_i \leq W_i^{max}\,, \tag{3.4}$$

where W_i is the weight of fuel in the fuel tank number i, W_{i0} is the initial weight of fuel in the fuel tank number i when the fuel occupies the same percentage of volume in all the fuel tanks, n_t is the total number of fuel tanks, W_i^{max} is the weight of fuel in the fuel tank number i when this tank is full, x_{CG} is the x-coordinate (chordwise) of the center of gravity, x_{CP} is the x-coordinate (chordwise) of the center of pressure. To solve this optimization problem we employ the program NEWSUMT-A [42].

The mesh generator described above has been used for several years at Virginia Tech, but it was only able to handle a narrow range of wing geometries. Additionally, several programs were used to generate loads, leading to much disk input-output (I/O) for communication. For the purpose of optimizing a large number of configurations the mesh generator was generalized and intermediate disk I/O was eliminated. The FE models in Figures 3.2 and 3.3 are created via the automated mesh generator. Some technical details about the mesh generator program are given in Appendix E.

3.5 Comparison of Coarse and Refined FE Models

This section describes how well the results obtained from the two FE models agree with each other and with FLOPS. We first compared the wing bending material weight for three HSCT configurations, denoted as Configuration 1, Configuration 2, and Configuration 3. Their planforms are presented in Figure 3.5.

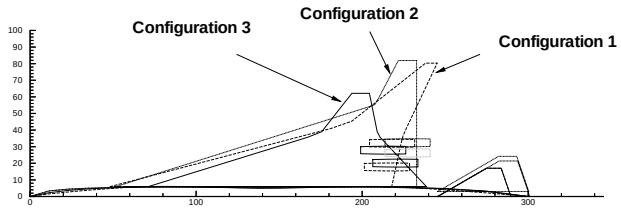

Figure 3.5: HSCT configurations to study differences between coarse and refined FE models.

The structural optimization was performed for these 3 HSCT configurations using coarse and refined FE models. The initial thicknesses of skin panels and cross-sectional areas of the spars and ribs were the same for the coarse and refined FE models. Figures 3.6—3.11 show the optimal thickness of the skin panels at the upper and lower surfaces wing surfaces for the coarse and refined FE models. For all three configurations the optimal distributions of the skin panels thicknesses for the coarse FE model differ significantly from the ones for the refined FE model. There are several reasons for these differences. The larger number of design variables in the refined FE model (Figures 3.2, 3.3) gives more flexibility in distributing the thicknesses and reducing the weight. However, presence of the cutout for the landing gear in the refined FE model decreases structural stiffness in comparison to the coarse FE model and thus increases weight. In addition, the large amount of fuel carried in the wing has to be redistributed in a different way than in the coarse FE model because of the landing gear cutout in the refined FE model, thus affecting the inertia loads.

In spite of the significant differences in the thickness distributions, the wing bending material weight of the optimal coarse and refined FE models show much less

drastic differences. This could be explained by the fact that the wing bending material weight is an integrated characteristic of the model. In Table 3.3 the wing bending material weights from the coarse and refined FE models and from FLOPS are compared.

Table 3.3: Comparison of the wing bending material weight from different models.

Model	Configuration 1	Configuration 2	Configuration 3
FLOPS	46,777 (*lb*)	27,945	13,534
Coarse FE model	68,464 (*lb*)	41,861	22,794
Refined FE model	72,650 (*lb*)	37,536	27,014

For all the configurations considered the FLOPS prediction of the wing bending material weight is significantly lower than the structural optimization results. The level of agreement between FLOPS results and the results from the structural optimization of the coarse FE model in Table 3.3 is worse (in magnitude) than that found by Huang *et al.* [16]. This could be partly attributed to the differences in the FE models used, partly to the differences in the structural optimization procedures applied, and partly to the differences in the aerodynamic loading due to different procedures of a wing camber optimization, that will be detailed in Chapter 5. The comparison between the coarse and refined FE models is not one sided: for Configurations 1 and 3 the weight prediction from the coarse FE model is lower than the one from the refined FE model, but for Configuration 2 it is higher.

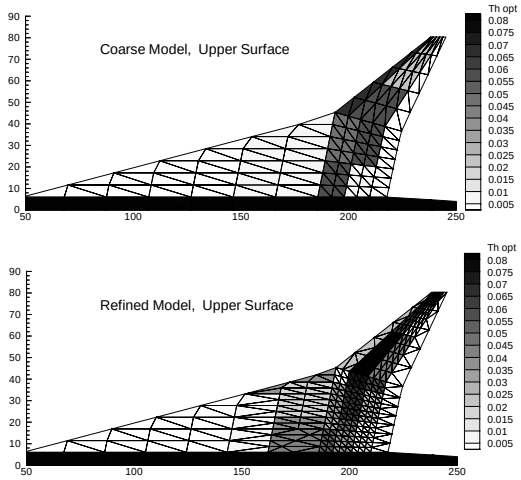

Figure 3.6: HSCT Configuration 1. Optimal thickness of wing upper surface panels.

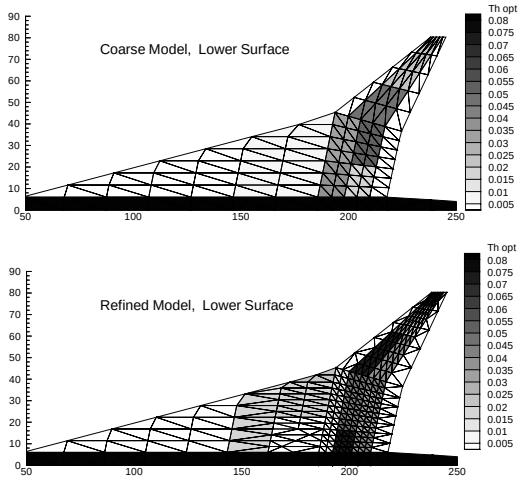

Figure 3.7: HSCT Configuration 1. Optimal thickness of wing lower surface panels.

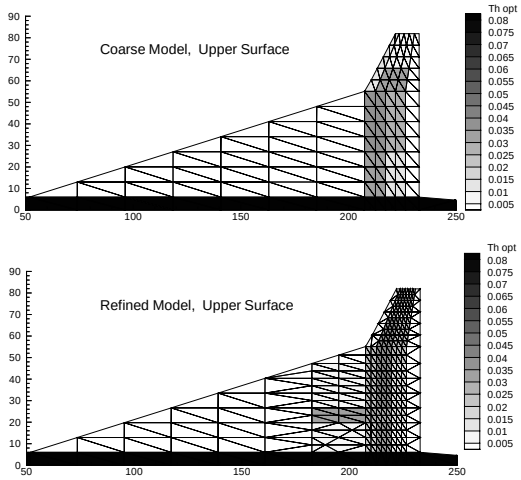

Figure 3.8: HSCT Configuration 2. Optimal thickness of wing upper surface panels.

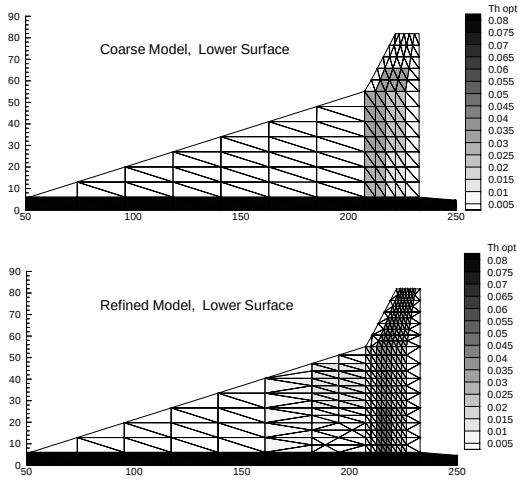

Figure 3.9: HSCT Configuration 2. Optimal thickness of wing lower surface panels.

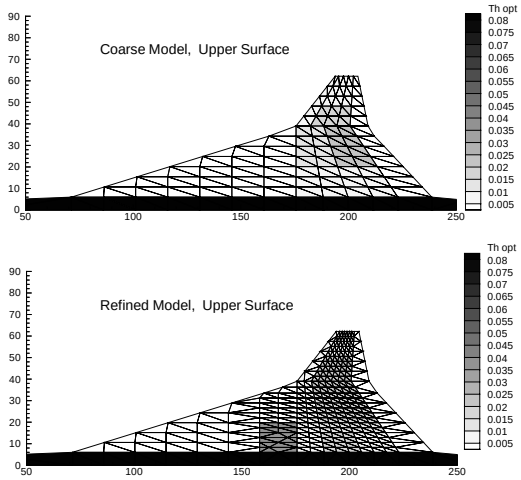

Figure 3.10: HSCT Configuration 3. Optimal thickness of wing upper surface panels.

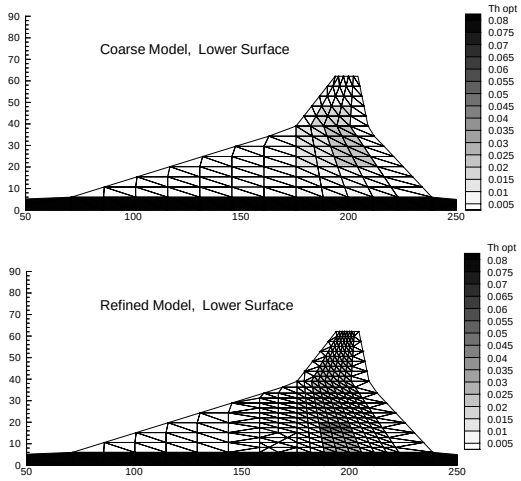

Figure 3.11: HSCT Configuration 3. Optimal thickness of wing lower surface panels.

Chapter 4

Parallelization of the Structural Optimization Procedure

To efficiently implement structural optimization in the overall design process, we must be able to perform a large number of structural optimizations in a short period of time. With the structural optimization of one configuration requiring about 40 minutes on an SGI workstation for a coarse model, the only way to perform the large number of structural optimizations is to take advantage of parallel computing.

Code parallelization can be implemented at either a fine-grained or coarse-grained level. In fine-grained parallelization, small segments of the code are made to run in parallel, while in coarse-grained parallelization larger segments are parallelized. Coarse-grained parallelization of an existing serial code does not require as much knowledge of the details of the code. For performing large numbers of structural optimizations, coarse-grained parallelization is adequate, with each processor performing one complete structural optimization. Each processor maintains its own data, so that interaction between the processors is minimal. We organized the parallel computation in a *"master-slave"* paradigm, with one processor free of computational work. This processor (the master) copies input and output files for the rest of the processors (the slaves), checks which processors have finished their work, and assigns new jobs to them. We implemented this version of coarse-grained parallelization on an Intel *Paragon* computer, which has a distributed memory architecture. The details about the parallelization procedure are given in Appendix G.

4.1 Description of the Structural Codes Involved

Originally, structural optimization for HSCT configuration optimization was performed using the Engineering Analysis Language (EAL) finite element program [48]. However, we faced the task of performing large numbers of structural optimizations efficiently. Because we did not have access to the source code of EAL and because EAL does not have its own internal optimizer, we considered two other software packages as candidates for parallelization: GENESIS [44] and MAESTRO [49].

MAESTRO is a computer program for optimum design of large complex thin-walled structures. It is currently used extensively for ship design, but is also applicable to aircraft design. It was originally written for computers with limited memory, and, therefore, performs extensive disk I/O.

GENESIS is a general purpose FE structural optimization code developed and supported by Vanderplaats, Miura, and Associates, Inc. It was created from the start to be a design program, with the necessary FE analysis available, in contrast to FE analysis codes which have optimization added later. GENESIS is able to modify both member sizes and geometrical shape in search of an optimal design. Design variables may be individual member dimensions and/or grid locations, or may be linear or nonlinear combinations of these. Dimension or shape variables may be linked to maintain symmetry and manufacturability. Basis vectors are used to create smooth variations in structural dimensions and shapes. The user may provide his own subroutines to calculate section properties as a function of the design variables. A variety of responses such as mass, stress, and displacement may be chosen as the design objective. Additionally, functions of the design variables and other responses may be created. These functions may be the objective or may be constraints. GENESIS provides three different optimization methods: method of feasible directions, sequential linear programming, and sequential quadratic programming. We used the method of feasible directions for our problem.

Both GENESIS and MAESTRO rely heavily on disk I/O. However, the large amount of I/O is a common feature of the majority of FE programs, and is not a special feature of MAESTRO or GENESIS.

4.2 Parallel Performance

For the Intel *Paragon*, disk I/O proved to be a bottleneck for parallel computations as the number of processors increased. For GENESIS we were able to get from the developer a version of the program with reduced I/O. For MAESTRO we systematically replaced disk I/O with memory usage. This was accomplished by converting all the temporary files into common blocks. The process required a significant amount of time to complete due to the size of the code. The structural analysis part of the code was completed, however, difficulties were encountered in the optimization part.

The effect of reducing the I/O in MAESTRO manifested itself even when the program was executed on a single node of the *Paragon*. The serial version took 501 seconds to execute a FE analysis of the HSCT model. The reduced I/O version took only about 132 seconds for the same job.

Figures 4.1 and 4.2 show speedups and efficiency for executing 50 structural optimizations using GENESIS and MAESTRO on a parallel distributed memory computer. The speedup of a parallel computation is defined as T_s/T_p where T_s is the serial execution time and T_p is the parallel execution time using p processors. In an ideal situation, speedup would be equal to the number p of processors being used. Efficiency is the ratio of the speedup to the number of processors that are used.

From Figures 4.1 and 4.2 we see that results both for MAESTRO and GENESIS with reduced I/O are close. For example, speedup for executing codes on 15 nodes is 10.2 for MAESTRO and 10.5 for GENESIS with reduced I/O. Figures 4.1 and 4.2 also show the benefits of the reduced I/O version of GENESIS. With the standard version, maximum speedup levels off at 2.3, regardless of the number of processors, while the reduced I/O version achieves a speedup of 10.5 using 15 processors.

We selected GENESIS as our tool for implementing the structural optimization because of our lack of success in creating a reduced I/O version of MAESTRO that could work for optimization. Additionally, GENESIS had an advantage of using input similar to NASTRAN, which is the aerospace industry standard, while MAESTRO's input is more oriented to naval applications.

The parallel implementation of GENESIS provides tremendous savings in real

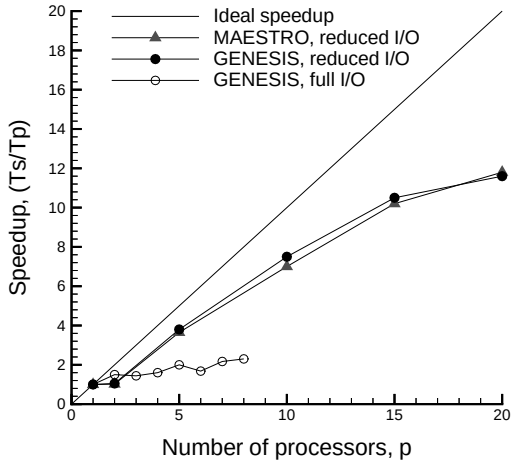

Figure 4.1: Ideal and actual speedup for parallel execution of 50 structural optimizations.

time for job execution: it takes 40 minutes of real time to execute one structural optimization of the coarse FE model on one processor of the *Paragon*), but only two hours to complete 50 structural optimizations on 20 processors. However, a small number of structural optimizations completed by each processor makes the dynamic task scheduling procedure that we implemented less efficient. This is the main reason for the drop in efficiency in Figure 4.2 for 20 processors: when 50 structural optimizations are executed on five processors, each processor completes on average 10 independent structural optimizations, while when the same task is executed on 20 processors, each processor completes on average only 2.5 independent structural optimizations.

To check if it was the small number of structural optimizations completed by each processor that reduced the parallel performance, we executed a large number of structural optimizations on different numbers of processors. For this large number of runs it was not feasible to run the same cases on a single processor. Therefore, speedups and efficiencies in this case are estimated on the basis of the average time for a run on a single processor, observed in the first set of runs — 40 minutes of wall time. The results are presented in Figure 4.3. Table 4.1 gives the description

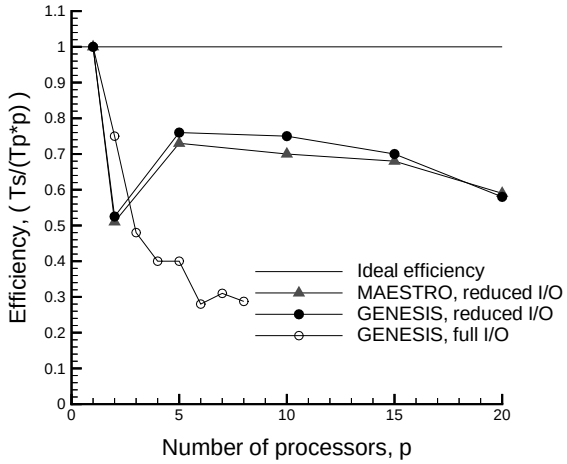

Figure 4.2: Ideal and actual efficiency for parallel execution of 50 structural optimizations.

of the parameters used to obtain each point in Figure 4.3. There is some scatter in the results due to the machine workload and the difference in computation time for different configurations. If two data points are available for the same number of processors, the estimated efficiency curve in Figure 4.3 is passed through the points corresponding to average calculated efficiency. The drop in estimated efficiency in Figure 4.3 for more than 45 processors can be explained by the amount of the disk I/O that the *Paragon* can handle at the same time.

Table 4.1: Parameters for executing many structural optimizations.

Number of processors	Number of structural optimizations performed	Real time
20	132	4.8 hours
35	466	10.8 hours
46	595	11.2 hours
46	590	13.6 hours
51	576	10.0 hours
51	678	19.6 hours
56	680	17.6 hours
56	896	19.6 hours

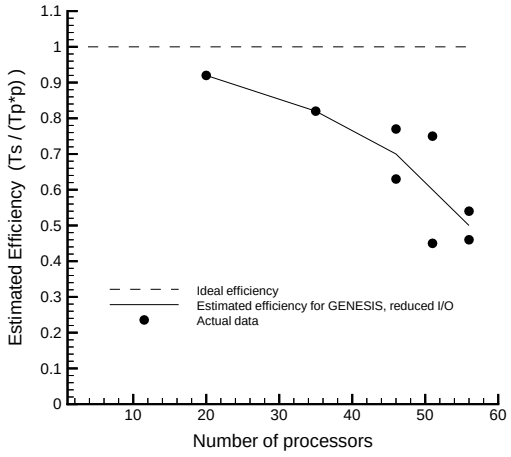

Figure 4.3: Ideal and estimated efficiency for parallel execution of many structural optimizations.

The results obtained indicate that using the procedure that was implemented on the Intel *Paragon* computer we can afford to execute thousands of coarse structural optimizations in a reasonable time. However, the implemented procedure does not scale to a large number of processors (say, 100, and more). The non-scaling is partly due to the particular approach to the coarse-grained parallelization that we used and partly due to the large amount of disk I/O that is a feature of the structural optimization code.

Chapter 5

Numerical Noise Issues

Unfortunately, the weight obtained by structural optimization is not a smooth function of the configuration design variables. This nonsmoothness is the result of changes in the set of active constraints as the configuration changes and numerical noise which includes incomplete convergence of the structural optimization as well as noise in the aerodynamic loads.

5.1 Design-Line Plots

A procedure which we use to detect noise in a response quantity is to plot the response along a straight line segment in design space. This plot is sometimes called a *design-line plot* or an *α-plot* [50]. The segment is obtained by connecting two points ($\mathbf{x_f}$ and $\mathbf{x_l}$) in the design space:

$$\mathbf{x} = (1 - \alpha)\mathbf{x_f} + \alpha\mathbf{x_l} \ , \quad 0 \leq \alpha \leq 1 \ .$$

In order to check the amount of noise in the results of the structural optimization, two close, conventional looking HSCT configurations were chosen as the endpoints of the segment in the design space (Figure 5.1). The design variables which define these two configurations differ by about 3%.

Figure 5.2 shows the variation in the wing bending material weight initially obtained from structural optimization for 20 HSCT configurations along the line segment

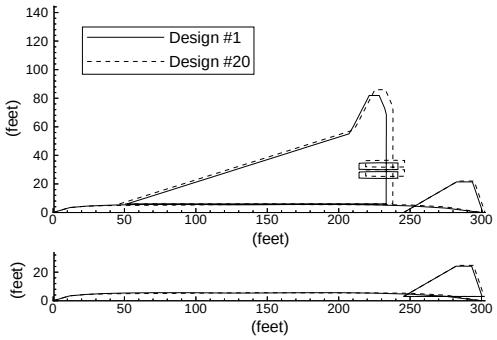

Figure 5.1: First and last configurations in the α-plot.

from Design # 1 (α=0) to Design # 20 (α=1) It appears from the figure that the noise in the structural optimization weight is on the order of 20–30%.

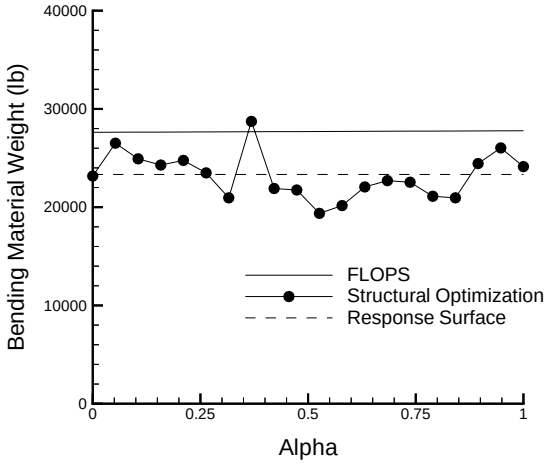

Figure 5.2: Initial noise in the wing bending material weight. (Response surface constructed from the "noisy" results of structural optimization).

5.2 Reduction of Numerical Noise

We first explored the possibility that most of the noise in the optimization results was due to unconverged structural optimization results. Accordingly we tried reducing move limits and tightening convergence criteria. Move limits were reduced from 30% to 10% and stopping convergence criteria were reduced from 1% to 0.1%. This had a favorable but small effect. The noise was reduced from 30% to about 29%. We looked for other optimization related noise sources and found that one of the possible sources was the objective function of the structural optimization (total wing structural weight). We found that the total wing structural weight varied less erratically than the bending material weight which was extracted from it. Apparently, the optimization procedure could find designs with very similar total weight, but with different distributions between the component defined as the bending material by FLOPS and the rest of the weight. Consequently, the optimization procedure converged to designs with similar total weights as we changed the aerodynamic shape, but with different bending-material weights. To overcome this difficulty we tried to make the objective function of the structural optimization closer to the definition of the wing bending material weight: we relaxed stress and buckling constraints for the portions of the wing whose weight was not included into wing bending material weight. Thus, we assumed that structural arrangement of these portions of the wing should be given. This manipulation of the objective function reduced the maximum noise by another 2%.

We also tried three different optimization methods available in GENESIS — method of feasible directions (FDM), sequential linear programming (SLP), and sequential quadratic programming (SQP) — to see if the noise was influenced by the method of performing structural optimization. The results are presented in Figure 5.3, which shows that none of the methods has a definite advantage over the others, and that noise is not related to the optimization method.

The biggest variation along the segment occurs for $\alpha \approx 0.37$. To eliminate any effect of optimization convergence, we optimized this configuration starting from the arithmetic mean of the configurations corresponding to $\alpha \approx 0.32$ and $\alpha \approx 0.42$.

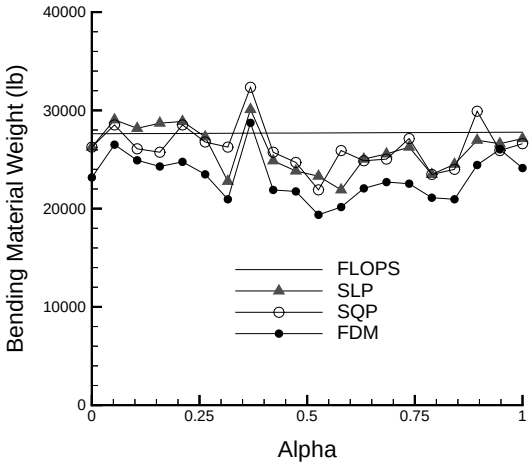

Figure 5.3: Wing bending material weight from different structural optimization methods.

This approach reduced the variation in the wing bending material weight for the configuration with $\alpha \approx 0.37$ by about 5%.

Next, we investigated the effect of the aerodynamic loads by using the arithmetic mean of the loads from the cases of $\alpha \approx 0.32$ and $\alpha \approx 0.42$ as a starting point for optimization of the configuration with $\alpha \approx 0.37$. This totally eliminated the variation, showing that the source of most of the noise arose from the loads that were applied to the structure. Figure 5.4, which shows the spanwise location of the center of pressure (CP) and of the inertia load center (IC) for the five load cases (LC), supports this conclusion. (The fifth load case is for taxiing, where only inertia loads are applied.)

Most of the curves in Figure 5.4 have some variation for $\alpha \approx 0.37$. The curve for the second load case (Mach number 2.4, load factor 1.0), which is critical, has the largest variation. In Ref. [51] it was shown that a change of 1.5 ft (approximately 0.018 of the semi-span) in the spanwise location of the center of pressure can change the stresses in the wing by about 20%. This sensitivity of the stresses to the location of the center of pressure is due to the large amount of fuel carried in the wing of the HSCT. The inertia loads associated with the fuel cancel most of the aerodynamic

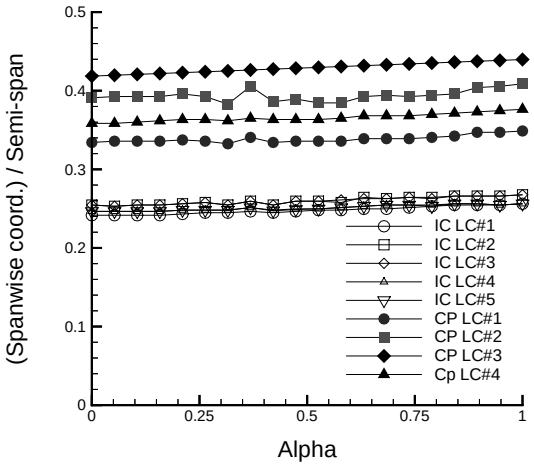

Figure 5.4: Spanwise location of the center of pressure and of the inertia load center for five load cases.

loads, so that small changes in the aerodynamic loads can have large effects on the resultant bending moment. These changes in bending moments and stresses in turn have substantial effect on the results of the structural optimization.

The variations in the inertia center location are mostly due to the fact that distribution of fuel between fuel tanks is optimized for each design [16]. Results of these independent optimizations are noisy, and they certainly affect the wing bending material weight calculations.

To further investigate the source of the noise in center of pressure location we studied the way camber is assigned to the wing. As mentioned earlier, the camber distribution is optimized by Carlson's program WINGDES [52]. Optimization of the camber distribution is done separately for each particular configuration. We found out that most of the variation in the center of pressure location was caused by a mistake in application of the WINGDES program. When we corrected the camber optimization procedure, we improved the camber design at the cruise C_L and obtained a much smoother wing camber distribution as a function of wing geometry. That in turn significantly reduced the amount of noise in the location of the center of pressure (Figure 5.5). Due to changes in camber distribution, the center of pressure for all the load cases moved outboard.

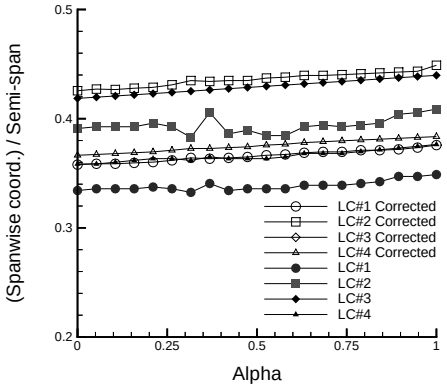

Figure 5.5: Spanwise location of the center of pressure for four load cases (initial and corrected camber).

After the camber optimization was corrected, we repeated the structural optimization for the designs of the α-plot (Figure 5.6). We obtained a significant reduction in the amount of noise in the wing bending material weight. Most of the remaining noise could be attributed to incomplete convergence of the structural optimization, separate optimization of fuel redistribution for each design, and noise left in the locations of center of pressure and center of inertia. The significant "shift up" in the absolute values of the wing bending material weight is due to significant changes in the spanwise coordinate of the center of pressure location.

The remaining noise in our results will be filtered out by the response surface approximations. Figures 5.2 and 5.6 show the response surface approximations to the wing bending material weight obtained from structural optimization results with the original and the reduced amount of noise, respectively. Even with the large amount of noise in the results of the structural optimization, the response surface model captures the general trend of the wing bending material weight. Details of the creation of the response surface models are described in Chapters 7–9.

It should be noted that the FLOPS results agree much better with the results from structural optimization obtained using uncorrected camber in this portion of the design space. This fact could partly explain why Huang *et al.* [16] got better agreement between the FLOPS results and results from the structural optimization.

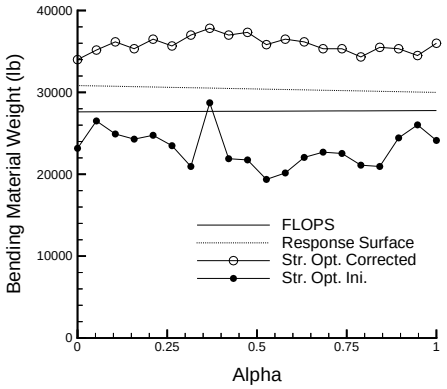

Figure 5.6: Wing bending material weight for the original and corrected camber distributions.

Chapter 6

Effect of the Aerodynamic Loads Model on the Results of the Structural Analysis and Optimization

We decided to investigate in more detail the influence of the model used for calculation of the aerodynamic loads on the results of the structural analysis and optimization. For this purpose we calculated aerodynamic loads using two different approaches: Euler analysis and linear aerodynamic theory. Pittman *et al.* [53] concluded that linear theory is useful in conceptual and preliminary stages of the aircraft design. We decided to check if in our case more precise and more computationally expensive aerodynamic loads calculations via Euler analysis result in wing bending material weight significantly different from the one calculated using aerodynamic loads obtained from linear aerodynamic theory. We compared the results of the structural analysis and optimization when aerodynamic loads from two approaches were applied to the coarse structural FE model. In this study we concentrated on three supersonic loads cases: Mach 2.4 cruise, 2.5-g pull-up at Mach 2.4, and Mach 1.2 cruise. The effect of differences in the loads on the Von Mises equivalent stresses is determined at these three conditions. Structural optimizations are then performed using the supersonic loads

from Euler solutions and from linear theory analyses to determine the sensitivity of the wing bending material weight to the accuracy of the aerodynamic loads.

The same three HSCT configurations were studied as the ones used for comparison between results of coarse and refined FE models (Figure 3.5). The detailed description of the study for HSCT Configuration 2 and results of the studies for the other two configurations are given in this chapter. Work by Knill *et al.* [51] provides additional details.

We used version 2.2 of the General Aerodynamic Simulation Program [54] (GASP) for the Euler calculations. The grids for the space-marching calculations on the HSCT wings and wing-fuselage combinations were created using 3-D grid generator originally developed by Barger [55] and modified by Knill [51]. The detailed description of the aerodynamic grids used and Euler code verification is given in Ref. [51].

6.1 HSCT Configuration 2

HSCT Configuration 2 is a modified version of an early optimal design described in Ref. [13]. The original wing planform has been altered so that there is no trailing edge sweep (Figure 6.1). This allows the aerodynamic grid generator to create a marching grid which models the wing trailing edge exactly. The design variables used to create this configuration are given in Table 6.1.

The loads computed from linear theory and Euler calculations on wing-alone and wing-fuselage configurations are presented for comparison. Cruise at Mach 2.4 for Design Case 1 is achieved with a lift coefficient of 0.070. The loads at this condition (Figure 6.1) show good agreement over most of the wing. Little variation is seen between the wing-alone and wing-fuselage loads. There is a slight peak in the linear theory loads at the wing trailing-edge cut, but this is a difference of only about 0.02 in ΔC_P. In Figure 6.1 ΔC_P denotes the difference in dynamic pressure between the wing lower and upper surfaces.

The wing model used for the structural optimization is shown in Figure 6.2. Figure 6.3 shows contours of the difference in wing bending stress computed from Euler and linear theory loads. The difference in stresses is negative over most of the wing,

Table 6.1: Design variables for HSCT Configuration 2.

Value	Description
181.00	Wing Root Chord ($ft.$)
156.00	L.E. Break, x ($ft.$)
49.20	L.E. Break, y ($ft.$)
181.00	T.E. Break, x ($ft.$)
64.00	T.E. Break, y ($ft.$)
170.00	L.E. Wing Tip, x ($ft.$)
11.00	Wing Tip Chord ($ft.$)
75.90	Wing Semi-Span ($ft.$)
0.4019	x-Loc. Airfoil Max. t/c (x/c)
3.6921	L.E. Radius Parameter
2.5789	t/c at Wing Root ($\%c$)
2.1594	t/c at L.E. Break ($\%c$)
1.8039	t/c at Wing Tip ($\%c$)
2.196	Fuselage X-Restraint #1
1.0610	Fuselage R-Restraint #1
12.200	Fuselage X-Restraint #2
3.4961	Fuselage R-Restraint #2
132.463	Fuselage X-Restraint #3
5.3410	Fuselage R-Restraint #3
248.668	Fuselage X-Restraint #4
4.6661	Fuselage R-Restraint #4

Table 6.2: Stress, center of pressure, and bending material weight comparisons for Configuration 2. Here $W_{\text{S/O-Euler}}$ denotes wing bending material weight calculated using Euler aerodynamic loads, $W_{\text{S/O-LT}}$ – wing bending material weight using aerodynamic loads from linear theory.

	$(\Delta\sigma)_{\max}$		$\Delta(\sigma_{\max})$		$\Delta y_{\text{c.p.}}$	
Load Case	psi	%	psi	%	ft	$\frac{W_{\text{S/O-Euler}}}{W_{\text{S/O-LT}}}$
M=2.4 n=1.0	-1971	(37.0%)	-1729	(23.6%)	-1.528	
M=1.2 n=1.0	-2710	(17.3%)	-641	(2.6%)	-1.342	0.944
M=2.4 n=2.5	-4696	(25.5%)	-4341	(16.7%)	-1.218	

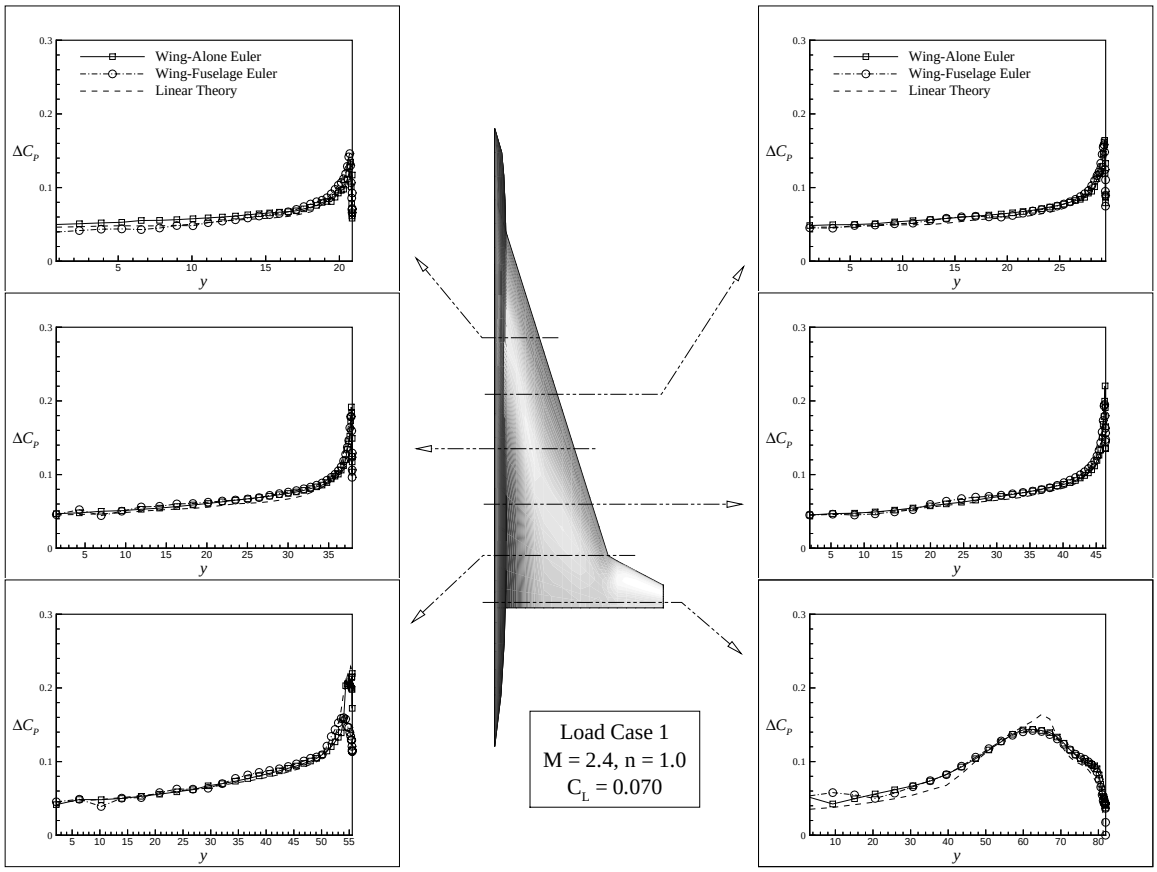

Figure 6.1: Aerodynamic loads for HSCT Configuration 2 at Mach 2.4 cruise.

indicating that the stresses computed from Euler loads are lower. The largest magnitude difference in stress occurs on the lower wing surface in a region inboard of the leading-edge break. The value of this maximum stress difference (Table 6.2) is

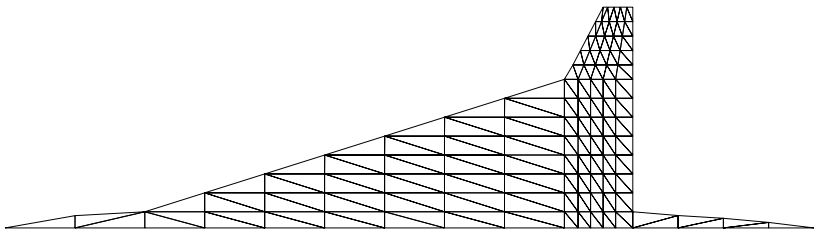

Figure 6.2: Structural mesh for HSCT Configuration 2.

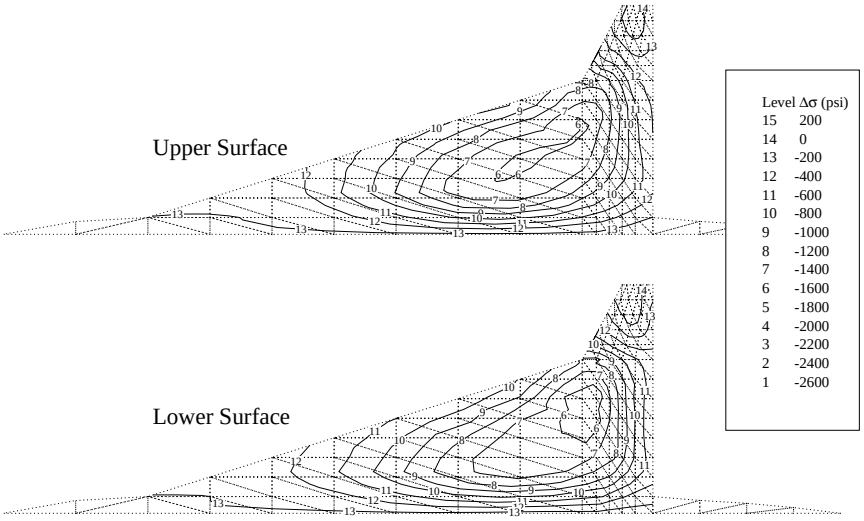

Figure 6.3: Stress differences for HSCT Configuration 2 at Mach 2.4 cruise.

-1971 *psi*, which represents 37.0% of the nominal value. The percentage variation in the maximum stress is lower at 23.6%, but is still high considering the agreement in the loads. Searching for explanations to this relatively large discrepancy led us to look at the predicted center of pressure location. The spanwise location of the center of pressure calculated from Euler analysis is 1.53 *ft* inboard of that computed from linear theory on a wing with a semi-span of 75.9 *ft*. This gives insight into why the Euler loads result in lower bending stress values. The sensitivity of the stresses to the predicted loads comes from the large amounts of fuel stored in the wings of our HSCT designs. Inertia relief from the fuel weight cancels much of the wing bending due to aerodynamic loading. This causes the wing bending stresses to become very sensitive to small changes in the loading and the spanwise location of the center of pressure.

The Mach 1.2 cruise load condition is examined next. Cruise at this Mach number

is obtained with a lift coefficient of 0.071. The Euler solution to the wing-fuselage configuration at Mach 1.2 cruise could not converge (see Ref. [51] for details). The wing-alone Euler calculations were successful, and the results (Figure 6.4) compare well with those from linear theory. As with the Mach 2.4 cruise condition, the loads near the trailing edge show the poorest agreement.

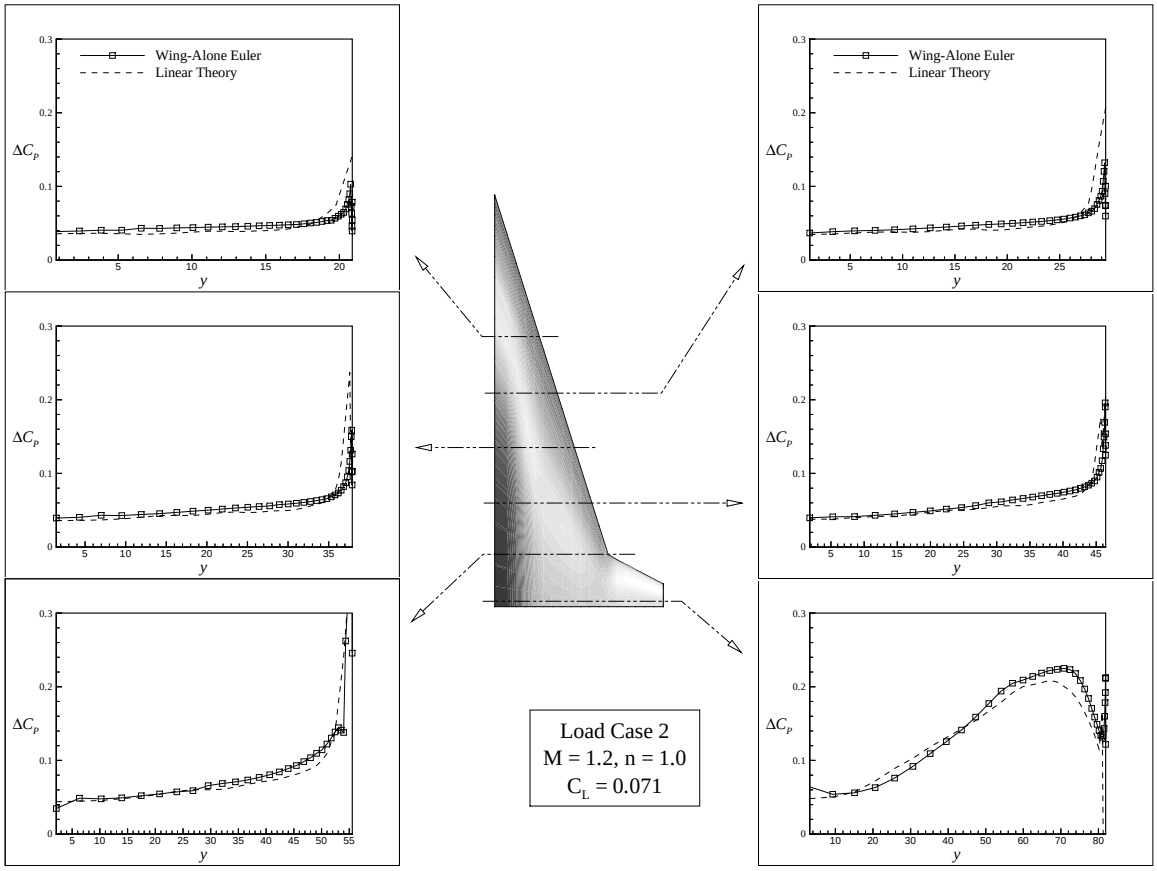

Figure 6.4: Aerodynamic loads for HSCT Configuration 2 at Mach 1.2 cruise.

The stress comparisons (Figure 6.5) for the Mach 1.2 cruise condition show that, overall, the stresses computed from Euler loads are lower than those from linear theory loads. The value of the maximum stress difference (Table 6.2) is -2710 *psi* which represents 17.3% of the stress value for that element, while the variation in the maximum stress is only -641 *psi* (2.6%). The maximum stress occurs near the leading edge break. The spanwise center of pressure location from Euler analysis is

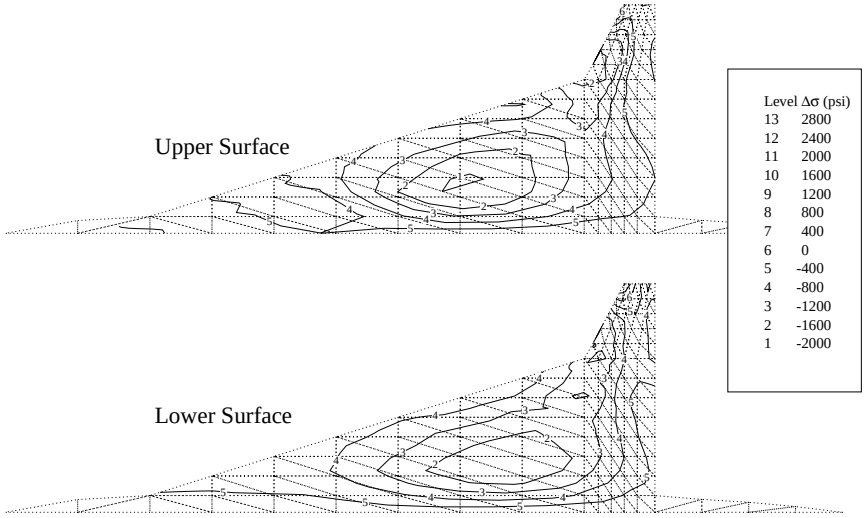

Figure 6.5: Stress differences for HSCT Configuration 2 at Mach 1.2 cruise.

1.34 ft inboard of that from linear theory.

The Mach 2.4 2.5-g pull-up case ($C_L = 0.154$) gives much more dramatic differences in the loading. The Euler solution (Figure 6.6) on the wing and wing-fuselage case reveals the formation of a shock on the upper wing surface. Linear theory loads match well inboard of the shock, but underpredict the load immediately outboard of it. Linear theory also overpredicts the leading edge suction peak along the entire subsonic leading-edge. The subsonic leading edge is that portion ahead of the leading-edge break in which the component of the Mach number normal to the leading edge is subsonic. After the wing break, the leading-edge loads predicted from linear theory match better with those from the Euler solutions, however, the peak caused by the error along the subsonic leading edge propagates and results in the peak seen at the aft-most wing station.

The effects of the differences in aerodynamic loading can be seen in the structural

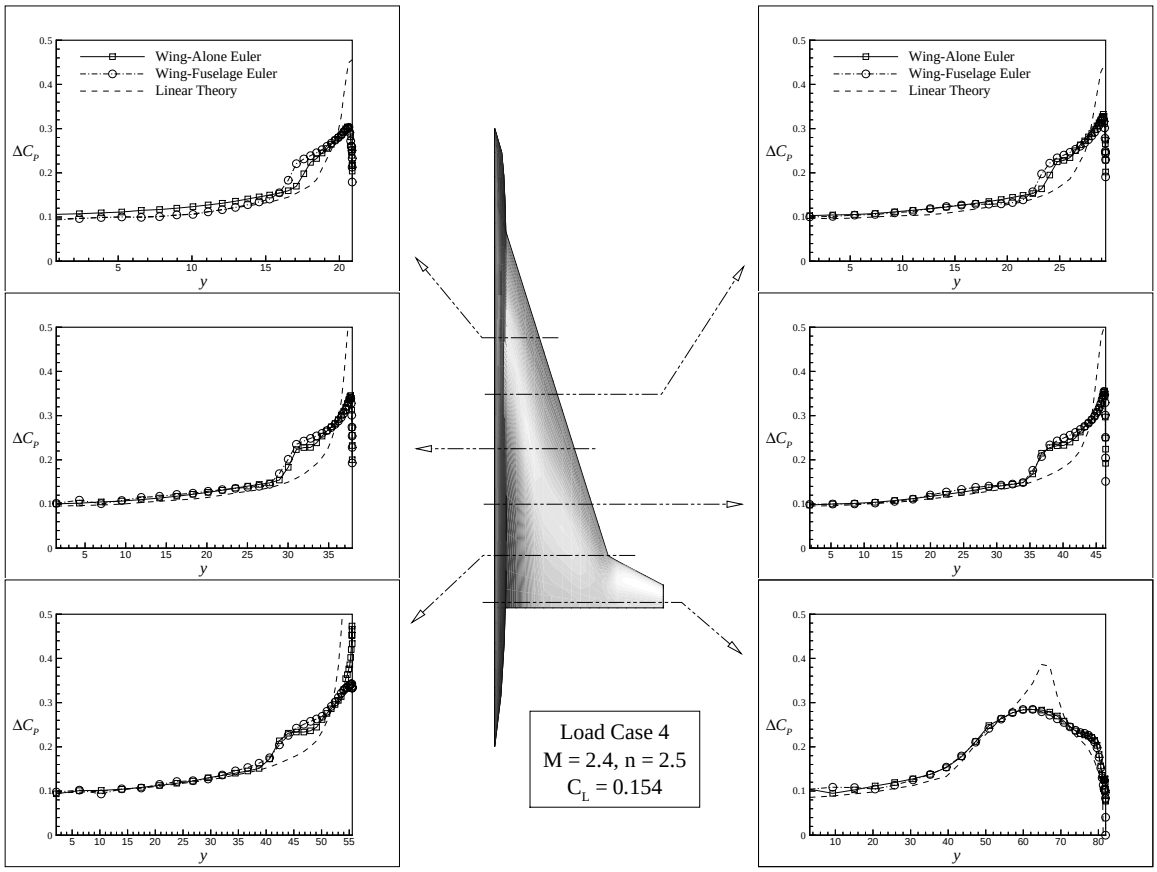

Figure 6.6: Aerodynamic loads for HSCT Configuration 2 at Mach 2.4 2.5-g pull-up.

analysis of the aircraft. As expected, we find that the largest magnitude difference in stresses (Table 6.2) computed from linear theory and Euler loads occurs for the Mach 2.4 2.5-g pull-up condition. The maximum difference in predicted stresses is 25.5% and the variation in the maximum stress is 16.7%. The maximum stress again occurs near the wing leading edge break. As with the previous two cases, the spanwise location center of pressure is farther inboard for the Euler loads. The stresses (Figure 6.7) from Euler loads are higher over the small outboard section of the wing, however over the remainder of the wing they are lower than the stresses found from linear theory loads. As with the other two load cases, the maximum difference in stresses occurs near the middle of the wing. While the regions aft of the leading-edge break show large variations in the aerodynamic loading from Euler and linear theory

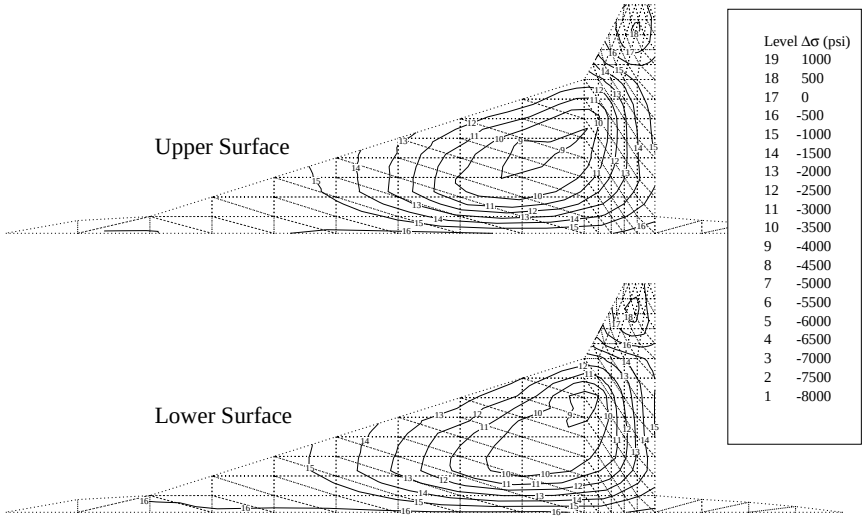

Figure 6.7: Stress differences for HSCT Configuration 2 at Mach 2.4 2.5-g pull-up.

results, they also have inertial loading from the nacelles. These inertial effects appear to explain why the maximum difference in stress does not occur farther aft on the wing.

The overall effect of these differences on the structural optimization is an optimal design whose wing bending-material weight is 1181 *lb* (5.6%) lighter by using the Euler loads instead of the linear theory loads. The lower stresses obtained with Euler loads result in a lighter wing. However, in spite of the difference in loads for the Mach 2.4 2.5-g pull-up and the relatively large variations in stresses for all load cases, the optimized wing-bending material weight shows only a small change.

6.2 Summary of Results from Three Configurations

Two other HSCT configurations (Figures 6.8, 6.9) were studied. The main results of these studies are summarized in Tables 6.3 and 6.4.

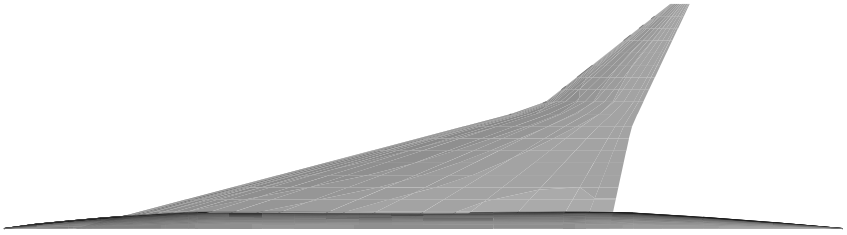

Figure 6.8: Planform of HSCT Configuration 1.

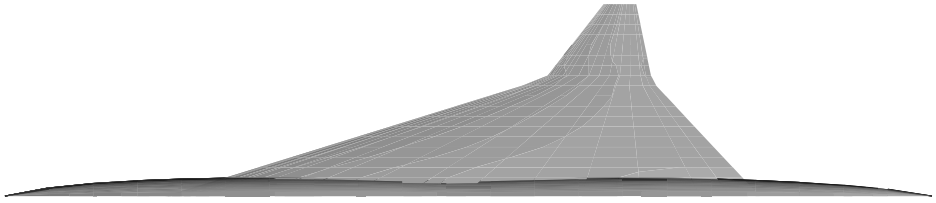

Figure 6.9: Planform of HSCT Configuration 3.

The HSCT configurations examined show that linear theory consistently overpredicts the lift. Linear theory pitching moments for the HSCT configurations show a stronger nose-up tendency than those from Euler analysis, because the aerodynamic center is located farther forward. Analysis of the three configurations shows that the nominal aerodynamic center location moves aft as the trailing edge of the wing becomes more aft-swept.

At supersonic cruise, linear theory compares well with Euler analysis. The same is not true for high-lift conditions, where crossflow shocks appear on the wings. In this case linear theory predicts the loads well inboard of the shock, underestimates the

Table 6.3: Stress, center of pressure, and bending material weight comparisons for Configuration 1. Here $W_{\text{S/O-Euler}}$ denotes wing bending material weight calculated using Euler aerodynamic loads, $W_{\text{S/O-LT}}$ – wing bending material weight using aerodynamic loads from linear theory.

Load Case	$(\Delta\sigma)_{\max}$ *psi*	%	$\Delta(\sigma_{\max})$ *psi*	%	$\Delta y_{\text{c.p.}}$ *ft*	$\frac{W_{\text{S/O-Euler}}}{W_{\text{S/O-LT}}}$
M=2.4 n=1.0	−2764	(23.4%)	−2520	(18.9%)	−1.713	
M=1.2 n=1.0	+4601	(21.2%)	+4594	(12.7%)	−0.056	1.051
M=2.4 n=2.5	−8745	(22.8%)	−8543	(21.1%)	−1.952	

Table 6.4: Stress, center of pressure, and bending material weight comparisons for Configuration 3. Here $W_{\text{S/O-Euler}}$ denotes wing bending material weight calculated using Euler aerodynamic loads, $W_{\text{S/O-LT}}$ – wing bending material weight using aerodynamic loads from linear theory.

Load Case	$(\Delta\sigma)_{\max}$ *psi*	%	$\Delta(\sigma_{\max})$ *psi*	%	$\Delta y_{\text{c.p.}}$ *ft*	$\frac{W_{\text{S/O-Euler}}}{W_{\text{S/O-LT}}}$
M=2.4 n=1.0	−706	(25.2%)	−265	(5.0%)	−0.532	
M=1.2 n=1.0	−2049	(49.0%)	−1496	(15.5%)	−0.197	0.971
M=2.4 n=2.5	−2088	(55.4%)	−1043	(6.3%)	−0.811	

loads immediately outboard of the shock, and overestimates the loads at the subsonic leading edge.

Despite the good agreement in loads at cruise, differences of 21%–49% are seen in Von-Mises stresses. The differences in maximum stress are lower, but still reach 23.6%. The magnitude of the differences in stresses is reflected in the differences in the spanwise center of pressure locations. Using Euler loads in the structural analysis results in a more inboard center of pressure and lower stresses over most of the wing. The Mach 1.2 cruise conditions show the largest regions on the wing where the stresses from Euler loads are bigger than those from linear theory loads. For HSCT Configurations 2 and 3, the wing bending material weights computed using Euler loads are lower than those from linear theory loads. However, in the case of HSCT Configuration 1, the largest stresses in the Mach 1.2 load case result in a heavier design using Euler loads. The bending material weights are not as sensitive as the wing stresses to the differences in loads. The differences in bending material weights are not greater than 5.6% for the three HSCT configurations considered.

Chapter 7

Response Surface Methodology and Design of Experiments

Response surface methodology (RSM) is not the only way to integrate structural optimization in the overall HSCT design process. For example, a multilevel decomposition approach was successfully used by Röhl [2] and an interlacing factor approach was used by a design group at Virginia Tech [13]. Currently, we employ RSM because it provides several attractive features not provided by other approaches. In particular, it allows disciplinary codes to be executed by specialists *a priori* to the overall design, rather than by generalists in the overall design process. RSM significantly simplifies multidisciplinary code integration and helps to filter out numerical noise. In our case, the objective function of an optimization is not a smooth function of problem parameters, and incomplete convergence adds numerical noise. Therefore, the smoothing properties of RSM are particularly useful for incorporating structural optimization in the overall configuration optimization. Finally, since the response surface is usually a low-order polynomial, the optimization task becomes computationally cheap.

7.1 General Description

Response surface methodology is a statistical technique in which smooth functions, typically linear or quadratic polynomials, are used to model system response. For

example, a quadratic response surface model for p variables has the form:

$$y = c_0 + \sum_{1 \le i \le p} c_i x_i + \sum_{1 \le i \le j \le p} c_{ij} x_i x_j \,, \tag{7.1}$$

where the x_i are the variables, the c_i are the polynomial coefficients, and y is the response. For p variables, (7.1) has $n = (p+1)(p+2)/2$ terms. In such a model the polynomial terms may be estimated using the method of least squares (Appendix B). To estimate the terms we need data at a number of points which is larger than the number of terms. Large ratios between the number of points and number of terms help filter out noise in the data as well as improve the fit of the polynomial to the response. Techniques for selecting analysis points in the design space are the subject of the theory of *design of experiments*.

For a quadratic polynomial in p variables the number of terms n in the model function grows at a rate $\mathcal{O}(p^2)$. Creating a response surface model for the n-term polynomial requires a number of points N which is larger than, but of the same order of magnitude as, n. However, to maintain good accuracy, we would like the points where we use the response surface model to be located within the convex hull of the data points used to construct the surface. To satisfy this for a p-dimensional box we must estimate the response at 2^p points (at the vertices of the box). Such an experimental design, where all the vertices of the p-dimensional box are evaluated, is called a *full-factorial design* and denoted according to the number of the points evaluated (2^p) ([20], pp. 79–111). Another commonly used experimental design which includes only $2^{(p-m)}$ vertices of the p-dimensional box (m is an integer number smaller than p) is called a $2^{(p-m)}$ *fractional factorial design* ([20], pp. 134–174). The idea behind selecting particular vertices in the fractional factorial design, while disregarding other vertices, is illustrated in Appendix C. For the twenty-nine design variables describing the HSCT configuration, the full-factorial design corresponds to more than 500 million points in the design space, which is certainly impossible to evaluate with present computational capabilities. This problem is often called the *curse of dimensionality*.

In addition to the curse of dimensionality, another source of inaccuracy in the response surface model is that quadratic polynomials cannot model higher order variations very well. Also estimations outside the data where the response surface was

created may produce inaccurate results.

Several measures can be taken to address this modeling error. First, the number of data points used to create the response surface can be increased so that the convex hull defined by the known data points encloses a larger portion of the design space. This option increases computational expense and we did not consider it for our high-dimensional problem. Second, the volume of the design space modeled by the RS model could be reduced. This will reduce the portion of the design space volume which is outside the convex hull of the data points. Another option is to reduce the complexity of the model function by eliminating unnecessary terms. A statistical technique, analysis of variance (ANOVA, described in part in Appendix B), enables the less significant terms in the polynomial approximation to be identified ([20], pp. 640–655). Finally, the points can be selected so as to minimize the modeling error. An example of an experimental design that minimizes the modeling error is given later in this chapter.

Once the response surface model (RS model) is generated, its predictive capabilities must be evaluated. This is accomplished by finding the response surface prediction at a series of data points with known responses. Measuring the difference between the known and the predicted response yields information including average error, maximum error, estimate of the standard deviation of the noise in the data, which is also a root mean square error estimate ($RMSE$), unbiased root mean square error estimate ($RMSE_{ub}$). The root mean square error estimate is the square root of the sum of squares of the differences between the actual (y_i) and predicted ($\hat{y}_i$) values of the responses at the data points divided by the total number of data points (N):

$$RMSE = \sqrt{\frac{\sum_{i=1}^{N}(y_i - \hat{y}_i)^2}{N}} \ . \tag{7.2}$$

However, the RMSE is a good predictor for estimating the standard deviation of the error in the response surface model only when the points used in Equation (7.2) were not used to fit the response surface model. If we use the same points, the standard deviation of the error at these points is underestimated and to get an unbiased

estimate we need to divide by the difference between the total number of data points (N) and the number of terms in the RS model function (n):

$$RMSE_{ub} = \sqrt{\frac{\sum_{i=1}^{N}(y_i - \hat{y}_i)^2}{N - n}} \ . \tag{7.3}$$

7.2 Design of Experiments for Response Surface Models

RSM typically employs a structured set of points such as a central composite design (CCD) ([20], pp. 297–341). Consider the p-dimensional box centered at the origin of the system of coordinates. Then a CCD comprises vertices of this box (factorial portion of the experimental design), the point at the center, and $2p$ points on the axes of the system of coordinates, located symmetrically with respect to the center of the box. These $2p$ points are called the axial points. However, a CCD is only effective for a low dimensional regularly shaped design space, which is unlikely to appear in this study, where our design problem is described by 29 design variables.

When one can not afford to evaluate the system response for the complete CCD, it is possible to reduce the number of points where system response should be evaluated, while still preserving the attractive geometrical structure of the CCD. Often this is done by reducing the factorial portion of the CCD, i.e., selecting a carefully chosen subset of the vertices of the p-dimensional box. The points in the $2^{(p-m)}$ fractional factorial design employed here for the factorial portion of the experimental design should be chosen in such a way that they allow estimation of all the necessary terms in the RS model function (in Appendix C we give brief explanation of the idea behind the selection of points). This experimental design, centered at the origin of the system of coordinates and represented by a $2^{(p-m)}$ subset of the vertices of the p-dimensional box, the point at the center, and $2p$ points along the axes of the system of coordinates is called a *small composite experimental design* (SCD) ([20], pp. 351–357).

For an irregularly shaped design space in high dimensions, there is no simple way

to create a finite number of points that span the entire region. Hence, a very large number of points is usually produced knowing that many of them will fall outside of the feasible design space. The infeasible points can then either be perturbed until they fall within the feasible region, or removed. This process will lead to a large number of points inside the feasible region, but whose geometric distribution is irregular. From these points, a small number could be chosen to construct the response surface model.

The D-optimality criterion [25], [56] provides a popular rational means for choosing the location of a given number of these points. This criterion seeks to minimize the variance in the terms of the response surface model due to noise in the data. This is accomplished by maximizing the determinant of the coefficient matrix in the normal equations used to obtain terms in the method of least squares (Equation (B.1) in Appendix B). The D-optimality criterion provides maximum protection against the effects of noise, but it is not well suited to handle modeling errors.

Another criterion, called minimum bias (e.g., [20], pp. 401–418), seeks to minimize the modeling error (also called bias error) which reflects the fact that the function we use for the response surface (quadratic polynomial here) is different from the true response function. Myers and Montgomery ([20], pp. 401–418) report on examples where minimum bias design sets of points also had good variance properties, but minimum variance sets of points did not have low bias properties.

To find a minimum bias set of points you have to postulate the true form of the approximated function. Since we employ a quadratic polynomial, we assume that the true wing bending material weight is a cubic polynomial. The minimum bias set of points satisfies the condition that

$$\frac{1}{V}\int_S m(x)dx = \frac{1}{N}\sum_{j=1}^{N} m(x_j)\,, \tag{7.4}$$

where V is the volume of the reasonable design space S, $m(x)$ is any monomial term obtained from multiplying a cubic polynomial by a quadratic polynomial, and N is the number of design points used to create the response surface.

7.3 Reasonable Design Space Approach

Most applications of RSM employ a region in design space that is a box defined in terms of lower and upper bounds on the design variables. For such a region a structured set of points, like a full factorial experimental design or CCD, works very well. For high dimensional problems, however, unless we analyze designs at most of the vertices of the box, the process of approximation inside the box can entail extrapolation rather than interpolation, with an attendant loss of accuracy. (The words "extrapolation" and "interpolation" are used here in their intuitive, rather than technical, senses.) With an n-dimensional box having 2^n vertices, it becomes impractical to evaluate the designs at all the vertices for values of n of the order of ten or more. However, other geometrical shapes in n dimensional space allow interpolation inside with many fewer points. For example, a simplex (the generalization of a triangle and a tetrahedron) has only $n + 1$ vertices. This reflects the fact that a simplex has a much smaller volume than the enclosing box, in fact, smaller by $n!$.

The reasonable design space approach seeks inexpensive constraints that eliminate from consideration large portions of the design box, and render it more similar to a simplex or at least an ellipsoid, which also has a much smaller volume than the enclosing box, with a ratio of about 10^{10} for $n = 25$. The volume V of a sphere with radius r in p dimensions is given by

$$V = \frac{\pi^{p/2} r^p}{\Gamma(\frac{p+2}{2})}, \tag{7.5}$$

where Γ is the Euler Gamma function (taken from [57], p. 206). For the sphere R of unit radius in p-dimensional space,

$$R = \{x \mid \sum_{i=1}^{p} x_i^2 \leq 1\}, \tag{7.6}$$

the following holds (taken from [57], p. 205):

$$\int_R \left(\prod_{i=1}^{p} x_i^{\delta_i} \right) dx = \begin{cases} \dfrac{\prod_{i=1}^{p} \Gamma\left(\frac{\delta_i+1}{2}\right)}{\Gamma\left(\frac{\sum_{i=1}^{p}(\delta_i+1)}{2}+1\right)}, & \text{for all } \delta_i \text{ even}, \\ 0, & \text{for any } \delta_i \text{ odd} \quad . \end{cases} \tag{7.7}$$

Expressions for the integrals of the second and fourth order monomial terms from Equation (7.4) could also be obtained as special cases of the general Equation (7.7):

$$\int_R x_i^2 dx = \frac{\pi^{p/2}}{(p+2)\Gamma(\frac{p+2}{2})}, \tag{7.8}$$

$$\int_R x_i^4 dx = \frac{\pi^{p/2}(3/4)}{\Gamma(\frac{p+6}{2})}, \tag{7.9}$$

$$\int_R x_i^2 x_j^2 dx = \frac{\pi^{p/2}(1/4)}{\Gamma(\frac{p+6}{2})}, \quad i \neq j. \tag{7.10}$$

The constraints that define the reasonable design space can come from simple geometric constraints that prevent combinations of design variables resulting in unreasonable geometry configurations. However, we also use inexpensive analysis tools to estimate the performance of candidate designs via aerodynamic and performance constraints. These analysis tools may not provide accurate estimates of performance, but they can identify designs with such inferior performance that we can discard them even based on very approximate results.

To define the reasonable design space for our particular case of HSCT configuration optimization we start with an HSCT configuration that lies well inside the design region. This configuration later on will be referred to as the *baseline HSCT configuration*. A box is constructed around this configuration by permitting each design variable to vary within the allowable bounds. Then one evaluates responses at a number of points in this box selected using some standard statistical design of experiments pattern.

For low dimensional cases a 3^n or 5^n full factorial experimental design (i.e., three or five levels in each variable) is constructed around the baseline HSCT configuration. The HSCT configurations corresponding to these full factorial points are analyzed using the inexpensive, low fidelity analysis tools and geometric constraints. The results are screened to eliminate from consideration any grossly inferior configurations. The remaining HSCT configurations form the approximation to the reasonable design space. This approach worked well for the low dimensional problem, as demonstrated by Giunta *et. al.* [32].

For high dimensional cases, some reasonable number of HSCT configurations on the boundary of the box are selected using a standard statistical design of experiments pattern, for example, CCD, SCD, or a design similar to a partially balanced incomplete block (PBIB) design described in Appendix D. Inexpensive analysis tools are used at this stage, along with geometric constraints to decide if an HSCT configuration is reasonable or not. As the set of the HSCT configurations in this case is sparse (even if we choose 1,000 HSCT configurations as our initial sample size, this number is still much smaller than the number of vertices of, say, a 29-dimensional box), the procedure of excluding points to estimate the reasonable design space would eliminate too many HSCT configurations. Instead the points corresponding to unreasonable HSCT configurations are moved to the edge of the reasonable design space in order to form an approximation of the boundary of the reasonable design space:

$$\mathbf{x}' = \beta\,(\mathbf{x} - \mathbf{x}_b) + \mathbf{x}_b,\ \beta > 0\,, \tag{7.11}$$

where $\mathbf{x}$ and $\mathbf{x}_b$ are the points corresponding to unreasonable and baseline HSCT configurations, respectively, and β is a parameter which is adjusted to make the HSCT configuration reasonable. In this process the points corresponding to the unreasonable HSCT configurations are moved towards the center of the design space (the baseline HSCT configuration) until the geometric, performance, and aerodynamic constraints are satisfied. In our particular case the constraints from Table 7.1 were used.

In Table 7.1 W_{b_F} denotes the wing bending material weight predicted by FLOPS, Λ_{le} denotes the leading edge sweep angle, AR is the wing aspect ratio, and c_{y_i} is wing section lift coefficient. Based on past experience with the weight function, reasonable

Table 7.1: Criteria for reasonable designs.

Number	Description
1-34	HSCT geometric constraints
35-36	20,000 lbs $< W_{b_F} <$ 120,000 lbs
37-58	Minimum fuselage radius
59	Inboard $\Lambda_{le} >$ Outboard Λ_{le}
60	$\Lambda_{le} > 0$
61-62	5,000 ft^2 $< S_w <$ 15,000 ft^2
63-64	$1.0 < AR < 3.2$
65	Inboard $\Lambda_{te} < 40^\circ$
65-83	$c_{y_{i+1}}/c_{y_i} < 1.0$
84	Approximate range $>$ 5,000 n. mi.
85-86	0.8*Thrust required $<$ Thrust available (approximate analysis)

HSCT configurations only occur when the FLOPS estimate for wing bending material weight W_{b_F} is between 20,000 lbs and 120,000 lbs, because of that the HSCT configurations with W_{b_F} falling outside that range were moved closer to the baseline HSCT configurations.

After the points corresponding to the unreasonable HSCT configurations have been moved inwards, we have a set of points residing on the edge of the reasonable design space. They form an approximation to the boundary of the reasonable design space. This process makes sense only if the baseline HSCT configuration $\mathbf{x}_b$ is located well inside the reasonable design space. If the baseline configuration is actually located on the boundary of the reasonable design space, many of the points that are pulled towards the baseline point could end up very close to the baseline point. In this case the representation of the shape of the reasonable design space could be incorrect. In our particular case we selected the baseline HSCT configuration by performing HSCT configuration optimization with tightened constraints, thus forcing the optimizer to end up with a configuration inside the region defined by constraints from Table 7.1, rather than on the boundary of this region.

After we have created the approximation to the reasonable design space or to the boundary of the reasonable design space, we can create a response surface model for the reasonable region using more accurate analysis or optimization tools than the ones used to define the reasonable design space.

7.4 Two-stage Approach for Constructing Response Surface Model

It is also possible to employ a two-stage approach for constructing response surface models. The general idea of this approach is the following. At the first stage (or stages) one constructs a relatively small (in terms of required number of points) experimental design in the part of the design space that is believed to be of interest. The RS model is constructed for this first-stage experimental design. It may even be a linear RS model if the number of design variables is large. The purpose of this RS model and small experimental design is to help *screen* the variables and determine the most influential ones. After the most important variables have been determined, one proceeds with constructing a large experimental design, but only for the most important variables. Then a more complicated RS model than one used at the first stage is fitted to the points of this design.

The reduced number of variables allows us to reduce the number of points where the response should be estimated at the second stage. We can use the *screening* procedure several times. In the process of doing so we may better define the region of interest: reduce it or shift it.

In our particular case we employed a two-stage approach involving SCD experimental design. In this approach we first construct SCD for our region of interest around a baseline HSCT configuration. We do so by allowing each of 29 configuration variable to vary between 60% and 140% of their baseline values. Next we move the points corresponding to unreasonable HSCT configurations towards the baseline point. Then, we employ results from the FLOPS weight equation to identify the important terms in the RS model. We construct a RS model based on FLOPS results at the SCD points and another RS model based on results of structural optimization for a subset of SCD points. We identify the important terms by comparing the terms in both RS models and focus our attention on these important terms at the second stage of the process. At the second stage we select points for additional structural optimizations and create the RS model from all the structural optimizations results

available. The advantage of the two-stage approach is that by identifying the important terms in the RS model we may more efficiently select HSCT configurations for structural optimization to improve the accuracy of the RS model. It should be noted that after we complete all the structural optimizations runs we should check if the terms that were eliminated after the first stage of constructing the RS model become important after we added additional structural optimization results during the second stage of the process.

Chapter 8

25-Design Variable Problem

In this chapter we describe the HSCT configuration optimization problem that was the first application of the reasonable design space approach. Twenty eight configuration variables were used to characterize a HSCT configuration at that time. Their description and baseline values are given in Table 8.1. Constraints used for this problem are given in Table 8.2. They are very similar to the constraints in the regular HSCT problem with 29 variables (Table 2.2).

Kaufman *et al.* [25] analyzed wing bending material weight for many diferent HSCT configurations using FLOPS weight equation results. The same 28 configuration variables were used as the ones in Table 8.1. It was found that three out of 28 variables — the wing leading edge radius parameter, the cruise climb rate, and the starting cruise altitude — do not have significant effect on the FLOPS estimates of the wing bending material weight. In spite of discrepancies in estimations of the wing bending material weight between the FLOPS weight equation and structural optimization, the FLOPS weight equation provides reasonable estimates of the wing bending material weight. Because of that we rely here on FLOPS to identify important variables, and we use only 25 out of 28 configuration variables for constructing the bending material weight RS model from the results of the structural optimization. However, as shown in the next chapter, identifying important variables for the RS model from higher fidelity results by using lower fidelity results, may not always work.

Table 8.1: HSCT baseline variables. 25-design variables problem.

Number	Value	Description
1	181.4780	Wing root chord (ft)
2	155.9070	LE Break, x (ft)
3	49.23480	LE Break, y (ft)
4	181.6030	TE Break, x (ft)
5	64.24340	TE Break, y (ft)
6	169.5730	LE of wing tip, x (ft)
7	7.003600	Tip chord (ft)
8	75.90870	Wing semi-span (ft)
9	0.401941	Chordwise location of max. t/c
10	3.692140	Airfoil LE radius parameter, r_t
11	0.025789	Airfoil t/c at root
12	0.021594	Airfoil t/c at LE break
13	0.018039	Airfoil t/c at tip
14	2.196000	Fuselage restraint 1, x (ft)
15	1.061000	Fuselage restraint 1, r (ft)
16	12.20000	Fuselage restraint 2, x (ft)
17	3.496100	Fuselage restraint 2, r (ft)
18	132.4630	Fuselage restraint 3, x (ft)
19	5.341000	Fuselage restraint 3, r (ft)
20	248.6680	Fuselage restraint 4, x (ft)
21	4.666100	Fuselage restraint 4, r (ft)
22	26.23010	Nacelle 1, x_9 (ft)
23	32.38760	Nacelle 2, x_{10} (ft)
24	322,617	Mission fuel (lbs)
25	64,794	Starting cruise altitude (ft)
26	33.89800	Cruise climb rate (ft/min)
27	697.8540	Vertical tail area (ft^2)
28	713.0590	Horizontal tail area (ft^2)

Table 8.2: Optimization constraints. 25-design variables problem.

Number	Description
1	Range $\geq 5,500$
2	Landing angle of attack $\leq 12^\circ$
3	Landing CL ≤ 1.0
4-21	Landing section Cl ≤ 2.0
22	Fuel volume $\leq$ half of wing volume
23-40	Wing chord $\geq$ 7.0ft
41	LE break, $y \leq$ wing semi-span
42	TE break, $y \leq$ wing semi-span
43	Root $t/c \geq 1.5\%$
44	LE break $t/c \geq 1.5\%$
45	TE break $t/c \geq 1.5\%$
46	Fuselage: $x_{rest_1} \geq 5ft$
47	Fuselage: $x_{rest_1} + 10\text{ft} \leq x_{rest_2}$
48	Fuselage: $x_{rest_2} + 10\text{ft} \leq x_{rest_3}$
49	Fuselage: $x_{rest_3} + 10\text{ft} \leq x_{rest_4}$
50	Fuselage: $x_{rest_4} + 10\text{ft} \leq 300\text{ft}$
51	Nacelle 1, $y \geq$ side-of-body
52	Nacelle 1, $y \leq$ nacelle 2, y
53	Engine out stability criterion
54	Minimum airfoil section spacing at wing tip
55-56	No engine scrape at landing angle-of-attack
57-58	No engine scrape at landing angle-of-attack, with 5° roll
59	No wing tip scrape at landing angle-of-attack, with 5° roll
60	No wing trailing-edge break point scrape at landing, with 5° roll
61	Crosswind landing capability with aileron deflection only
62	Crosswind landing capability with aileron and rudder deflection
63	Tail deflection $\leq 22.5^\circ$ for landing
64	Takeoff rotation must occur prior to reaching 90% of takeoff velocity
65	No negative sweep of wing inboard trailing-edge
66	Root trailing-edge must not overlap root leading-edge of horizontal tail
67-68	Required engine thrust $\leq$ available thrust

8.1 Identifying The Reasonable Design Space

The first step in identifying the reasonable design space was to construct a suitably large hypercube, defined by the twenty-five design variables (Table 8.1), that encompasses this entire region of space. Each of the variables, except the fuel weight, was allowed to assume values between 20% and 180% of its baseline value, given in Table 8.1. The fuel weight was only allowed to vary between 75% and 125% of its baseline value because of its strong influence on the range of the HSCT and therefore feasibility. 19,651 configurations were obtained by perturbing one, two, and three variables at a time in such a way that perturbed variables reach their extreme allowable values (see Appendix D). Note, that a full quadratic RS model in 25 variables has 351 terms in it. Of the initial HSCT configurations, 83% violated one or more of the HSCT's constraints that define the reasonable design space (Table 7.1). These constraints are the same for our general case of 29 HSCT configuration variables (Table 2.1) and for the case of 25 HSCT configuration variables, which are a subset of the HSCT configuration variables given in Table 8.1. The unreasonable HSCT configurations were moved towards the baseline design for the 25-variable problem according to Equation (7.11).

8.2 RS Models Based on Minimum Bias and Minimum Variance Experimental Designs

Due to the computational expense of the structural optimization, it was not possible to estimate wing bending material weight for all 19,651 points using structural optimization. It was necessary to choose points in the reasonable design space for creating the wing bending material weight response surface.

To create a response surface model that minimizes modeling error, we had to satisfy the condition from equation (7.4). This condition is difficult to satisfy for an irregular domain, and therefore we first transformed the domain to a 25-dimensional sphere. We scaled the design domain so that minimum and maximum values of each coordinate of all 19,651 points we had in the reasonable design space were assigned

values -1 and 1, respectively. We also adjusted our domain to assure that points with only one coordinate equal -1 or 1 with the rest of the coordinates being zero had to correspond to reasonable aircraft configurations. With this criterion satisfied for extreme points, we ensured that our reasonable design space is close to a sphere.

After we obtained the spherical domain, we selected the points for the experimental design in such a way that coordinates of the points satisfied Equation (7.4). In a sphere, integrals of all monomials with any odd power are zero (Equation (7.7)). One possible way to satisfy Equation (7.4) is to construct a symmetric experimental design, so that all odd order monomial sums in Equation (7.4) are zero. Substituting the expressions for the volume of a p-dimensional sphere (Equation (7.5)), second and fourth order monomials (Equations (7.8)–(7.10)) into Equation (7.4) we get the conditions for the second and fourth order monomials that should be satisfied in the minimum bias design:

$$[ii] = \frac{1}{N}\sum_{j=1}^{N} {x_{i,j}}^2 = \frac{1}{p+2} \ , \ i = 1, \ldots, p \, , \tag{8.1}$$

$$[iiii] = \frac{1}{N}\sum_{j=1}^{N} {x_{i,j}}^4 = \frac{3}{(p+2)(p+4)} \ , \ i = 1, \ldots, p \, , \tag{8.2}$$

$$[iijj] = \frac{1}{N}\sum_{j=1}^{N} {x_{i,j}}^2 {x_{r,j}}^2 = \frac{1}{(p+2)(p+4)} \ , \ i \neq r \ , \ i, r = 1, \ldots, p \ , \tag{8.3}$$

where p is the dimension of the problem (i.e., number of coordinates used), i, r are indices of particular coordinates, $x_{i,j}$ is the i coordinate of the j point in the design space. These conditions are described in detail in Ref. [57], pp. 205–214.

In our case of 25 variables, we selected a modified small composite experimental design that satisfied all the necessary requirements. While a central composite design includes a full factorial design (all the vertices of the p-dimensional box), in a small composite design the full factorial portion is replaced by a fractional factorial portion. We employed a $2^{(25-15)}$ fractional factorial portion accounting for 1024 points. These 1024 points constitute a *resolution V* fractional factorial experimental design ([20], pp. 138–139, and Appendix C). They were generated using procedure

$FACTEX$ in the program SAS [58]. SAS selects the points in such a way that the location of the points allows estimation of all the cross-product terms of the type $x_i * x_j$ in the RS model function. Appendix C describes the idea behind this point selection technique. We also augmented our small composite design with additional 50 axial points for a total of 100 axial points. Including the central point, this experimental design consisted of 1125 points. The coordinates of the points in this experimental design were selected by solving the system of Equations (8.1)–(8.3). In our particular case the value of p is equal to 25 and the values of the coordinates $(x_{i,j})$ were set to the following values.

(i) If the point is one of the 1024 factorial points, then all the coordinates of each point were assigned to have the values of $+g$ or $-g$ correspondingly.

(ii) If the point is one of the axial points (recall, that we have 4 axial points on each axis), then one of the coordinates of the point was set to either $+a$, or $+b$, or $-a$, or $-b$, while all the other coordinates of that point were set to be zero.

The assigned values of the coordinates were substituted into the system of equations (8.1)–(8.3), yielding

$$[ii] = \frac{2a^2 + 2b^2 + 1024g^2}{1125} = \frac{1}{27}\,, \tag{8.4}$$

$$[iiii] = \frac{2a^4 + 2b^4 + 1024g^4}{1125} = \frac{3}{783}\,, \tag{8.5}$$

$$[iijj] = \frac{1024g^4}{1125} = \frac{1}{783}\,. \tag{8.6}$$

This new system of equations (8.4)–(8.6) was solved for the values of a, b, and g: $a = 0.8022$, $b = 1.006$, $g = 0.1935$.

In low dimensions the minimum bias requirement causes the points to be located close to the center of the design space. However, in high dimensional spheres most of the volume is near the surface, and so we obtained a design where all but 50 axial points were located very close to the surface of the sphere that bounded our design domain. (Note, that the distance of the factorial points from the origin is $\sqrt{25}g = 0.9675$.) This fact led us to hope that in addition to good bias properties

our design would possess good variance properties also (experimental designs which minimize variance consist of points that are usually located at the perimeter of the design space). A response surface model in 25 design variables was constructed based on this minimum bias experimental design.

We also considered a minimum variance response surface model which was based on the *D*-optimal experimental design. The *D*-optimal set of 1,125 points for the minimum variance design was found by the "k-exchange" method of Mitchell [59] as a subset of the 19,651 points residing on the boundary of the reasonable design space (the procedure for identifying 19,651 points is described in Section 8.1).

The minimum variance response surface model is denoted $RS1_{25}$. The minimum bias response surface model is denoted $RS3_{25}$. Each RS model is constructed based on results of structural optimizations at 1125 points and checked based on additional results of structural optimizations at 1,000 points selected based on the *D*-optimality criterion. The structural optimization was performed using the coarse FE model. The terms in the RS models were selected using the program JMP [60]. The backward elimination procedure describe in Appendix C was employed with the threshold *p*-value of 0.05 (Appendix B).

The approach used here to construct the minimum variance RS model is the same as the approach used by Kaufman *et al.* [25]. However the structural optimization data used by Kaufman *et al.* was noisy. In our case we reduced the amount of noise considerably (see Figure 5.6). The accuracy of the response surfaces in the current work is compared with a similar model from Ref. [25] and the FLOPS weight function (Table 8.3). In Table 8.3 the error percentage is calculated with respect to the average value of the wing bending material weight at 1,000 points that are used for checking the RS model. In this table $RS2_{25}$ refers to the response surface constructed by Kaufman *et al.* for 25 variables based on *D*-optimal point selection and FLOPS refers to the FLOPS weight function.

From Table 8.3 it is seen that all RS models have lower errors than the FLOPS weight function. This reduced error is the consequence of customizing the response surfaces to the particular design conditions of the HSCT problem.

Comparing $RS1_{25}$ and $RS3_{25}$ to the more noisy results obtained with $RS2_{25}$, we

Table 8.3: Comparison of the absolute errors for the RS models as percentage of the average bending material weight. 25 variables.

Model	Average Error	RMSE	Maximum Error
$RS1_{25}$ (D-opt.)	4.29 %	6.61 %	71.08 %
$RS2_{25}$ (D-opt, prev.)	7.72 %	12.78 %	114.58 %
$RS3_{25}$ (min. bias)	4.43 %	6.45 %	52.77 %
FLOPS	49.07 %	297.29 %	297.29 %

see the improvement for the 25-variable RS1. That reflects the reduced effect of the noise. Comparing the RS model for the minimum bias design ($RS3_{25}$) to the RS model for the minimum variance design ($RS1_{25}$), we observe similar performance, indicating no substantial advantage of one over the other.

Another effect of the reduced noise levels is in the number of polynomial coefficients that are characterized well by the data. Kaufman *et al.* found that only 61 coefficients out of 351 were retained for $RS2_{25}$ when ANOVA techniques were employed to eliminate poorly characterized coefficients. In contrast, 163 coefficients were retained for $RS1_{25}$ and 81 coefficients for $RS3_{25}$.

8.3 HSCT Configuration Optimization

Complete HSCT configuration optimizations were performed to evaluate the effects of using the response surface models for the wing bending material weight, $RS1_{25}$, and $RS3_{25}$. At the completion of the optimizations, RS model results were compared with structural optimization results. Implementation of each response surface was accomplished by modifying the gross takeoff weight calculations within the weight module of FLOPS. In place of FLOPS estimates for wing bending material weight, response surface predictions were used. (See Appendix A for a more detailed description of how wing bending material weight was calculated in FLOPS). $RS1_{25}$ and $RS3_{25}$ were intended for use in the reasonable design space and their predictions could not be relied upon outside this region. Therefore, all calculations outside the reasonable design space were done with FLOPS. With two exceptions, the criteria listed in

Table 7.1 were used to identify the reasonable design space in the process of HSCT configuration optimization. First, the range criterion was not evaluated because of its relatively high computational expense. Second, an additional criterion was added to exclude unreasonable predictions by the response surface models. Similar to the criterion on the wing bending material weight calculated by FLOPS (W_{b_F} in Table 7.1), if the RS model value for the wing bending material weight ($W_{b_{RS}}$) falls outside the range 20,000 lbs $< W_{b_{RS}} <$ 120,000 lbs, the design is considered unreasonable.

At the edge of the reasonable design space, a transition function was implemented into the HSCT configuration optimization code by Kaufman [25] to prevent discontinuity between wing bending material weight calculated by FLOPS and the response surface prediction. The transition function for the wing bending material weight is

$$W_b = \begin{cases} W_{b_{RS}}, & r_{max} \leq 0, \\ f(W_{b_{RS}}, W_{b_F}), & 0.10 > r_{max} > 0, \\ W_{b_F}, & r_{max} \geq 0.10, \end{cases}$$

where

$$f(a,b) = a\left[1 - \sin^2(5r_{max}\pi)\right] + b\sin^2(5r_{max}\pi) \tag{8.7}$$

is based on the maximum violation r_{max} among the aforementioned criteria.

Three HSCT configuration optimizations were performed, each starting from the baseline design detailed in Table 8.1. During the first optimization, the FLOPS wing bending material weight was used to find the takeoff gross weight. The next two optimizations were performed using $RS1_{25}$ and $RS3_{25}$ respectively. Results from these optimizations are given in Table 8.4 and the planforms are plotted in Figures 8.1, 8.2, and 8.3.

Comparing the results in Table 8.4 and Figures 8.1 – 8.3, we see that the optimizations using FLOPS and $RS3_{25}$ obtained HSCT configurations that could be more structurally efficient (low W_b), but less efficient aerodynamically (low L/D). The optimization using $RS1_{25}$ found the HSCT configuration which is more aerodynamically efficient with higher structural weight. The response surface errors in W_b at the optima are of similar relative magnitude, but because $RS1_{25}$ has a conservative error (it overestimates the weight) it probably corresponds to a slightly superior design. It should be noted that restricting RS models to the reasonable design space

Table 8.4: Parameters for the optimal HSCT configurations. 25 variables. Here "*Bend. Mat. Weight by Model*" designates wing bending material weight calculated either by the corresponding RS model or by FLOPS.

FLOPS	$RS1_{25}$	$RS3_{25}$	Parameter
Planform Geometry			
161.5	141.0	158.2	Wing root chord (ft)
7.44	7.51	7.66	Wing tip chord (ft)
60.9	62.4	60.4	Wing semi-span (ft)
1.74	1.84	1.76	Aspect Ratio
10,263	10,160	10,049	Wing Area (ft^2)
Performance Data			
5,510	5,516	5,498	Range ($n.\ mi.$)
11,87	11.84	11.99	Landing AOA ($^\circ$)
8.98	9.16	8.92	L/D_{max} (M=2.4)
Range and Weight Data			
331,821	328,709	331,618	Required Fuel Weight (lb)
18,755	41,221	17,674	Bend. Mat. Weight by Model (lb)
22,848	36,767	20,244	Bend. Mat. Weight by Str. Opt. (lb)
622,551	622,439	620,488	Gross Take Off Weight (lb)

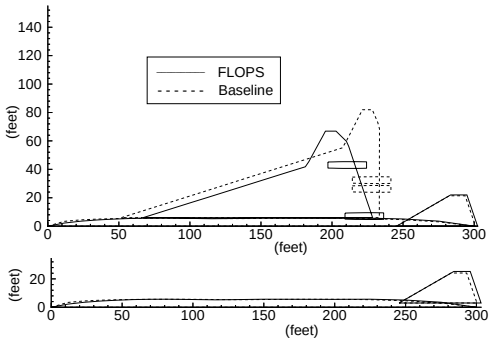

Figure 8.1: Optimal HSCT planform using FLOPS. 25 variables.

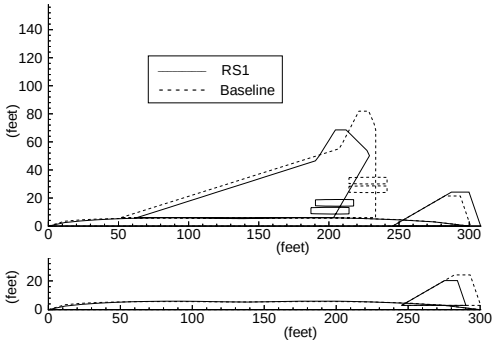

Figure 8.2: Optimal HSCT planform using RS model from D-optimal design. 25 variables.

was essential to achieve good accuracy of the RS models. The error in the FLOPS estimate of W_b at the optimum is highest, but the difference is smaller than may be expected from Table 8.3. This indicates that FLOPS works well for optimal designs since this weight equation was created based on actual aircraft data. Overall, the use of the response surface led to a small improvement in performance compared to the use of the FLOPS weight equation.

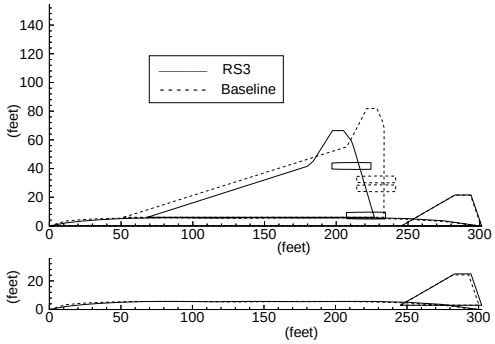

Figure 8.3: Optimal HSCT planform using RS model from minimum bias design. 25 variables.

Chapter 9

29-Design Variable Problem

In this chapter we describe the HSCT configuration optimization for the standard set of 29 variables (Table 2.1) and 68 constraints (Table 2.2). We constructed RS models for the wing bending material weight based on all 29 variables. There are 465 coefficients in the full-quadratic RS model for the 29 variables.

9.1 Two Approaches for Constructing RS Models

Following the procedure described in Chapter 7 we constructed a suitably large hypercube that encompasses the large portion of the design space in 29 variables. This time we compared the RS models obtained using two completely different approaches. The first approach is identical to the one used for the 25-variable problem: at first we construct a PBIB experimental design, then move the points corresponding to unreasonable HSCT configurations towards the baseline point. Next we select the subset of D-optimal points from the points residing on the boundary of the reasonable design space, perform structural optimization for HSCT configurations corresponding to these points, and create a RS model from the obtained results.

The second approach is a two-stage approach involving SCD experimental design, described in Chapter 7. In this approach we first construct a SCD rather than a PBIB design and move the points corresponding to unreasonable HSCT configurations towards the baseline point. One reason for this is that selecting D-optimal points

becomes computationally expensive as the dimension of the problem grows. Then, we employ results from the FLOPS weight equation to identify the important terms in the RS model. We construct a RS model based on FLOPS results at the SCD points and another RS model based on results of structural optimization for a subset of SCD points. Comparing the terms in both RS models, we determine what terms could be important in the final RS model. The second stage of the process is selecting points for additional structural optimizations and creating a RS model from all the structural optimizations results. By identifying the important terms in the RS model we try to more efficiently select HSCT configurations for structural optimization to improve the accuracy of the RS model. After we complete all the structural optimization runs we check if the terms that were eliminated after the first stage of constructing the RS model become important after adding additional structural optimization results during the second stage of the process.

9.2 Identifying Reasonable Design Space. RS Model for D-optimal Points

To identify the reasonable design space we used the same move limits in 29 design variables both for PBIB and for SCD. The design variables vary between 60% and 140% of their baseline values (Table 2.1). The criteria used to identify the reasonable design space are the same as in the 25-variable problem (Table 7.1). If a point does not satisfy these constraints it is moved towards the baseline point according to Equation (7.11).

For the RS model based on the D-optimal points, at first a PBIB design was constructed in 29 variables which included 30,915 points. About 90% of the points did not satisfy the criteria for a reasonable design. After the unreasonable points were moved toward the baseline point, a subset of 1,500 points (about three times the number of polynomial coefficients) was chosen from 30,915 points using the D-optimality criterion.

Approximate aerodynamic analysis was used when the points were moved towards

the baseline point due to the computational expense of moving 30,915 points. For 1,500 D-optimal points the range was checked using more accurate aerodynamic analysis. The HSCT configurations with the range less than 4,900 nautical miles were disregarded. 1,466 points were left in the final set.

For this set of points we performed structural optimization to get wing bending material weight. After that, regression analysis was performed with SAS [58] using the backward elimination procedure and the stepwise regression procedure followed by backward elimination. The unbiased root mean square error estimate obtained during the regression procedures is shown in Figure 9.1. The number of terms in the full-quadratic RS model in 29 variables is 465. The model with the minimum value of $RMSE_{ub}$ had 136 terms in it. As the average value of the wing bending material weight for this set of 1466 points was about 65,000 lb, the minimum $RMSE_{ub}$ corresponds to about 4.2% of error. However, some of the terms in the model function with 136 terms were poorly defined: their p-values were about 0.8. (See Appendix B for a definition of p-value). Consequently we chose a model with 73 terms for the HSCT configuration optimization. The p-values for this model were much better: all the coefficients had p-values less than 0.05. Also, exactly the same model with 73 terms was obtained using both the backward elimination procedure and the stepwise regression procedure followed by backward elimination.

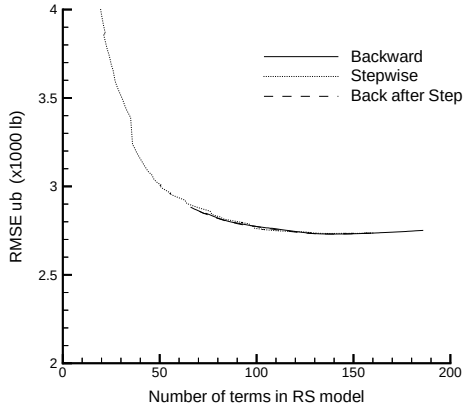

Figure 9.1: $RMSE_{ub}$ for 1466 D-optimal points. 29-variable problem.

9.3 Preliminary RS Models Based on FLOPS Results

Though FLOPS estimation of the wing bending material weight is not as accurate as the one from the structural optimization, it still provides reasonable estimates of the wing bending material weight. Estimation of wing bending material weight using FLOPS is also very computationally inexpensive. Because of that we made use of the FLOPS estimates of the wing bending material weight at the first stage of the process of creating the response surface model.

At the first stage of our process we constructed a SCD consisting of 1083 points and estimated the wing bending material weight in these points using the FLOPS weight equation. The SCD was constructed assuming that the design space is a box centered at the baseline HSCT configuration with each of the 29 configuration design variables varying from 60% to 140% of their baseline (central) values. We included in the SCD one central point, 58 axial points (two points on each of the 29 axis), and 1024 vertices of a 29-dimensional cube. As in the case of the 25-dimensional problem, the 1024 points, representing a subset of all the vertices of the 29-dimensional cube, constitute a *resolution V* fractional factorial experimental design ([20], pp. 138–139, and Appendix C). They were chosen using the procedure $FACTEX$ in SAS. The idea used in SAS for selecting particular vertices and ignoring others is described in Appendix C. Axial points were originally located at the centers of the faces of the cube. After the SCD was constructed, all the points were pulled towards the central point until they resided on the boundary of the reasonable design space. The FLOPS weight equation was used to estimate the wing bending material weight at the final locations of the 1083 points. Then a response surface model was constructed based on these results.

The stepwise regression procedure followed by backward elimination was applied to remove poorly defined terms in the response surface model using SAS. The threshold p-value was set to 0.1, which is higher than the one used for the D-optimal model. The reason for choosing a higher p-value is that the model we get using FLOPS serves only for eliminating unimportant terms in the RS model from structural optimization.

Thus more care should be taken when terms are eliminated from the model. There were 161 terms left in the model function after all the terms with p-values higher than 0.1 were eliminated.

To check if a smaller number of points can adequately represent the design space, we decided to employ a smaller SCD with 571 points to construct a reduced RS model from FLOPS results. This number of points allowed us to estimate only 203 out of 465 terms in the full quadratic polynomial in 29 variables. This 571 point design included: one central point (considered to be in the center of coordinates), 58 axial points (two points on each of 29 axes), and 512 vertices of a 29-dimensional cube. This time the vertices of the 29-dimensional cube constitute only a *resolution IV* fractional factorial experimental design. The points were chosen using the procedure $FACTEX$ in the program SAS. It was not possible to find a fractional factorial design that allows estimating all 465 terms in the model function using only 512 points. Only 203 out of 465 terms could be estimated using this design. The limits for the 29 variables were the same as the ones used in creating the 1083 point SCD. All 571 points were pulled towards the baseline design.

The stepwise regression procedure followed by backward elimination was applied to remove poorly defined terms in the response surface model using SAS. The threshold p-value was set to 0.1 as it was in the previous case. Only 79 terms out of the original 203 had a p-value less than or equal to 0.1.

As a second check, a third response surface was created using FLOPS results. This time the superset of the previous two sets of points (1594 points) was used to construct the response surface. The same method, software, and threshold value were used to determine the well-defined terms in this model function. This time 152 terms had acceptable p-values.

Figure 9.2 shows the unbiased root mean square error estimate in the three RS models constructed using FLOPS results versus the number of terms in the model function. $RMSE_{ub}$ in Figure 9.2 levels out approximately after 80 terms are present in the RS model. These results indicate that the RS model function with approximately 80 terms could be used instead of the full quadratic model function with 465 without significantly affecting the accuracy of the response surface model. The average value

of the wing bending material weight calculated by FLOPS is about 45,000 lb. Thus the "flat" portion of the $RMSE_{ub}$ in the plot is about a 0.5% error.

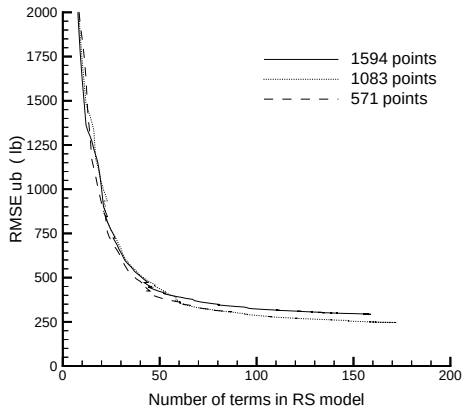

Figure 9.2: $RMSE_{ub}$ in the wing bending material weight RS models from FLOPS results.

9.4 Preliminary RS Model Based on Structural Optimization Results

From past experience ([25]), however, we know that estimates of the wing bending material weight from structural optimizations are sometimes significantly different from the ones obtained using FLOPS. Thus, it is dangerous to assume that the same terms model well results from FLOPS and results from the structural optimization. Taking into account computational expense, we constructed a reduced RS model from the results of the structural optimization for the same set of 571 points that were used to construct a reduced response surface model from FLOPS results.

To better understand the RS model from structural optimization results we used two different approaches to eliminate poorly defined terms in the RS model: the backward elimination procedure, and the stepwise regression procedure followed by backward elimination (Appendix B, [20], pp. 640–655). The threshold p-value was again set to be 0.1, because this model is used only for screening important terms.

There were 73 terms in this RS model.

Figure 9.3 shows the the unbiased root mean square error estimate for the RS models obtained from the results of the structural optimization. The average value of the wing bending material weight from the structural optimization is about 59,000 *lb*. So the minimum error corresponds to about 3.9%.

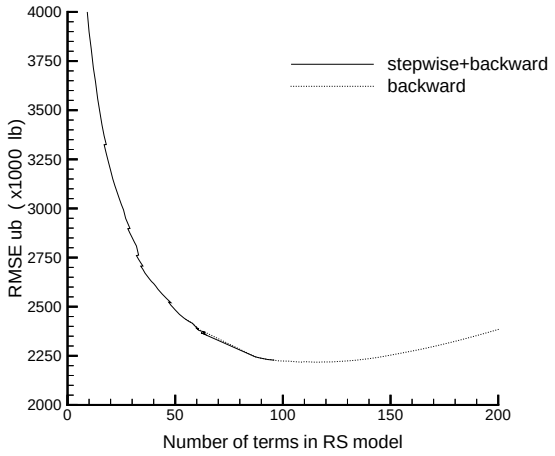

Figure 9.3: $RMSE_{ub}$ in the wing bending material weight RS models from 571 structural optimizations.

Though the RS models created from FLOPS results were not exactly the same as the RS models created from structural optimization results, these RS models shared many common terms. It should be noted that the error in the RS model based on results of the structural optimization is on average about 8 times higher than the error in the RS model based on FLOPS results. These numbers are somewhat misleading, because of the numerical noise in the results of the structural optimization. There is no such noise in the algebraic expressions used to evaluate bending material weight in FLOPS. A large portion of the difference in the measures of accuracy of the RS models could be caused by this factor.

9.5 Second-Stage RS Model based on structural optimization results

The first stage of the process was intended to help us select important terms in the RS model describing wing bending material weight. Table 9.1 shows the linear terms that were left in different RS models after the insignificant terms were eliminated. The linear terms in the RS models correspond to 29 configuration design variables (Table 2.1).

We decided to include in the second stage of constructing the RS model the following linear terms: terms picked up by any of the RS models from the results of the structural optimization and terms picked up at least by two RS models from FLOPS results. The last column in Table 9.1 represents these linear terms selected for further use in the final RS model. However, it should be recalled that all the terms that are eliminated at this stage will be reevaluated later to check if they become significant.

In all the RS models there were important *interaction* terms (terms that represent the product of two variables, say $x1 * x2$, for example). We included in the second stage all interaction terms picked up by any of the RS models from results of the structural optimization. In addition we included all the interactions that we could not estimate in the first-stage RS model from the results of the structural optimization due to the small number of points used to construct this model. The total number of terms kept for the second stage was 235. Thus, at the first screening stage, we were able to reduce the number of terms in the RS model for 29 design variables from 465 (full quadratic polynomial) to 235.

The number and the location of the points in the design space for which we already had results of the structural optimization did not allow us to estimate the terms that we needed. To evaluate all the necessary terms in the final RS model with acceptable accuracy, we constructed a new small composite experimental design augmented with Box-Behnken experimental design [61]. The Box-Behnken experimental design for p variables consists of all combinations with two variables at their limits while the other $(p-2)$ variables are held at their nominal values.

Table 9.1: Linear terms in different RS models.

N	Description	Str.opt. Step+Back 571 pnt	Str.opt. Back 571 pnt	FLOPS 571 pnt	FLOPS 1083 pnt	FLOPS 1594 pnt	selected
1	Wing root chord		x	x	x	x	x
2	LE break point, x	x	x				x
3	LE break point, y	x	x	x	x	x	x
4	TE break point, x	x	x	x	x	x	x
5	TE break point, y				x	x	x
6	LE wing tip, x	x	x	x	x	x	x
7	Wing tip chord			x	x	x	x
8	Wing semi-span	x		x	x	x	x
9	Chordwise location of max. t/c	x	x				x
10	LE radius parameter		x				x
11	Airfoil t/c at root	x	x	x	x	x	x
12	Airfoil t/c at LE break	x			x		x
13	Airfoil t/c at tip		x		x		x
14	Fuselage restraint 1, x		x				
15	Fuselage restraint 1, r						
16	Fuselage restraint 2, x		x	x	x	x	x
17	Fuselage restraint 2, r						
18	Fuselage restraint 3, x						
19	Fuselage restraint 3, r	x	x				x
20	Fuselage restraint 4, x						
21	Fuselage restraint 4, r						
22	Nacelle 1, y						
23	Nacelle 2, y			x	x	x	x
24	Mission fuel			x	x	x	x
25	Starting cruise altitude						
26	Cruise climb rate						
27	Vertical tail area						
28	Horizontal tail area						
29	Max. sea level thrust/engine				x		

In particular, we used a SCD to estimate the 17 linear terms (shown in the last column of Table 9.1) and all mutual interactions of these linear terms. The design consists of 291 points: one central point, 34 axial points, and 256 factorial points. The 256 factorial points constitute a *resolution V* fractional factorial experimental design ([20], pp. 138–139, and Appendix C), chosen using procedure $FACTEX$ in SAS. As we already had the results of the structural optimization for the central and the axial points, we only needed to perform structural optimization for 256 points in this experimental design. We used Box-Behnken experimental designs to estimate 80 interaction terms that contained design variables not included in the main 17 linear terms, which led to another 320 points for structural optimizations (four points for each interaction term). All in all it was necessary to perform structural optimization for 576 new HSCT configurations corresponding to the new points in the design space.

To get better estimates of all the terms in our RS model, we combined the new set of 576 points with 571 points used for the first stage of the process. As in the first stage, we used two different approaches to eliminate poorly defined terms in the RS model: the pure backward elimination procedure and the stepwise regression procedure followed by backward elimination. This time we set the threshold p-value to be 0.05. It was possible to estimate 87 terms in the RS model function for which the p-values of the coefficients were less than or equal to 0.05. The same model was obtained using both the backward elimination procedure and the stepwise regression procedure followed by backward elimination.

Figure 9.4 shows the unbiased root mean square error estimate for the second-stage RS models obtained from the results of the structural optimization. The RMS_{ub} for the second-stage RS model increased by about 400 *lb* with respect to the RMS_{ub} for the preliminary-stage RS model from structural optimization results (Figure 9.3). The increase in the RMS_{ub} error for the new RS models could be attributed to the fact that now the model has to fit the results at a larger number of points than at the preliminary stage. Also because the overall number of points used to determine the coefficients of the RS models is not large enough, it is harder to fit a quadratic polynomial to 1147 points than to 571 points. It should be noted, however, that if we had enough points to estimate most of the coefficients in a full-quadratic polynomial

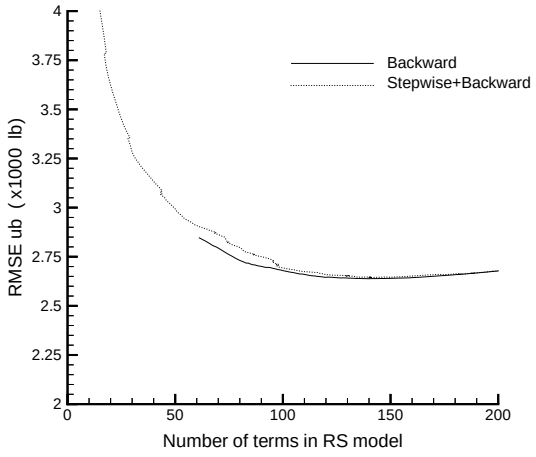

Figure 9.4: RMS_{ub} in the second-stage wing bending material weight RS models from structural optimizations.

with acceptable accuracy, the value of RMS_{ub} should go down for this large number of points with respect to the value of RMS_{ub} that we have now.

In order to check if we have eliminated some important terms after the preliminary stage, all the terms that were eliminated were reinstalled into the model function and we performed the backward elimination procedure and the stepwise regression procedure followed by backward elimination starting from the full-quadratic model. With the specified p-value of 0.05 we ended up with the same model as we had at the end of the second stage. That is, the eliminated terms could not be estimated with an acceptable level of accuracy using the set of points that we have.

9.6 Cross-Validation of the Second-Stage Response Surface Models

We performed one more check of the accuracy of the RS models intended for use in HSCT configuration optimization. We checked the accuracy of the final RS models at the points that were not used for creation of the RS models. Particularly, the accuracy of the RS model from D-optimal points (RS1) was calculated at 1147 SCD

points and compared with that at 1466 D-optimal points, and the accuracy of the RS model from the SCD points (RS2) was calculated at 1466 D-optimal points and compared with that at 1147 SCD points. The results for calculated absolute errors are presented in Table 9.2. In Table 9.2 $RMSE$ and $RMSE_{ub}$ were calculated according to formulas 7.2 and 7.3. The performance of both RS models at the set of points that were not used in the creation of the RS models is rather poor, and the large standard deviation relative to the median for RS1 suggests faulty data.

Table 9.2: Absolute errors of RS models at two sets of points.

Method	RMSE	$RMSE_{ub}$	Average	Median	Maximum	Std. Dev.
RS1 at 1466 points	2,775 lb	2,847 lb	1,557 lb	842 lb	23,378 lb	2,298 lb
RS1 at 1147 points	6,873 lb	—	4,144 lb	2,349 lb	46,282 lb	5,486 lb
RS2 at 1147 points	2,534 lb	2,656 lb	1,814 lb	1,305 lb	18,674 lb	1,769 lb
RS2 at 1466 points	5,866 lb	—	3,976 lb	2,705 lb	45,300 lb	4,314 lb

9.7 HSCT Configuration Optimization at the Second Stage

Complete HSCT configuration optimizations were performed to evaluate the effects of using the response surface models for the wing bending material weight. The procedure was almost exactly the same as the one used for the 25-variable problem described in the previous chapter. The only difference was in the number of variables used in the problem and in the baseline HCST configuration from which we start our configuration optimization. Implementation of the response surface model was accomplished by modifying the gross take off weight calculations within the weight module of FLOPS as was done for the 25-variable problem. At the completion of the configuration optimizations, results were compared with structural optimization results.

Three HSCT configuration optimizations were performed, each starting from the baseline design detailed in Table 2.1. During the first optimization, the FLOPS weight equation was used to calculate wing bending material weight. The next optimization

was performed using the RS model from D-optimal points (RS1) for the same purpose. The third optimization was conducted employing the RS model from the SCD points (RS2). Parameters for the optimal HSCT configurations are given in Table 9.3 along with the corresponding baseline configuration parameters. In Table 9.3 the gross take off weight is given as calculated by the corresponding optimization. The planforms for the aircraft are plotted in Figures 9.5 – 9.7. The 29 configuration design variables for the three optimal HSCT configurations are detailed in Table 9.4. For the baseline design the gross take off weight is calculated using FLOPS estimates for the wing bending material part.

Table 9.3: Parameters for the baseline and optimal HSCT configurations.

Baseline	FLOPS	RS1	RS2	Parameter
Planform Geometry				
178.2	178.1	179.5	171.5	Wing root chord (ft)
9.2	9.7	9.9	9.9	Wing tip chord (ft)
82.6	72.5	77.3	73.5	Wing semi-span (ft)
2.22	1.84	1.98	1.97	Aspect Ratio
14,157	13,356	13,987	12,810	Wing Area (ft^2)
2.82	2.82	2.96	3.03	Root t/c (%)
Performance Data				
5.534	5,502	5,499	5,498	Range ($n.\ mi.$)
8.98	9.02	8.98	8.79	L/D_{max} at $M = 2.4$
Weight Data				
464,743	421,212	431,506	424,066	Required Fuel Weight (lb)
41,267	28,133	35,109	33,924	Bend. Mat. Weight by FLOPS (lb)
58,281	33,889	20,049	24,280	Bend. Mat. Weight by RS1 (lb)
56,520	48,355	35,298	20,020	Bend. Mat. Weight by RS2 (lb)
56,779	33,713	34,575	34,808	Bend. Mat. Weight by Str Opt (lb)
876,488	801,287	808,735	788,341	Gross Take Off Weight (lb)

Comparing the results in Table 9.3 and Figures 9.5 – 9.7 we see that configuration optimization exploits weaknesses in both the FLOPS and the RS models: for all optimal HSCT configurations the wing bending material weight obtained by the particular method used is much lower than the weight from the other methods. It is also obvious that accuracy of the RS models in some regions of the design space

Table 9.4: HSCT configuration variables for the optimal configurations from the second stage.

Num.	FLOPS	RS1	RS2	Description
1	178.0	179.5	171.5	Wing root chord (ft)
2	110.1	121.7	117.3	LE break point, x (ft)
3	40.2	41.0	37.0	LE break point, y (ft)
4	174.0	186.4	179.5	TE break point, x (ft)
5	12.3	11.3	10.5	TE break point, y (ft)
6	134.0	137.0	139.0	LE wing tip, x (ft)
7	9.7	9.9	9.9	Wing tip chord (ft)
8	72.5	77.3	73.5	Wing semi-span (ft)
9	0.49	0.47	0.47	Chordwise max. t/c location
10	2.85	2.32	2.09	LE radius parameter
11	2.55	2.96	3.03	Airfoil t/c at root (%)
12	1.82	2.04	2.15	Airfoil t/c at LE break (%)
13	1.74	1.65	1.54	Airfoil t/c at tip (%)
14	2.59	2.59	2.88	Fuselage restraint 1, x (ft)
15	0.35	0.43	0.54	Fuselage restraint 1, r (ft)
16	14.0	13.7	13.7	Fuselage restraint 2, x (ft)
17	2.44	2.40	2.63	Fuselage restraint 2, r (ft)
18	111.6	114.7	113.6	Fuselage restraint 3, x (ft)
19	5.44	5.37	5.27	Fuselage restraint 3, r (ft)
20	184.0	186.4	188.2	Fuselage restraint 4, x (ft)
21	5.37	5.45	5.44	Fuselage restraint 4, r (ft)
22	9.1	10.7	9.8	Nacelle 1, y (ft)
23	34.0	30.6	31.6	Nacelle 2, y (ft)
24	421,212	431,506	424,066	Mission fuel (lbs)
25	58,831	58,290	58,185	Starting cruise altitude (ft)
26	38.30	38.06	37.78	Cruise climb rate (ft/min)
27	885.2	887.9	831.0	Vertical tail area (ft^2)
28	882.3	1008.6	951.3	Horizontal tail area (ft^2)
29	53,200	52,580	51,487	Max. sea level thrust/engine, (lb)

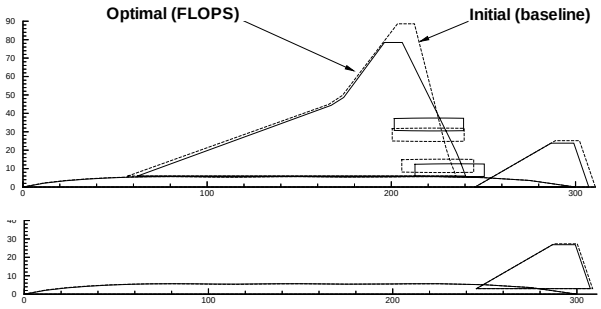

Figure 9.5: Initial and optimal HSCT planforms obtained using FLOPS weight equation.

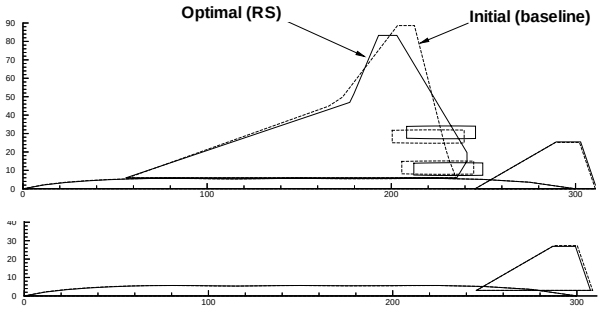

Figure 9.6: Initial and optimal HSCT planforms obtained using RS model from D-optimal design.

is not acceptable and the RS models should be improved. We see that the screening procedure of identifying important terms in the response surface models based on the low fidelity analysis (FLOPS) did not work out. The relatively small errors of FLOPS results with respect to structural optimization results indicate that FLOPS works well for optimal designs since this weight equation was created based on actual aircraft data.

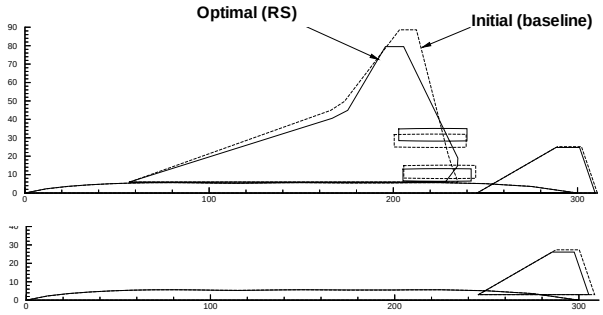

Figure 9.7: Initial and optimal HSCT planforms obtained using RS model from SCD.

9.8 Third Stage of Constructing RS Model

Results from Table 9.3 indicate that both RS1 and RS2 were not accurate enough at their own optima. To improve the accuracy of the RS models we constructed a smaller 29-dimensional box around the optimal HSCT configurations that we obtained and constructed a new RS model for this smaller region. The upper and lower limits for the 29 configuration design variables were defined based on the initial HSCT configuration and optimum HSCT configurations from FLOPS, from RS1, and from RS2. Knowing the values of 29 configuration design variables for all of these designs (Tables 2.1 and 9.4) we defined the upper and lower limits for the new 29-dimensional box given in Table 9.5.

We scaled the values of the configuration variables in such a way that the lower limits for the design variables from Table 9.5 corresponded to -1 and the upper limits from Table 9.5 corresponded to $+1$. After that we constructed the SCD for the new multidimensional box region in the design space. Because we shrunk our operability region, the influence of noise in the results of the structural optimization could be more significant. Therefore we used a SCD with 2048 points in the factorial portion of the SCD instead of 1024 points as in the previous cases. All in all our new SCD included 2107 points (one central point, 58 axial points, and 2048 vertices). Axial points were located at the centers of the faces of the box. Similarly to the previous

Table 9.5: Upper and lower limits for the HSCT configuration design variables at the third stage.

Number	Lower limit	Upper limit	Description
1	163.00	180.50	Wing root chord (ft)
2	109.10	123.00	LE break point, x (ft)
3	36.75	43.90	LE break point, y (ft)
4	172.40	187.40	TE break point, x (ft)
5	10.40	13.65	TE break point, y (ft)
6	133.00	147.40	LE wing tip, x (ft)
7	9.19	10.28	Wing tip chord (ft)
8	72.37	82.71	Wing semi-span (ft)
9	0.4479	0.5384	Chordwise max. t/c location
10	2.080	2.858	LE radius parameter
11	2.544	3.124	Airfoil t/c at root (%)
12	1.807	2.168	Airfoil t/c at LE break (%)
13	1.535	1.753	Airfoil t/c at tip (%)
14	2.59	3.01	Fuselage restraint 1, x (ft)
15	3.49	5.61	Fuselage restraint 1, r (ft)
16	13.10	14.90	Fuselage restraint 2, x (ft)
17	2.32	2.64	Fuselage restraint 2, r (ft)
18	110.60	115.70	Fuselage restraint 3, x (ft)
19	5.26	5.49	Fuselage restraint 3, r (ft)
20	180.50	189.20	Fuselage restraint 4, x (ft)
21	5.33	5.46	Fuselage restraint 4, r (ft)
22	9.11	12.82	Nacelle 1, y (ft)
23	24.51	34.06	Nacelle 2, y (ft)
24	420,200	465,700	Mission fuel (lbs)
25	57,680	58,930	Starting cruise altitude (ft)
26	37.50	38.40	Cruise climb rate (ft/min)
27	788.1	922.2	Vertical tail area (ft^2)
28	950.3	1,018.6	Horizontal tail area (ft^2)
29	50,380	57,370	Max. sea level thrust/engine, (lb)

cases, 2048 vertices of the 29-dimensional cube constitute a *resolution V* fractional factorial experimental design, obtained using procedure $FACTEX$ in SAS. This time we did not move the points at the vertices towards the center of the box, because HSCT configurations corresponding to all 2107 points of the SCD were inside the reasonable design space. Structural optimization was performed for all new 2107 HSCT configurations that corresponded to the points in the SCD. After that the RS model was created based on the results of these new structural optimizations.

We used two different approaches to eliminate poorly defined terms in the RS model: the backward elimination procedure and the stepwise regression procedure followed by backward elimination using SAS. We set the threshold p-value to be 0.05. It was possible to estimate 96 terms in the RS model function for which the p-values of the coefficients were less than or equal to 0.05. The same model was obtained using both the backward elimination procedure and the stepwise regression procedure followed by backward elimination. Figure 9.8 shows the unbiased root mean square error estimate for the third-stage RS models obtained from the results of the structural optimization. The average value of the wing bending material weight for the 2107 points calculated by structural optimization was about 44,000 lb. Taking this into account the minimum value of the RMS_{ub} on the plot in Figure 9.8 corresponds to about 4% error.

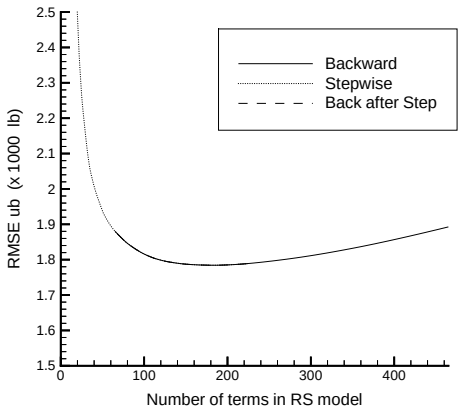

Figure 9.8: RMS_{ub} in the third-stage wing bending material weight RS models from structural optimizations.

9.9 Third-Stage HSCT Configuration Optimization

Complete HSCT configuration optimizations were performed to evaluate the effects of using the response surface model for the wing bending material weight. This was accomplished in a way similar to the second-stage HSCT configuration optimization. The only difference was that now additional side constraints were included in the problem to prevent the optimizer from moving outside the box defined in Table 9.5. This was not necessary in the previous stage, because the optimizer did not go outside the region where RS models were defined.

We performed five HSCT configuration optimizations. At first we repeated HSCT configuration optimization employing the FLOPS weight equation to estimate wing bending material weight, in order to see if the small box limits would influence significantly the FLOPS optimum. We started this configuration optimization from the baseline HSCT configuration (recall that both the baseline configuration and the optimum configuration from previous stage obtained using the FLOPS weight equation are included in our new box). The next four configuration optimizations were performed employing the new RS model to estimate wing bending material weight. Each of these four configuration optimizations was started from a different initial point: (i) the baseline HSCT configuration, (ii) the optimum configuration obtained by FLOPS, (iii) the optimum configuration obtained using RS1, and (iv) the optimum configuration obtained using RS2. Some parameters of the new optimal HSCT configurations are given in Table 9.6. The gross take off weight presented in this table was calculated using the approximate bending material weight employed in the corresponding configuration optimization. The planforms of the aircraft are plotted in Figure 9.9. The 29 configuration design variables for the five optimal HSCT configurations are detailed in Table 9.7.

Comparing the results in Tables 9.6, 9.7, and in Figure 9.9 one can see that though the optimizations were started from different initial HSCT configurations, the optimal HSCT configurations obtained using the RS model are very similar. The HSCT configuration obtained using the FLOPS weight equation is different from the configurations obtained using the RS model. However, their gross take off weights

Table 9.6: Parameters of optimal HSCT configurations from the third stage. $FLOPS$ – using FLOPS weight equation; RS_b – using RS model, starting from the baseline; RS_{FLOPS} – using RS model, starting from the FLOPS optimum; RS_{RS1} – using RS model, starting from optimum of RS1; RS_{RS2} – using RS model, starting from optimum of RS2.

$FLOPS$	RS_b	RS_{FLOPS}	RS_{RS1}	RS_{RS2}	Parameter
Planform Geometry					
180.2	180.4	180.4	180.5	180.5	Wing root chord (ft)
10.3	10.3	10.3	10.3	10.3	Wing tip chord (ft)
72.9	72.4	72.4	72.4	72.4	Wing semi-span (ft)
1.89	1.80	1.81	1.81	1.81	Aspect Ratio
13,214	13,637	13,559	13,551	13,572	Wing Area (ft^2)
2.59	2.74	2.73	2.74	2.73	Root t/c (%)
Performance Data					
5,501	5,500	5,499	5,500	5,500	Range ($n.\ mi.$)
9.01	9.00	8.98	8.99	9.00	L/D_{max} at $M = 2.4$
Weight Data					
420,336	422,480	423,815	422,425	422,067	Required Fuel Weight (lb)
27,491	27,909	26,860	26,837	27,098	Bend. Mat. Weight by FLOPS (lb)
33,359	22,990	23,512	23,073	24,280	Bend. Mat. Weight by RS (lb)
33,823	28,319	28,644	28,511	28,158	Bend. Mat. Weight by Str Opt (lb)
797,529	797,167	798,693	796,556	796,545	Gross Take Off Weight (lb)

Table 9.7: HSCT configuration variables for five optimal configurations from the third stage. Optimizations were started from different initial points. $FLOPS$ – using FLOPS weight equation; RS_b – using RS model, starting from the baseline; RS_{FLOPS} – using RS model, starting from the FLOPS optimum; RS_{RS1} – using RS model, starting from optimum of RS1; RS_{RS2} – using RS model, starting from optimum of RS2.

Num.	$FLOPS$	RS_b	RS_{FLOPS}	RS_{RS1}	RS_{RS2}	Parameter
1	180.2	180.4	180.4	180.4	180.5	Wing root chord (ft)
2	119.3	122.6	120.9	121.5	121.4	LE break point, x (ft)
3	42.3	42.5	42.5	42.5	42.5	LE break point, y (ft)
4	172.7	185.0	182.7	182.9	183.3	TE break point, x (ft)
5	10.7	10.4	10.4	10.4	10.4	TE break point, y (ft)
6	141.1	135.5	134.4	134.9	134.6	LE wing tip, x (ft)
7	10.26	10.27	10.28	10.28	10.27	Wing tip chord (ft)
8	72.9	72.4	72.4	72.4	72.4	Wing semi-span (ft)
9	0.50	0.49	0.50	0.50	0.50	Chordwise max t/c location
10	2.85	2.09	2.09	2.16	2.15	LE radius parameter
11	2.59	2.74	2.73	2.74	2.73	Airfoil t/c at root (%)
12	1.89	2.17	2.17	2.17	2.17	Airfoil t/c at LE break (%)
13	1.54	1.54	1.54	1.54	1.54	Airfoil t/c at tip (%)
14	2.70	2.85	2.76	2.95	2.94	Fuselage restraint 1, x (ft)
15	0.44	0.55	0.38	0.56	0.56	Fuselage restraint 1, r (ft)
16	13.1	13.2	13.1	13.3	13.3	Fuselage restraint 2, x (ft)
17	2.41	2.37	2.32	2.34	2.33	Fuselage restraint 2, r (ft)
18	110.9	110.7	110.8	110.7	111.1	Fuselage restraint 3, x (ft)
19	5.41	5.49	5.49	5.49	5.49	Fuselage restraint 3, r (ft)
20	183.9	180.8	181.1	182.1	181.8	Fuselage restraint 4, x (ft)
21	5.34	5.34	5.34	5.35	5.35	Fuselage restraint 4, r (ft)
22	9.1	9.1	9.1	9.1	9.1	Nacelle 1, y (ft)
23	33.9	30.6	30.5	30.6	30.7	Nacelle 2, y (ft)
24	420,336	422,480	423,386	422,425	422,067	Mission fuel (lbs)
25	58,651	58,440	58,511	58,473	58,474	Starting cruise altitude (ft)
26	38.27	38.00	38.15	38.02	38.03	Cruise climb rate (ft/min)
27	867.1	789.0	788.1	788.3	788.5	Vertical tail area (ft^2)
28	951.8	950.9	950.5	950.4	950.6	Horizontal tail area (ft^2)
29	52,202	51,686	52,033	51,790	51,739	Max. sea level thrust/engine (lb)

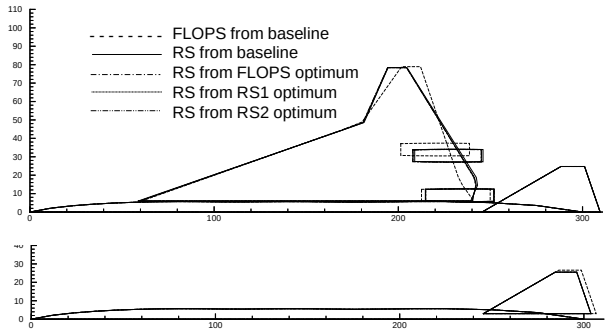

Figure 9.9: Optimal HSCT configurations from the third stage.

are comparable. Again the optimizer exploited weaknesses of both the RS model and the FLOPS weight equation: for all optimal HSCT configurations the wing bending material weight obtained by the approximation method used in the configuration optimization is lower than the weight from the other approximation method. One may notice that the accuracy of the RS model at its own optimum is much better than at the second stage and comparable with the accuracy of the FLOPS weight equation at the FLOPS optimum. Once again, we see that the FLOPS weight equation is a very good approximation for the aircraft weight, and for the wing bending material weight in particular.

It should be noted, however, that for some configuration design variables, the values at the optima are either at their lower or at their upper limits, defined in Table 9.5. Thus to further improve the design it may be necessary to shift the design window.

In general, from our experience with the 29-design variable problem, we may conclude that the reasonable design space approach and other zooming procedures, like shifting and shrinking the box where the response surface model is applicable, were essential to achieve good accuracy of the response surface model. Another important issue is that the number of points required to construct the quadratic response surface model with acceptable accuracy grows faster than the number of design variables squared.

Chapter 10

Correction Response Surface Models

The time required to perform structural optimization for the refined FE model is an order of magnitude larger than the time required to perform structural optimization for the coarse FE model. Therefore it was not feasible to perform the same number of refined structural optimizations as coarse structural optimizations. Consequently, it was not possible for us to create a quadratic RS model using results of refined structural optimizations. Instead, we introduced *linear correction RS models* from the results of structural optimization of the refined FE model. These correction RS models correct the RS model based on the coarse FE models. Correction RS models can be constructed using a relatively small number of refined structural optimizations.

10.1 Data Sets for Correction RS Models

Several approaches could be considered when introducing corrections to the results of the RS model constructed using the coarse FE model. In all of these approaches we assume that the coarse structural optimization is performed at a large set S_c of points and the refined structural optimization at a small subset S_r of these points. In our particular case S_c consists of 2107 points used in the third stage and S_r is represented by 100 D-optimal points selected from 2107 points plus a point in the

center of the box, defined by 2107 points. We added the point in the center of the box to the set of 100 points, because all the selected D-optimal points were located at the vertices of the 29-dimensional box from the third stage. Another set of 100 points S_r^{check} was randomly selected from S_c (2107 points) to check the performance of the *linear correction RS models* at a set of points different from the set of points used to create the correction RS models. This number of points (100) is approximately three times the number of coefficients in the linear correction RS models.

Refined structural optimization was performed for S_r and S_r^{check}. The average value of the wing bending material weight from refined structural optimization was about 55,000 lb both for S_r and for S_r^{check}. From the third stage we already had the results of the coarse structural optimization both for S_r and for S_r^{check}. The differences between the wing bending material weight calculated by the coarse structural optimization and by the refined structural optimization for the two sets of points S_r and S_r^{check} are summarized in Table 10.1. From Table 10.1 we see that on average the refined structural optimization predicts 25% heavier wing bending material weight than the coarse structural optimization.

Table 10.1: Differences in wing bending material weight from coarse and refined. structural optimizations at two sets of points: S_r and S_r^{check}. Here Wb_{crs} is the bending material weight from the coarse structural optimization, Wb_{ref} is the bending material weight from the refined structural optimization. Average value of Wb_{ref} is 55,000 lb for both S_r and S_r^{check}

Parameter	Minimum	Average	Median	Maximum	Std. Dev.
Wb_{ref} - Wb_{crs} at S_r	-5,253 lb	10,813 lb	10,382 lb	29,572 lb	5,285 lb
Wb_{ref} - Wb_{crs} at S_r^{check}	-5,253 lb	11,364 lb	11,867 lb	25,818 lb	4,915 lb
Wb_{crs} / Wb_{ref} at S_r	0.5904	0.8047	0.8073	1.073	0.08833
Wb_{crs} / Wb_{ref} at S_r^{check}	0.6516	0.7944	0.7795	1.073	0.08560

We evaluated the errors of the coarse RS model from stage three with respect to the refined structural optimization results at S_r and S_r^{check} (Table 10.2). The average, median, and maximum values of the error of the RS model from stage three agree well with the differences between the refined and the coarse structural optimization

results from Table 10.1, which indicates that there is not much difference between a comparison of the actual data and the response surface values for this particular case.

Table 10.2: Errors of RS model from the third stage at two sets of points with respect to the results from the refined FE model.

Set of points	RMSE	Average	Median	Maximum	Std. Dev.
S_r	11,880 lb	10,685 lb	10,279 lb	28,463 lb	5,220 lb
S_r^{check}	12,356 lb	11,409 lb	11,252 lb	23,620 lb	4,768 lb

10.2 Construction and Performance Evaluation of Correction RS Models

We tried several approaches for introducing corrections to the results of the RS model constructed using the coarse FE model. To better describe these approaches we introduce the following notations:

d_a — average difference between the results of refined and coarse structural optimizations at S_r (101 points);

r_a — average ratio of the results of coarse structural optimizations to the results of refined structural optimizations at S_r;

Wb_c — bending material weight from coarse structural optimizations at S_c (2107 points);

Wb_c^{corr} — corrected bending material weight at S_c (2107 points);

$RS3$ — RS model from stage three (constructed from the coarse structural optimizations (Wb_c);

RS_{ac} — linear additive correction RS model (constructed at S_r);

RS_{mc} — linear multiplicative correction RS model (constructed at the set of points S_r);

$RS3^{corr}$ — corrected quadratic RS model.

One may use the correction techniques to correct either the results of the quadratic RS model constructed from the coarse structural optimizations results, or to correct the data used for construction of the quadratic RS model. Using the notations above, these approaches can be summarized as follows:

(i $_a$, $_b$) $RS3^{corr} = RS3 + d_a$ or $RS3^{corr} = RS3/r_a$;
(ii $_a$, $_b$) $RS3^{corr} = RS3 + RS_{ac}$ or $RS3^{corr} = RS3/RS_{mc}$.
(iii) and (iv) are similar to (i) and (ii), but coarse data is corrected instead of coarse RS models:
(iii $_a$, $_b$) $Wb_c^{corr} = Wb_c + d_a$ or $Wb_c^{corr} = Wb_c/r_a$;
(iv $_a$, $_b$) $Wb_c^{corr} = Wb_c + RS_{ac}$ or $Wb_c^{corr} = Wb_c/RS_{mc}$.

If (iii) or (iv) are completed, $RS3^{corr}$ is obtained by passing a new RS model at the corrected data points. In fact, approaches (i_a) and (iii_a) are identical, because (iii_a) results in shifting all data by the same amount, thus, preserving all the features of $RS3$, except for the constant term. As the shift in (i_a) and (iii_a) is the same, the predicted responses are also the same for $RS3^{corr}$ from (i_a) and for $RS3^{corr}$ created from Wb_c^{corr} of (iii_a).

In general, correction of the data is preferable, because when the results of the two RS models are added both of them may have the same sign error at a point. This does not happen when the data points are corrected and the new RS model is passed through corrected data.

For the linear correction RS models RS_{ac} and RS_{mc}, as in all the previous cases, we used two different approaches to eliminate poorly defined terms in the RS models: the backward elimination procedure and the stepwise regression procedure followed by backward elimination. For the threshold p-value of 0.05 it was possible to estimate only four out of the original 30 terms for the difference RS model, RS_{ac}, and nine out of 30 terms for the ratio RS model, RS_{mc}.

The accuracy of the wing bending material weight calculations using approaches (i) and (ii) above, where the correction is applied to the coarse RS model ($RS3$), is summarized in Figures 10.1 and 10.2 for the sets S_r and S_r^{check}, respectively. Note that the values in Figures 10.1 and 10.2 for one term in the model function correspond to the usage of the average difference, d_a, and the average ratio, r_a.

To separate the errors associated with the coarse RS model from the errors of the linear correction RS models we recalculated the errors without using the coarse RS model, but instead correcting the coarse data points of sets S_r and S_r^{check}. The

resulting errors for sets S_r and S_r^{check} are presented in Figures 10.3 and 10.4, respectively. Comparing the results in Figures 10.1 and 10.2 with the results in Figures 10.3 and 10.4 we see that using the coarse RS model introduces additional inaccuracy of less than 500 lb.

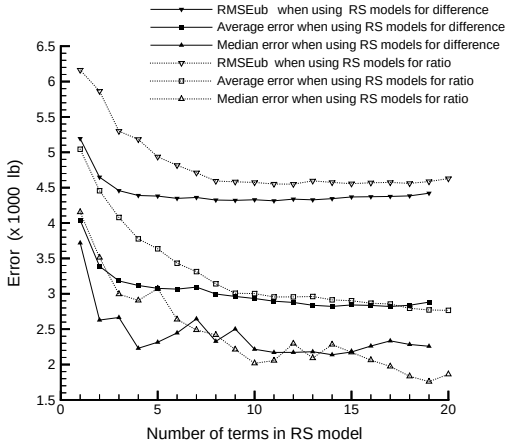

Figure 10.1: Absolute error at the set of points S_r when using RS model from the third stage and linear correction RS models.

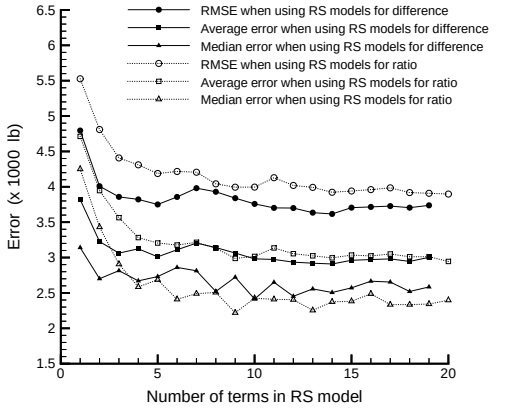

Figure 10.2: Absolute error at the set of points S_r^{check} when using RS model from the third stage and linear correction RS models.

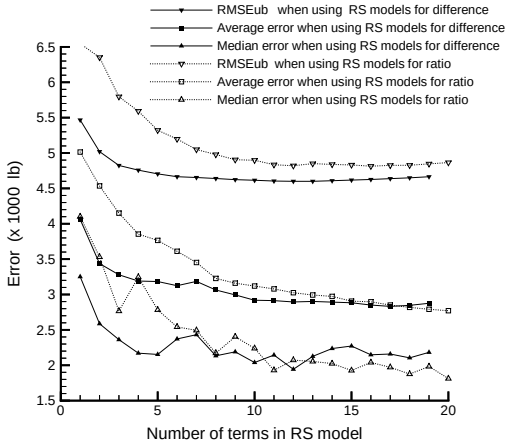

Figure 10.3: Absolute error at the set of points S_r when using coarse FE model results and linear correction RS models.

Finally, we completed this procedure by correcting all 2107 points (data Wb_c at the set of points S_c) using approach (iv) described above, that is, passing a RS model through the corrected data. For RS_{ac} we used four terms and for RS_{mc} we used nine terms.

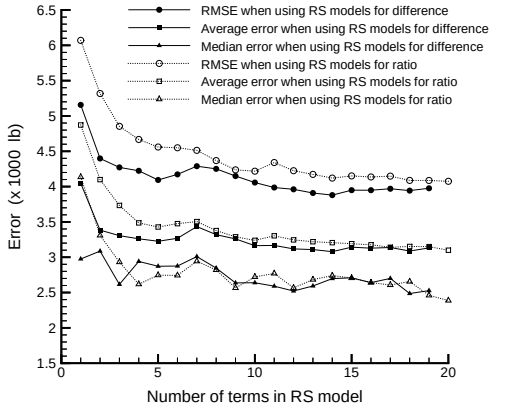

Figure 10.4: Absolute error at the set of points S_r^{check} when using coarse FE model results and linear correction RS models.

From Figures 10.1 and 10.2 it can be seen that these numbers of terms correspond to the beginning of the flat portion of the error plots. The individual terms in these particular RS models had the p-values less than 0.05.

After the data Wb_c was corrected (data Wb_c^{corr} was obtained), two quadratic RS models were recreated from the corrected data set of 2107 points. The RS model created using the linear additive correction RS model RS_{ac} is denoted $RS3_{ac}^{corr}$. The RS model created using linear multiplicative correction RS model RS_{mc} is denoted $RS3_{mc}^{corr}$. The same 96 terms were picked up for both $RS3_{ac}^{corr}$ and $RS3_{mc}^{corr}$ by backward elimination and by stepwise regression followed by backward elimination, when the threshold p-value was set to 0.05. The terms in the $RS3_{ac}^{corr}$, $RS3_{mc}^{corr}$, and original $RS3$ models are the same. However, the values of the coefficients in the terms are different. The plots of the unbiased root mean square error estimates for $RS3_{ac}^{corr}$ and $RS3_{mc}^{corr}$ at the set of points S_c with respect to the data Wb_c^{corr} are shown in Figures 10.5 and 10.6.

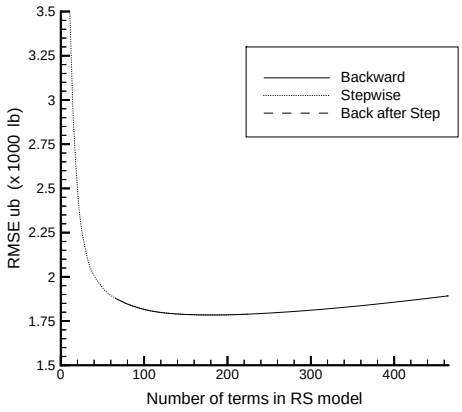

Figure 10.5: $RMSE_{ub}$ for the RS model created from 2107 points when additive four-term correction RS model was used to correct the results at the data points.

The errors of $RS3_{ac}^{corr}$ and $RS3_{mc}^{corr}$ evaluated at the sets of points S_r and S_r^{check} are presented in Table 10.3. The results obtained are very close to the corresponding results from Figures 10.1 and 10.2, when RS_{ac} and RS_{mc} were used to correct the results of $RS3$. From that we may conclude that there is not much difference in

approaches (ii) and (iv), i.e., it does not matter much if we correct the results of the coarse RS model ($RS3$) or we correct the data Wb_c and recreate the quadratic RS model from the corrected data.

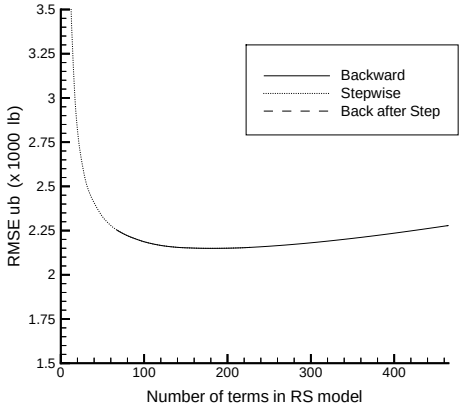

Figure 10.6: $RMSE_{ub}$ for the RS model created from 2107 points when multiplicative nine-term correction RS model was used to correct the results at the data points.

Table 10.3: Absolute errors of $RS3^{corr}_{ac}$ and $RS3^{corr}_{mc}$ at the sets of points S_r and S^{check}_r with respect to the results from the refined FE model.

RS and Set	RMSE	Average	Median	Maximum	Std. Dev.
$RS3^{corr}_{ac}$ at S_r	4,324 lb	3,118 lb	2,230 lb	17,540 lb	3,011 lb
$RS3^{corr}_{ac}$ at S^{check}_r	3,822 lb	3,123 lb	2,670 lb	9,830 lb	2,214 lb
$RS3^{corr}_{mc}$ at S_r	4,422 lb	3,072 lb	2,240 lb	18,747 lb	3,196 lb
$RS3^{corr}_{mc}$ at S^{check}_r	3,992 lb	3,051 lb	2,292 lb	12,723 lb	2,587 lb

Analyzing the results in Figures 10.1 and 10.2 and Tables 10.2 and 10.3 we may conclude that the error of the coarse RS model ($RS3$) can be reduced by more than 50% by using the constant correction (d_a or r_a). The few additional terms in the linear correction RS models improve the accuracy just a little more. It is also possible to conclude that on average the linear additive correction RS model is slightly better than the linear multiplicative correction RS model.

10.3 HSCT Configuration Optimization employing Correction RS Models

HSCT configuration optimizations were performed to evaluate the effects of using the correction RS models. Three different approaches were tried for estimating wing bending material weight:

(1) Approach (i) described above was used, with the coarse RS model ($RS3$) corrected by the average difference (d_a).

(2) $RS3^{corr}_{ac}$ was used to estimate the wing bending material weight.

(3) $RS3^{corr}_{mc}$ was used to estimate the wing bending material weight.

The RS models were used in the configuration optimization in the same way as at stage three. Additional side constraints for the configuration design variables from stage three were also included in the configuration optimization. Each configuration optimization was started from the baseline HSCT configuration. Some parameters of the obtained optimal HSCT configurations are given in Table 10.4. The gross take off weight presented in this table was calculated using the approximate bending material weight employed in the corresponding configuration optimization. The planforms of the aircraft are plotted in Figure 10.7. The 29 configuration design variables for the three optimal HSCT configurations are detailed in Table 10.5. For comparison, we also give in Table 10.5 the parameters of the optimal configurations obtained at stage three using FLOPS and $RS3$, when optimization was started from the baseline HSCT configuration.

From Tables 10.4 and 10.5 and from Figure 10.7 we see that when the corrected RS models $RS3^{corr}_{ac}$ and $RS3^{corr}_{mc}$ were used, the configuration optimization converged to very similar designs. The configuration obtained using the average difference correction looks slightly different from the configurations obtained using $RS3^{corr}_{ac}$ and $RS3^{corr}_{mc}$. The gross take off weights obtained for the three optimum designs are comparable. The gross take off weight is lower for the design obtained using the average difference correction. However, the error of the average difference correction is not conservative for this configuration. If we correct the wing bending material weight for this configuration using the refined structural optimization and add the fuel needed

Table 10.4: Parameters of optimal HSCT configurations when correction RS models were used. Optimizations were started from the baseline HSCT configuration. In this table $WBMW_{FLOPS}$ denotes bending material weight by FLOPS; $WBMW_{RS3}$ – bending material weight by $RS3$; $WBMW_{CRS}$ – bending material weight by coarse structural optimization; $WBMW_{RS3_{d_a}}$ – bending material weight by $RS3$ corrected with d_a; $WBMW_{RS3_{ac}}$ – bending material weight by $RS3^{corr}_{ac}$; $WBMW_{RS3_{mc}}$ – bending material weight by $RS3^{corr}_{mc}$; $WBMW_{REF}$ – bending material weight by refined structural optimization. An asterisk denotes weight used in the optimization.

FLOPS	$RS3$	$RS3 + d_a$	$RS3^{corr}_{ac}$	$RS3^{corr}_{mc}$	Parameter
Planform Geometry					
180.2	180.4	169.1	163.4	162.8	Wing root chord (ft)
10.3	10.3	9.5	10.0	10.0	Wing tip chord (ft)
72.9	72.4	74.7	76.7	77.1	Wing semi-span (ft)
1.89	1.80	1.85	1.98	2.03	Aspect Ratio
13,214	13,637	14,086	13,828	13,607	Wing Area (ft^2)
2.59	2.74	2.84	2.74	2.82	Root t/c (%)
Performance Data					
5,501	5,500	5,487	5,497	5,501	Range $(n.\ mi.)$
9.01	9.00	8.97	8.98	9.00	L/D_{max} at $M = 2.4$
Weight Data					
420,336	422,480	453,687	459,980	456,730	Required Fuel Weight (lb)
$27,491^*$	27,909	39,590	45,455	46,630	$WBMW_{FLOPS}$ (lb)
33,359	$22,990^*$	37,202	43,088	46,566	$WBMW_{RS3}$ (lb)
33,823	28,319	37,611	45,721	49,000	$WBMW_{CRS}$ (lb)
44,067	33,697	$47,910^*$	53,796	57,274	$WBMW_{RS3_{d_a}}$ (lb)
41,777	35,148	47,596	$51,616^*$	54,784	$WBMW_{RS3_{ac}}$ (lb)
42,458	34,773	47,026	51,638	$52,888^*$	$WBMW_{RS3_{mc}}$ (lb)
36,954	37,280	51,260	50,315	57,846	$WBMW_{REF}$ (lb)
797,529	797,167	859,019	872,653	868,503	Gross Take Off Weight (lb)

Table 10.5: HSCT configuration variables of optimal HSCT configurations when correction RS models were used. Optimizations were started from the baseline HSCT configuration.

Num.	$RS3 + d_a$	$RS3^{corr}_{ac}$	$RS3^{corr}_{mc}$	Parameter
1	169.1	163.4	162.8	Wing root chord (ft)
2	111.8	111.8	112.0	LE break point, x (ft)
3	42.3	42.7	41.7	LE break point, y (ft)
4	179.8	174.2	173.3	TE break point, x (ft)
5	11.4	11.4	11.3	TE break point, y (ft)
6	141.7	144.2	143.8	LE wing tip, x (ft)
7	9.5	10.0	10.0	Wing tip chord (ft)
8	74.7	76.7	77.1	Wing semi-span (ft)
9	0.50	0.50	0.50	Chordwise max t/c location
10	2.46	2.48	2.49	LE radius parameter
11	2.84	2.74	2.82	Airfoil t/c at root (%)
12	1.87	2.02	1.85	Airfoil t/c at LE break (%)
13	1.67	1.71	1.70	Airfoil t/c at tip (%)
14	2.64	2.76	2.74	Fuselage restraint 1, x (ft)
15	0.26	0.42	0.41	Fuselage restraint 1, r (ft)
16	13.5	14.1	13.8	Fuselage restraint 2, x (ft)
17	2.40	2.45	2.44	Fuselage restraint 2, r (ft)
18	113.5	113.7	113.7	Fuselage restraint 3, x (ft)
19	5.34	5.36	5.36	Fuselage restraint 3, r (ft)
20	187.1	185.8	185.4	Fuselage restraint 4, x (ft)
21	5.39	5.39	5.39	Fuselage restraint 4, r (ft)
22	9.2	10.1	9.3	Nacelle 1, y (ft)
23	28.3	28.7	26.9	Nacelle 2, y (ft)
24	453,688	459,977	456,730	Mission fuel (lbs)
25	58,305	58,322	58,370	Starting cruise altitude (ft)
26	38.22	37.97	37.98	Cruise climb rate (ft/min)
27	807.5	855.4	804.9	Vertical tail area (ft^2)
28	1,010.6	1,012.8	1,013.8	Horizontal tail area (ft^2)
29	55,359	56,634	56,525	Max. sea level thrust/engine (lb)

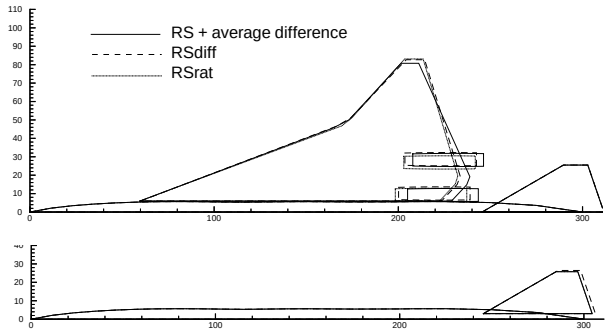

Figure 10.7: Optimal HSCT configurations employing correction RS models. Optimizations were started from the baseline HSCT configuration. Here (*RS + average difference*) denotes using ($RS3+d_a$); *RSdiff* denotes using $RS3^{corr}_{ac}$; *RSrat* denotes using $RS3^{corr}_{mc}$.

to carry the additional weight, the gross take off weight for this configuration will be much closer to the other two optimum configurations.

We also performed HSCT configuration optimization starting from the optimal configuration obtained by FLOPS at the third stage. The same approximations were used to estimate the wing bending material weight: ($RS3 + d_a$), $RS3^{corr}_{ac}$, and $RS3^{corr}_{mc}$. Some parameters of the obtained optimal HSCT configurations are given in Table 10.6. The gross take off weight presented in this table was calculated using the approximate bending material weight employed in the corresponding configuration optimization. The planforms of the aircraft are plotted in Figure 10.8. The 29 configuration design variables for the three optimal HSCT configurations are detailed in Table 10.7. For comparison, we also give in Table 10.7 the parameters of the optimal configurations obtained at stage three using FLOPS and $RS3$, when optimization using $RS3$ was started from the FLOPS optimum of the second stage

Though the optimal configurations obtained are different from the ones when optimization was started from the baseline configuration, the gross take off weights of the aircraft are comparable. From Tables 10.4 and 10.6 we can see that the accuracy

Table 10.6: Parameters of optimal HSCT configurations when correction RS models were used. Optimizations were started from the FLOPS optimum. In this table $WBMW_{FLOPS}$ denotes bending material weight by FLOPS; $WBMW_{RS3}$ – bending material weight by $RS3$; $WBMW_{CRS}$ – bending material weight by coarse structural optimization; $WBMW_{RS3_{d_a}}$ – bending material weight by $RS3$ corrected with d_a; $WBMW_{RS3_{ac}}$ – bending material weight by $RS3^{corr}_{ac}$; $WBMW_{RS3_{mc}}$ – bending material weight by $RS3^{corr}_{mc}$; $WBMW_{REF}$ – bending material weight by refined structural optimization. An asterisk denotes weight used in the optimization.

FLOPS	$RS3$	$RS3 + d_a$	$RS3^{corr}_{ac}$	$RS3^{corr}_{mc}$	Parameter
Planform Geometry					
180.2	180.4	180.1	180.5	180.5	Wing root chord (ft)
10.3	10.3	10.1	10.2	10.2	Wing tip chord (ft)
72.9	72.4	74.8	75.8	75.8	Wing semi-span (ft)
1.89	1.81	1.83	1.89	1.86	Aspect Ratio
13,214	13,559	14,296	14,181	14,378	Wing Area (ft^2)
2.59	2.73	2.76	2.71	2.79	Root t/c (%)
Performance Data					
5,501	5,499	5,496	5,503	5,501	Range $(n.\ mi.)$
9.01	8.98	8.96	8.94	8.96	L/D_{max} at $M = 2.4$
Weight Data					
420,336	423,815	458,481	458,926	459,085	Required Fuel Weight (lb)
$27,491^*$	26,860	34,349	30,381	34,862	$WBMW_{FLOPS}$ (lb)
33,359	$23,512^*$	28,517	29,557	29,828	$WBMW_{RS3}$ (lb)
33,823	28,644	33,045	32,599	34,203	$WBMW_{CRS}$ (lb)
44,067	34,220	$39,225^*$	40,265	40,536	$WBMW_{RS3_{d_a}}$ (lb)
41,777	34,917	40,424	$39,063^*$	41,659	$WBMW_{RS3_{ac}}$ (lb)
42,458	34,868	39,309	38,810	$38,790^*$	$WBMW_{RS3_{mc}}$ (lb)
36,954	38,099	43,231	42,337	46,933	$WBMW_{REF}$ (lb)
797,529	798,693	868,261	868,132	869,566	Gross Take Off Weight (lb)

Table 10.7: HSCT configuration variables of optimal HSCT configurations when correction RS models were used. Optimizations were started from the FLOPS optimum.

Num.	$RS3 + d_a$	$RS3^{corr}_{ac}$	$RS3^{corr}_{mc}$	Parameter
1	180.1	180.5	180.5	Wing root chord (ft)
2	114.9	115.9	117.8	LE break point, x (ft)
3	40.7	43.9	42.9	LE break point, y (ft)
4	187.3	179.0	187.3	TE break point, x (ft)
5	10.8	10.4	10.4	TE break point, y (ft)
6	135.5	136.8	133.1	LE wing tip, x (ft)
7	10.1	10.2	10.2	Wing tip chord (ft)
8	74.8	75.8	75.8	Wing semi-span (ft)
9	0.50	0.51	0.48	Chordwise max t/c location
10	2.19	2.53	2.85	LE radius parameter
11	2.76	2.71	2.79	Airfoil t/c at root (%)
12	2.17	2.17	1.92	Airfoil t/c at LE break (%)
13	1.75	1.75	1.75	Airfoil t/c at tip (%)
14	3.00	3.00	3.00	Fuselage restraint 1, x (ft)
15	0.55	0.56	0.56	Fuselage restraint 1, r (ft)
16	13.1	13.1	13.1	Fuselage restraint 2, x (ft)
17	2.36	2.32	2.32	Fuselage restraint 2, r (ft)
18	113.1	113.0	114.4	Fuselage restraint 3, x (ft)
19	5.35	5.41	5.30	Fuselage restraint 3, r (ft)
20	187.1	183.5	188.0	Fuselage restraint 4, x (ft)
21	5.37	5.35	5.39	Fuselage restraint 4, r (ft)
22	9.1	9.1	9.1	Nacelle 1, y (ft)
23	27.5	27.7	24.5	Nacelle 2, y (ft)
24	458,481	458,926	459,085	Mission fuel (lbs)
25	58,604	58,736	58,735	Starting cruise altitude (ft)
26	38.39	38.39	38.38	Cruise climb rate (ft/min)
27	795.4	800.2	788.5	Vertical tail area (ft^2)
28	986.5	958.2	974.5	Horizontal tail area (ft^2)
29	57,089	57,363	57,356	Max. sea level thrust/engine (lb)

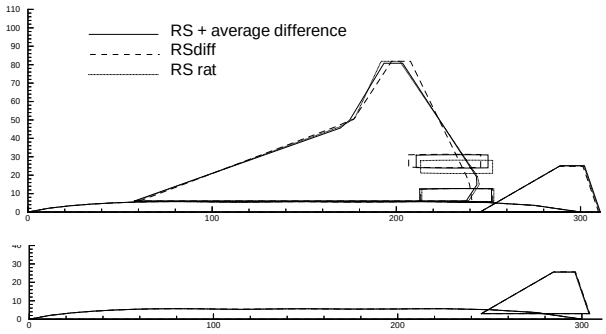

Figure 10.8: Optimal HSCT configurations employing correction RS models. Optimizations were started from the FLOPS optimum. Here (*RS + average difference*) denotes using $(RS3 + d_a)$; *RSdiff* denotes using $RS3^{corr}_{ac}$; *RSrat* denotes using $RS3^{corr}_{mc}$.

of the RS models used is rather good at the optima. For all optimal HSCT configurations some design variables are at their upper or lower limits defined in Table 9.5. Thus to further improve the HSCT configuration, it may be necessary to shift the design window. Convergence to different HSCT configurations when starting from different initial points reflects the nonconvexity of the design domain. In addition the aerodynamic constraints used in the configuration optimization have numerical noise in them [32]. Thus several local optima are very likely to exist.

Once again we see that the FLOPS weight equation performs really well. Results obtained by FLOPS are even not that far from the results of the refined structural optimization for the optimal configurations!

It is also possible to conclude that using the linear correction RS models does not give us a lot in comparison to using just the average difference between the results of structural optimization of refined and coarse FE models. But in general, we have observed that the linear or constant correction is a an effective way of using a relatively small number of high fidelity results to correct the RS model created from the low fidelity data.

Chapter 11

Concluding Remarks

The goal of the work was to explore the possibility of improving weight prediction for the aerodynamic configuration optimization. This was accomplished by using response surface methodology and parallel computing.

A procedure to generate a customized weight equation for the wing bending material weight of the High Speed Civil Transport was implemented using multiple structural optimizations. The customized weight equation was a quadratic response surface model. Coarse-grained parallelization on an Intel *Paragon* computer permitted execution of thousands of coarse structural optimizations which were used for the creation of the response surface model.

In the process of the work it was confirmed that the FLOPS weight equation is an extremely good approximation for the aircraft weight at optimal designs, and for the wing bending material weight in particular. Even for an unconventional aircraft configuration like HSCT, FLOPS wing bending material weight predictions for the optimal configurations were never far from the results of the coarse and even refined structural optimizations. It was very difficult to improve upon FLOPS results with a quadratic response surface model.

It was found that the effect of dimensionality is very strong. The number of points required to construct the quadratic response surface model with acceptable accuracy grows faster than the number of design variables squared.

When structural optimization is integrated into aircraft configuration optimization, the structural weight is inherently a non-smooth function of the configuration shape variables. Additional noise is created due to numerical noise in aerodynamic loads and incomplete convergence of the structural optimization. It was shown that the response surface model is an effective tool to filter out that noise.

The reasonable design space approach and other zooming procedures, like shifting and shrinking the box where the response surface model is applicable, were essential to achieve good accuracy of the response surface model. Simple analysis tools were very useful for the process of identifying the reasonable domain. They helped to eliminate *nonsense* regions of the design space, thus customizing the weight equation to aircraft with the given range, Mach number, etc. However, the screening procedure of identifying important terms in the response surface models based on the low fidelity analysis (FLOPS) did not work out.

Linear or constant correction proved to be a cost effective way to use a relatively small number of high fidelity structural optimization results to improve the accuracy of a response surface model created from low fidelity structural optimization results. In general, response surface approximation to the wing bending material weight for HSCT configuration optimization has been shown to be an effective way to deal with the expense of structural optimizations, the nonsmoothness of structural optima, and the practical difficulties of code integration. Practical considerations that balance response surface accuracy with its development cost are nontrivial. The techniques described here are not limited to the wing bending material weight application and can be used in other areas of multidisciplinary design.

Bibliography

[1] Haftka, R. T. and Sobieszczanski-Sobieski, J., "Multidisciplinary Aerospace Design Optimization: Survey of Recent Developments," in *34th Aerospace Sciences Meeting and Exhibit*, (Reno, NV), January 15–18, 1996. AIAA 96–0711.

[2] Röhl, P. J., Mavris, D. N., and Schrage, D. P., "HSCT Wing Design Trough Multilevel Decomposition," 1995. AIAA 95–3944.

[3] DeLaurentis, D. A., Cesnik, C. E. S., Lee, J.-M., Mavris, D. N., and Schrage, D. P., "A New Approach to Integrated Wing Design in Conceptual Synthesis and Optimization," in *Proceedings of the 6th AIAA/NASA/ISSMO Symposium on Multidisciplinary Analysis and Optimization*, (Bellevue, WA), pp. 1835–1843, September 4–6, 1996. AIAA 96–4000–CP.

[4] Mavris, D. N., Bandte, O., and Schrage, D. P., "Application of Probabilistic Methods for the Determination of an Economically Robust HSCT Configuration," in *Proceedings of the 6th AIAA/NASA/ISSMO Symposium on Multidisciplinary Analysis and Optimization*, (Bellevue, WA), pp. 968–987, September 4–6, 1996. AIAA 96–4090–CP.

[5] Sobieszczanski-Sobieski, J., "Optimization by Decomposition: A Step from Hierarchic to Non-Hierarchic," in *2nd NASA/Air Force Symposium on Recent Advances in Multidisciplinary Analysis and Optimization*, (Hampton, Virginia), September 1988. NASA CP-3031, Part 1. Also NASA TM-101494.

[6] Lokanathan, A. N., Brockman, J. B., and Renaud, J. E., "Concurrent Design of Manufacturable Integrated Circuits," in *Proceedings of the 6th*

AIAA/NASA/ISSMO Symposium on Multidisciplinary Analysis and Optimization, (Bellevue, WA), pp. 1010–1018, September 4–6, 1996. AIAA 96–4094–CP.

[7] Sellar, R. S. and Batill, S. M., "Concurrent Subspace Optimization Using Gradient-Enhanced Neural Network Approximations," in *Proceedings of the 6th AIAA/NASA/ISSMO Symposium on Multidisciplinary Analysis and Optimization*, (Bellevue, WA), pp. 319–330, September 4–6, 1996. AIAA 96–4019–CP.

[8] Sobieszczanski-Sobieski, J., "Sensitivity of Complex Internally Coupled Systems," in *AIAA Journal*. vol. 28, no. 1, pp. 153–160, 1990.

[9] Braun, R., Gage, P., Kroo, I., and Sobieski, I., "Implementation and Performance Issues in Collaborative Optimization," in *Proceedings of the 6th AIAA/NASA/ISSMO Symposium on Multidisciplinary Analysis and Optimization*, (Bellevue, WA), pp. 295–305, September 4–6, 1996. AIAA 96–4017–CP.

[10] Braun, R. D., *Collaborative Optimization: An Architecture for Large-Scale Distributed Design*. PhD thesis, Stanford University, June, 1996.

[11] Unger, E. R., Hutchison, M. G., Rais-Rohani, M., Haftka, R. T., and Grossman, B., "Variable-Complexity Design of a Transport Wing," in *International Journal of Systems Automation: Research and Applications (SARA)*. no. 2, pp. 87–113, 1992.

[12] Hutchison, M. G., Unger, E. R., Mason, W. H., Grossman, B., and Haftka, R. T., "Variable-Complexity Aerodynamic Optimization of an HSCT Wing Using Structural Wing-Weight Equations," in *Journal of Aircraft*. vol. 31, no. 1, pp. 110–116, 1994.

[13] Dudley, J., Huang, X., MacMillin, P. E., Grossman, B., Haftka, R. T., and Mason, W. H., "Multidisciplinary Optimization of the High-Speed Civil Transport," in *33rd Aerospace Sciences Meeting and Exhibit*, (Reno, NV), Sept, 1995. AIAA 95-0124.

[14] Torenbeek, E., "Development and Application of a Comprehensive, Design-Sensitive Weight Prediction Method for Wing Structures of Transport Category Aircraft," in *Report LR-693*, (Delft University of Technology), Sept, 1992.

[15] Scott, P. W., "Developing Highly Accurate Empirical Weight Estimation Relationships: Obstacles and Tactics," in *Proceedings of the 51th International Conference of the Society of Weight Engineers*, May, 1992. SAWE Paper No. 2091.

[16] Huang, X., Dudley, J., Haftka, R. T., Grossman, B., and Mason, W., "Structural Weight Estimation for Multidisciplinary Optimization of a High-Speed Civil Transport," in *Journal of Aircraft*. vol. 33, no. 3, pp.608–616, 1996.

[17] McCullers, L. A., "Aircraft Configuration Optimization Including Optimize Flight Profiles," in *Proceedings of a Symposium on Recent Experiences in Multidisciplinary Analysis and Optimization*, pp. 395–412, April, 1984. J. Sobieski, compiler, NASA CP–2327.

[18] MacMillin, P., Golovidov, O., Mason, W., Grossman, B., and Haftka, R., "Trim, Control and Performance Effects in Variable-Complexity High-Speed Civil Transport Design," in *MAD Center Report 96-07-01*, (Virginia Tech), July, 1996.

[19] Balabanov, V., Kaufman, M., Knill, D. L., Haim, D., Golovidov, O., Giunta, A. A., Haftka, R. T., Grossman, B., Mason, W. H., and Watson, L. T., "Dependence of Optimal Structural Weight on Aerodynamic Shape for a High-Speed Civil Transport," in *Proceedings of the 6th AIAA/NASA/ISSMO Symposium on Multidisciplinary Analysis and Optimization*, (Bellevue, WA), pp. 599–612, September 4–6, 1996. AIAA 96–4046–CP.

[20] Myers, R. H. and Montgomery, D. C., *Response Surface Methodology. Process and Product Optimization Using Designed Experiments*. New York, N. Y.: John Willey & Sons, Inc., 1995.

[21] Montgomery, D. C., *Design and Analysis of Experiments*. New York, N. Y.: John Willey & Sons, Inc., 1991.

[22] Fox, E. P., "Methods of Integrating Probabilistic Design within Orginization's Design System Using Box-Behnken Matrices," 1993. AIAA 93–1380.

[23] Giunta, A. A., Dudley, J. M., Narducci, R., Grossman, B., Haftka, R. T., Mason, W. H., and Watson, L. T., "Noisy Aerodynamic Response and Smooth Approximation in HSCT Design," in *Proceedings of the 5th AIAA/USAF/NASA/ISSMO Symposium on Multidisciplinary Analysis and Optimization*, (Panama City Beach, FL), pp. 1117–1128, September 7–9, 1994. AIAA 94–4376.

[24] Chen, W., Schrage, D. P., Allen, J. K., and Mistree, F., "Statistical Experimentation for Affordable Concurrent Design," in *Proceedings of the 6th AIAA/NASA/ISSMO Symposium on Multidisciplinary Analysis and Optimization*, (Bellevue, WA), pp. 921–930, September 4–6, 1996. AIAA 96–4085–CP.

[25] Kaufman, M., Balabanov, V., Burgee, S. L., Giunta, A. A., Grossman, B., Haftka, R. T., Mason, W. H., and Watson, L. T., "Variable-Complexity Response Surface Approximations for Wing Structural Weight in HSCT Design," in *Computational Mechanics*. no. 18(2), pp. 112–126, 1996.

[26] Carpenter, W., "Effect of Design Selection on RS Performance," June, 1993. NASA CR–4520.

[27] Sacks, J., Welch, W. J., Mitchell, T. J., and Wynn, H. P., "Design and Analysis of Computer Experiments," in *Statistical Science*. vol. 4, no. 4, pp. 409–435, 1989.

[28] Welch, W. J., Buck, R. J., Sacks, J., Wynn, H. P., Mitchell, T. J., and Morris, M. D., "Screening, Predicting, and Computer Experiments," in *Technometrics*. vol. 34, no. 1, pp. 15–25, February 1992.

[29] Osio, I. G. and Amon, C. H., "An Engineering Design Methodology with Bayesian Surrogates and Optimal Sampling," in *EDRC Report 24–112–94*, (Dept. of Mech. Engineering and Engineering Design Research Center, Carnegie Mellon University), September, 1994.

[30] Toropov, V. V., van Keulen, F., Markine, V. L., and de Boer, H., "Refinements in the Multi-Point Approximations Method to Reduce the Effects of Noisy Structural Responses," in *Proceedings of the 6th AIAA/NASA/ISSMO Symposium on Multidisciplinary Analysis and Optimization*, (Bellevue, WA), pp. 941–951, September 4–6, 1996. AIAA 96–4087–CP.

[31] Toropov, V. and Markine, V., "The Use of Simplified Numerical Models as Mid-Range Approximations," in *Proceedings of the 6th AIAA/NASA/ISSMO Symposium on Multidisciplinary Analysis and Optimization*, (Bellevue, WA), pp. 952–958, September 4–6, 1996. AIAA 96–4088–CP.

[32] Giunta, A. A., Balabanov, V., Haim, D., Grossman, B., H., M. W., Watson, L. T., and T., H. R., "Wing Design for a High-Speed Civil Transport Using a Design of Experiment Methodology," in *Proceedings of the 6th AIAA/NASA/ISSMO Symposium on Multidisciplinary Analysis and Optimization*, (Bellevue, WA), pp. 168–183, September 4–6, 1996. AIAA 96–4001–CP.

[33] Oakley, D., Sues, R. H., and Rhodes, G. S., "Multilevel Parallel Computing for Multidisciplinary Optimization and Probabilistic Mechanics," in *Proceedings of the 37th AIAA/ASME/ASCE/AHS/ASC Structures, Structural Dynamics, and Materials Conference and Exhibit*, (Salt Lake City, UT), pp. 620–628, April 15–17, 1996. AIAA 96–1387–CP.

[34] Giunta, A. A., Balabanov, V., Burgee, S., Grossman, B., Haftka, R. T., Mason, W. H., and Watson, L. T., "Variable-Complexity Multidisciplinary Design Optimization Using Parallel Computers," in *Computational Mechanics'95 – Theory and Applications*. pp. 489–494, 1995. Editors: Alturi, S. N., Yagawa, G., Cruse, T. A., Springer, Berlin.

[35] Bertin, J. and Smith, M., *Aerodynamics for Engineers*. Prentice Hall, Second ed., 1989.

[36] Carlson, H., Mack, R., and Barger, R., "Estimation of Attainable Leading Edge Thrust for Wings at Subsonic and Supersonic Speeds," 1979. NASA TP–1500.

[37] Carlson, H. and Miller, D., "Numerical Methods for the Design and Analysis of Wings at Supersonic Speeds," 1974. NASA TN D–7713.

[38] Harris, Jr, R. V., "An Analysis and Correlation of Aircraft Wave Drag," 1964. NASA TM X–947.

[39] Hoak, D. E. *et al.*, *USAF Stability and Control DATCOM.* Flight Control Division, Air Force Flight Dynamics Laboratory, WPAFB, Ohio, 45433-0000, 1978. Revised.

[40] Roskam, J., "Methods for Estimating Stability and Control Derivatives of Conventional Subsonic Airplanes," 1971. Kansas: Roskam Aviation and Engineering Corporation.

[41] Kay, J., Mason, W., Durham, W.and Lutze, F., and Benoliel, A., "Control Power Issues in Conceptual Design: Critical Conditions, Estimation Methodology, Spreadsheet Assessment, Trim and Bibliography," in *Aero–200*, (Virginia Tech), November, 1993.

[42] Grandhi, R. V., Thareja, R., and Haftka, R. T., "NEWSUMT-A: A General Purpose Program for Constrained Optimization Using Constraint Approximation," in *ASME J. Mechanisms, Transmissions and Automation in Design.* vol. 107, pp. 94–99, 1985.

[43] Vanderplaats Research & Development, Inc., Colorado Springs, CO, *DOT Users Manual, Version 4.20*, 1995.

[44] Vanderplaats, Miura and Associates, Inc., 5960 Mandarin Avenue, Suite F, Goleta, CA 93117, *GENESIS User Manual, Version 1.3*, December, 1993.

[45] Barthelemy, J. F. M., Wrenn, G. A., R., D. A., Coen, P. G., and Hall, L. E., "Supersonic Transport Wing Minimum Weight Design Integrating Aerodynamics and Structures," in *Journal of Aircraft.* vol. 31, no. 2, pp. 330–338, March–April, 1994.

[46] Harder, R. L. and Desmarais, R. N., "Interpolation using Surface Spline," in *Journal of Aircraft*. vol. 9, no. 2, pp. 189–191, 1972.

[47] Craidon, C. B., "Description of a Digital Computer Program for Airplane Configuration Plots," 1970. NASA TM X–2074.

[48] Whestone, W. D., *Engineering Analysis Language Reference Manual*. Engineering Information System, Inc., 1983.

[49] Ross-McNatt Naval Architects, 301 Pier One Road, Suite 200, Stevensville, MD 21666, *MAESTRO Basic Features Manual, Version 6.2*, September, 1993.

[50] Giunta., A. A., Narducci, R., Burgee, S., Grossman, B., Mason, W. H., Watson, L. T., and Haftka, R. T., "Variable-Complexity Response Surface Aerodynamic Design of an HSCT Wing," in *Proceedings of 13th AIAA Applied Aerodynamics Conference*, (San Diego, CA), pp. 994–1002, June 19–22, 1995. AIAA 95–1886.

[51] Knill, D. L., Balabanov, V., Grossman, B., Mason, W. H., and Haftka, R. T., "Certification of a CFD code for High-Speed Civil Transport Design Optimization," in *34th Aerospace Sciences Meeting and Exhibit*, (Reno, NV), January 15–18, 1996. AIAA 96–0330.

[52] Carlson, H. and Walkley, K., "Numerical Methods and a Computer Program for Subsonic and Supersonic Aerodynamic Design and Analysis of Wings with Attainable Thrust Corrections," 1984. NASA CP–3808.

[53] Pittman, J. L., Bonhaus, D. L., Siclari, M. J., and Dollyhigh, S. M., "Euler Analysis of a High-Speed Civil Transport Concept at Mach 3," in *Journal of Aircraft*. vol. 28, no. 4, pp. 239–245, April, 1991.

[54] McGrory, W. D., Slack, D. C., Applebaum, M. P., and Walters, R. W., *GASP Version 2.2 Users Manual*. Aerosoft, Inc., 1993.

[55] Barger, R. L., Adams, M. S., and Krishnan, R. R., "Automatic Computation of Euler-Marching and Subsonic Grids for Wing-Fuselage Configurations," in *NASA TM 4573*. July, 1994.

[56] Box, M. J. and Draper, N. R., "Factorial Designs, the $|\mathbf{X}^T\mathbf{X}|$ Criterion, and Some Related Matters," in *Technometrics*. vol. 13, no. 4, pp. 731–742, 1971.

[57] Myers, R. H., *Response Surface Methodology*. Blacksburg, VA: published by Author, 1976.

[58] SAS Institute Inc., SAS Campus Drive, Cary, NC 27513, *SAS Users Guide, Version 6, Fourth Edition*, 1990.

[59] Mitchell, T. J., "An Algorithm for the Construction of D-Optimal Experimental Designs," in *Technometrics*. vol. 16, no. 2, pp. 203–210, May, 1974.

[60] SAS Institute Inc., SAS Campus Drive, Cary, NC 27513, *JMP Statistics and Graphics Guide, Version 3.1*, 1995.

[61] Box, G. E. P. and Behnken, D. W., "Some New Three Level Designs for the Study of Quantitative Variables," in *Technometrics*. vol. 2, no. 4, pp. 455–475, 1960.

[62] Kaufman, M. D., "Variable-Complexity Response Surface Approximations for Wing Structural Weight in HSCT Design," Master's thesis, Virginia Polytechnic Institute and State University, Blacksburg, VA, February, 1996.

Appendix A

Calculation of the Wing Bending Material Weight in FLOPS

The general wing weight function in FLOPS is based on an analytic expression to relate wing bending material weight to wing geometry, material properties, and loading. Other terms are added to account for shear material, control surfaces, etc. In addition, constants are included to correlate with a wide range of existing transports and to reflect features such as composite materials, strut braced wings, etc. The wing weight W_w used within FLOPS is given as

$$W_w = \frac{W_g K_e W_b + W_s + W_n}{1 + W_b}\,, \tag{A.1}$$

where

$$W_s = 0.68\,(1 - 0.17 f_c)\,(S - S_b)^{0.34}\,W_g^{0.6},$$
$$W_n = 0.35\,(1 - 0.3 f_c)\,S^{1.5},$$
$$W_b = K f_{ul} b\,(1 - 0.4 f_c)\,(1 - .01 f_a)\,,$$
$$K = 8.8 B_z \left(1 + (6.25/b)^{0.5}\right) \times 10^{-6},$$
$$K_e = 1.0 - (B_{ze}/B_e)\,(W_{pod}/W_g)\,,$$

and

B_z is the bending material factor,

B_{ze} is the engine relief factor,
S is the wing area (ft^2),
S_b is the wing box area (ft^2),
W_b is the wing bending material weight (lbs),
W_g is the gross takeoff weight (lbs),
W_n is the wing control surfaces and non-structural weight (lbs),
W_{pod} is the engine pod weight (lbs),
W_s is the wing shear material and flaps weight (lbs),
b is the wing span (ft),
f_a is the composite material factor,
f_c is the aeroelastic tailoring factor,
f_{ul} is the ultimate load factor.

The system is closed except for the bending material factor B_z and the engine relief factor B_{ze}. The parameter B_z accounts for the distribution of load on the wing, neglecting the engines, and is calculated by approximately determining the required material volume of the upper and lower skins in a simple wing box description of the wing. The parameter B_{ze} accounts for the reduced amount of structural weight necessary due to the presence of the engines on the wing.

First, the weighted average of the load sweep angle at a 75% chord position is found:

$$\Lambda_L = \int_0^1 (1 + 2y)\Lambda(y)\, dy.$$

Next it is necessary to determine the bending moment assuming a simple elliptic pressure distribution.

$$M(y) = \int_0^y p(\xi)\xi\, d\xi.$$

With this bending moment distribution it is possible to calculate the necessary flange areas

$$A(y) = \frac{M(y)}{t(y)c(y)\cos\Lambda(y)},$$

and the required volume as

$$V = \int_0^1 A(y)\, dy.$$

The total load is

$$L = \int_0^1 p(y)\, dy,$$

and the bending material factor is finally given as

$$B_z = \frac{2V}{Ld},$$

where

$$d = AR^{0.25}[1 + (0.5f_a - 0.16)\sin^2 \Lambda_L + 0.3K_a$$
$$(1 - 0.5f_a)\sin \Lambda_L],$$

where AR is the aspect ratio and K_a is given by

$$K_a = \begin{cases} AR - 5, & \text{if } AR > 5, \\ 0, & \text{otherwise.} \end{cases}$$

B_{ze} accounts for the reduced amount of structural weight necessary due to the presence of the engines on the wing:

$$B_{ze} = 16 \int_{y_{root}}^{y_{tip}} NE \left(\frac{y_{tip} - y}{\cos^2 \Lambda(y)} \right) \left(\frac{y_{tip} - y_{root}}{c(y) Max(t/c)} \right) dy,$$

where NE is given by

$$NE = \begin{cases} 2, & y < y_{nacelle_1}, \\ 1, & y_{nacelle_1} < y < y_{nacelle_2}, \\ 0, & y > y_{nacelle_2}. \end{cases}$$

Appendix B

Least Squares Method, Analysis of Variance, and Regression Procedure

B.1 Least Squares Method and Analysis of Variance

Statistical techniques known as regression analysis and analysis of variance (ANOVA) provide the means to identify and remove poorly characterized terms in response surface polynomial models, thereby improving the accuracy of those models. Regression analysis is the procedure by which the c_i coefficients for the response surface model are obtained and typically involves the method of least squares, as follows. Let there be N measurements Y_i at N distinct design points $(x_1^{(i)}, \ldots, x_p^{(i)})$, $i = 1, \ldots, N$, and let the basis functions for the regression model be $\varphi_1(x), \ldots, \varphi_n(x)$, where $x = (x_1, \ldots, x_p)$. A choice for the φ_i might be

$$1, x_1, x_2, \ldots, x_p, x_1^2, x_1 x_2, \ldots, x_p^2,$$

corresponding to a quadratic model. The regression model is

$$y \approx c_1 \varphi_1(x) + \cdots + c_n \varphi_n(x),$$

which leads to the overdetermined matrix problem

$$Y \approx \mathbf{X}c\,, \tag{B.1}$$

where $Y = (Y_1, ..., Y_N), c = (c_1, ..., c_n)$, and $\mathbf{X}$ is the $N \times n$ $(N \geq n)$ matrix

$$\begin{pmatrix} \varphi_1(x^{(1)}) & \dots & \varphi_n(x^{(1)}) \\ \vdots & \ddots & \vdots \\ \varphi_1(x^{(N)}) & \dots & \varphi_n(x^{(N)}) \end{pmatrix}.$$

The least squares solution is that (unique, assuming rank $\mathbf{X} = n$) vector $\hat{c}$ which minimizes the 2-norm $||Y - \mathbf{X}\hat{c}||_2$, or the sum of squares of the components of $Y - \mathbf{X}\hat{c} = e$, the *errors*:

$$\hat{c} = (\mathbf{X}^T\mathbf{X})^{-1}\mathbf{X}^T Y \tag{B.2}$$

The regression or response surface model of the data is then taken as

$$\hat{c}_1\varphi_1(x) + \cdots + \hat{c}_n\varphi_n(x) \tag{B.3}$$

The least squares solution $(\hat{c})$ of equation B.1 is also the unbiased estimator of c ([20], p. 24). The variance property of $\hat{c}$ is expressed by the covariance matrix:

$$Cov(\hat{c}) = \sigma^2(\mathbf{X}^T\mathbf{X})^{-1}\,, \tag{B.4}$$

where σ^2 is the variance in the observed response data. Square roots of the diagonal terms of the matrix $Cov(\hat{c})$ are called *standard errors* of the regression coefficients $\hat{c}_i$: It can be shown ([20], p. 26) that the unbiased estimator of σ^2 is given by:

$$\hat{\sigma}^2 = \frac{e^T e}{N - n} = \frac{Y^T Y - \hat{c}^T\mathbf{X}^T Y}{N - n} \tag{B.5}$$

Note, that the unbiased estimator of σ^2 from B.5 is model dependent: n - is the number of terms in the response surface model B.3.

To quantify the error in the coefficients of the response surface model B.3 the following measure called t-statistics ([20], p. 32) is often used:

$$t = \frac{\hat{c}_i}{\sqrt{\hat{\sigma}^2 (\mathbf{X}^T \mathbf{X})^{-1}_{ii}}}, \tag{B.6}$$

where the quantity in the denominator is the standard error of the regression coefficient $\hat{c}_i$. Thus, the smaller the error in estimating the value of the coefficient, the larger the corresponding t-statistics value.

Another way of quantifying how well the coefficients of the polynomial are determined is by specifying the significance level of a coefficient – p-value. This is the probability that the value of the particular coefficient is actually zero, rather than the one that was computed. It is the prerogative of the user to select an appropriate significance level for the coefficients in a polynomial. Often p-values of 0.05 or less for all coefficients are considered as an evidence that the polynomial fits the data. Analysis of variance procedures implemented in the standard statistical programs like JMP [60] and SAS [58] provide calculation of both t-statistics and p-value.

B.2 Regression Procedure

There are several ways of selecting the appropriate subset of terms in a RS model. The most widely used methods are: forward selection, backward elimination, and stepwise regression. They are described in detail in Ref. [20], pp. 640–655, and only a very brief description is given here.

The forward selection procedure begins with the assumption that initially there are no terms in the RS model other than the constant term. An effort is made to find an optimal subset by inserting terms in the model one by one. At each step the term with the largest t-statistics value (which correspond to the smallest p-value) is inserted. The p-value should be specified so that it does not allow poorly defined terms to be entered into the RS model.

Backward elimination attempts to find a good model by starting with the one that includes all candidate terms. Then the term with the largest p-value is eliminated. At each step the term with the smallest t-statistics value (which correspond to the largest p-value) is eliminated. The procedure is continued until the threshold value

is reached for eliminating the terms and all the terms in the model have p-values less than the specified threshold value.

In the forward selection procedure once the term is inserted in the model, it can not be removed from the model. The stepwise regression algorithm is a modification of the forward selection procedure. However, at each step all the terms that are already in the model are reevaluated. Some of the terms could be removed if the reevaluated t-statistics value is less than the required threshold value.

There is no guarantee that the algorithms described above converge to the same RS model. Often, there is no best subset model, but there are several equally good ones. However, backward elimination is often less affected by the mutual correlation of the terms in the model than forward selection. It is also often helpful to run stepwise regression followed by backward elimination.

For our particular calculations we decided to use two approaches: backward elimination only and stepwise regression followed by backward elimination. After applying each of the approaches we try to select the RS model that both approaches came up with and that satisfies our criterion for the p-value.

Appendix C

Estimation of RS Model Coefficients in Two-Level Factorial Design

In response surface methodology smooth functions, typically polynomials, are used to model an objective function. For example, a bi-linear response surface model for p variables has the following form:

$$y = c_0 + \sum_{1 \le i \le p} c_i x_i + \sum_{1 \le i < j \le p} c_{ij} x_i x_j \,, \tag{C.1}$$

Here the x_i are the variables, the c_i are the polynomial coefficients, and y is the measured response. To maintain good accuracy, we would like the points where we use the response surface model to be located within the convex hull of the data points used to construct the surface. To satisfy this for a p-dimensional box we must estimate response at 2^p points (at the vertices of the box). Such experimental design, when all the vertices of the p-dimensional box are evaluated, is called *full-factorial design* and denoted according to the number of the vertices evaluated (2^p) ([20], pp.79–111). The variables that are involved in the RS model are often called *factors* in statistics. That is why the design is called *factorial*. A very important case of factorial design is that where each of the p variables (factors) has only two possible values – *levels*. In this case designs are called 2^p factorial designs. When each factor is evaluated at

three levels, the experimental design is called a 3^p factorial design.

The simpliest design in the 2^p-series is one with only two factors, say A and B, each evaluated at two levels. This design is called a 2^2 factorial design. The values of the factors may be arbitrarily called "low" and "high". The factor-level combinations in the design are often represented by lower case letters, as shown in Figure C.1.

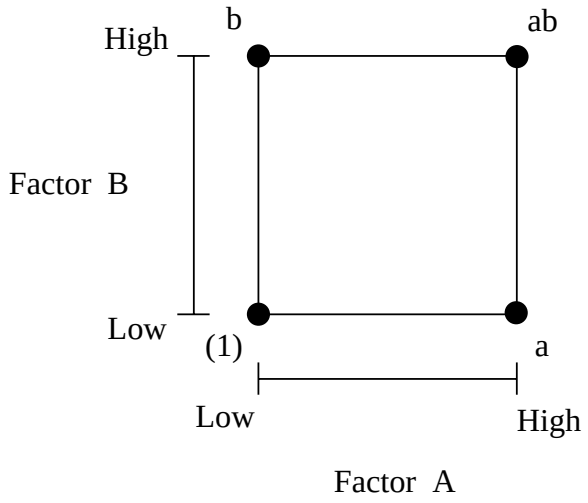

Figure C.1: 2^2 experimental design.

In Figure C.1 the high level of a factor at a point in the design is denoted by a corresponding lower case letter and the low level of a factor is denoted by the absence of this letter. Thus, a represents the combination of factor levels with A at the high level and B at the low level, b represents A at the low level and B at the high level, and ab represents both factors at the high level. (1) is used to denote the point where both factors are at the low level.

The *effect of a factor* is defined as the change in response produced by a change in the level of that factor averaged over the levels of the other factor. Thus, the effect of A can be found as the difference in the average response of the two points on the right-hand side of the square in Figure C.1 and the two points on the left-hand side. Denoting the effects of the factors by the same capital letters as the factors themselves, the formula for the effect A can be written as:

$$A = \frac{ab + a}{2} - \frac{b + (1)}{2} = \frac{1}{2}\left[ab + a - b - (1)\right] . \tag{C.2}$$

The effect of factor B is found as the difference between the average of the response at the two points on the top of the square and the average of the response at the two points on the bottom:

$$B = \frac{ab+b}{2} - \frac{a+(1)}{2} = \frac{1}{2}\left[ab+b-a-(1)\right] . \tag{C.3}$$

The *two-factor interaction effect* AB is the average of the responses on the right-to-left diagonal points in the square [ab and (1)] minus the average of the responses on the left-to-right diagonal points [a and b]:

$$AB = \frac{ab+(1)}{2} - \frac{a+b}{2} = \frac{1}{2}\left[ab+(1)-a-b\right] . \tag{C.4}$$

The values of effects may be used to find the coefficients of the RS model from equation (C.1). The constant term in this equation (c_0) is the average of all observations. The rest of the coefficients are the corresponding factor effect estimates divided by one-half of the distance between the high and the low levels of the corresponding factors.

The procedure for estimating the coefficients in the RS model using the method of least squares is described in Appendix B. However, for the factorial designs the procedure presented here and the least squares method always yield identical results.

Now consider the experimental design with three factors – A, B, and C. In this case to get the full-factorial design we need to estimate the response at eight points – vertices of the cube. However, if we are only concerned about linear effects A, B, and C we may be able to estimate them using only 4 carefully selected points. The experimental design obtained in such a way is called according to the number of points used: $2^{(3-1)}$ *fractional factorial* design. An example of such a design is given in Figure C.2.

The equations for the effects A, B, and C in the particular case of points in Figure C.2 are:

$$A = \frac{ab+ac}{2} - \frac{bc+(1)}{2} = \frac{1}{2}\left[ab+ac-bc-(1)\right] , \tag{C.5}$$

$$B = \frac{ab+bc}{2} - \frac{ac+(1)}{2} = \frac{1}{2}\left[ab+bc-ac-(1)\right] , \tag{C.6}$$

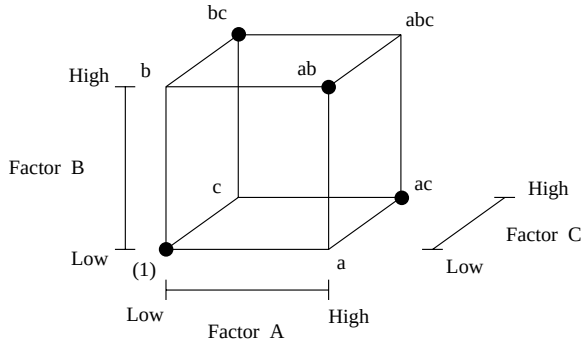

Figure C.2: Example of $2^{(3-1)}$ experimental design.

$$C = \frac{ac+bc}{2} - \frac{ab+(1)}{2} = \frac{1}{2}\left[ac+bc-ab-(1)\right] , \tag{C.7}$$

However, if we would like to estimate two-factor interaction effect in our particular set of points from Figure C.2, we shall not be able to do it. For example:

$$AB = \frac{ab+(1)}{2} - \frac{bc+ac}{2} = \frac{1}{2}\left[ab+(1)-bc-ac\right] = -C\,, \tag{C.8}$$

The expression defining interaction effect AB is proportional to the expression defining effect C. In this situation effects AB and C are called *confounded* or *aliased*. That is, we are not able to distinguish between AB and C if we use only the set of points from Figure C.2. In the case represented in Figure C.2 the other pairs of confounded effects are: AC and B, and BC and A. Such a design where the main effects are confounded with two-factor interactions is called a *resolution III* design.

In general, a design is of resolution G if no p-factor effect is aliased with another effect containing less than $(G-p)$ factors. For example, *resolution III* design is a design in which no main effects are aliased with any other main effect, but main effects are aliased with two-factor interactions and two-factor interactions may be aliased with each other; *resolution IV* design is a design in which no main effect is aliased with any other main effect or with any two-factor interaction, but two-factor interactions are aliased with each other; *resolution V* design is a design in which no main effect or two-factor interaction is aliased with any other main effect or two-factor interaction, but two-factor interactions are aliased with three-factor interactions ([20], pp. 138–139).

However, if we choose the four points not as it is shown in Figure C.2, but, say as

it is shown in Figure C.3, we shall be able to estimate effects A, C, and AC, but we shall not be able to estimate B, BC, and AB. The reason is that in the deign from Figure C.3 there are no points that correspond to the high level of the factor B.

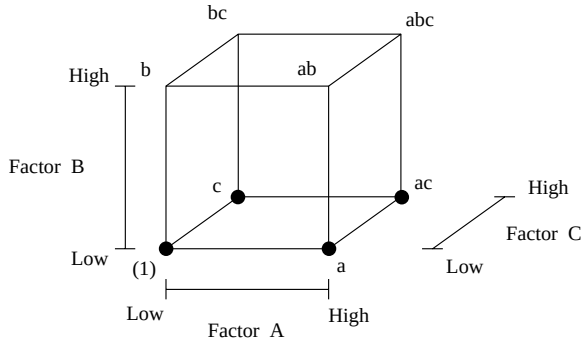

Figure C.3: Example of $2^{(3-1)}$ experimental design.

From the illustrations presented it is clear that the desired form of the RS model function dictates the location of the points in the experimental design. Particularly, if one uses only some fraction of the factorial design, one must be sure that the selected set of points gives an opportunity to estimate all the desired effects clearly, without them being confounded with the other effects in the model.

When the number of factors in the experimental design is large, it is hard to select a fraction of the factorial design by just looking at the picture. There are special computer programs that can do selection of smaller subsets of points from a full-factorial design based on the model that will be fitted to the points in the experimental design. Examples of such programs are JMP [60] and SAS [58]. The detailed description of the related topics can be found in [20], pp. 79–111.

Appendix D

Point Selection Technique Similar to PBIB

In the development of a response surface, a large number of data points that *cover* the design space are required. A systematic approach for producing the locations of these points has been developed by Kaufman ([62]). It is assumed that the initial design space is a p-dimensional box centered at the origin with vertices $(\pm 1, \ldots, \pm 1)$ and a quadratic polynomial (Equation (7.1)) is used as the RS model function. The *level* of a variable in a point selection system refers to the number of values that the variable is allowed to take on within a set of data points; for example, if a variable assumes the values $\{-1, 0, +1\}$ within a set of points, then it is said to have a level of three [61].

Consider a combination of two level-point selection systems based on the partially balanced incomplete block design (PBIB) ([21], pp. 176–196). For a two-level system, each variable can take on the values $\{-1, +1\}$. Similar to the PBIB design, a pattern of blocks is created, each of which contains a fraction of the total number of variables. The variables within a block are evaluated at the two levels ± 1, while the variables outside of the block are held fixed at the third level 0. Three different blocking systems are incorporated to produce a satisfactory number of points. Every block pattern containing one, two, and three variables is considered, as well as the center point $(0, \ldots, 0)$.

All possible two-variable block patterns for a problem in three variables, and the corresponding design points are given in Table D.1. For example, for twenty-five variables, 19,651 points are produced using the three blocking systems and one center point. For an arbitrary number p of variables the total number of points created is

$$1 + \sum_{i=1}^{3} 2^i \frac{p!}{i!\,(p-i)!}.$$

Table D.1: Two-variable block pattern example.

	x_1	x_2	x_3
Block #1	*	*	
Block #2		*	*
Block #3	*		*

	x_1	x_2	x_3
Block #1	1	1	0
	-1	1	0
	1	-1	0
	-1	-1	0
Block #2	0	1	1
	0	-1	1
	0	1	-1
	0	-1	-1
Block #3	1	0	1
	-1	0	1
	1	0	-1
	-1	0	-1

Appendix E

Finite Element Mesh Generator

The finite element mesh generator program *mesh2* creates an input file for the finite element structural optimization code *GENESIS*. The file is usually named *hsctgo.dat*. The description of the input file for *GENESIS* can be found in Ref. [44]. The mesh generator program requires three input files to operate: the Craidon geometry description file, the file with information about the weight of all nonstructural items of the aircraft, and the file with the location and values of the aerodynamic forces acting on aerodynamic panels of the aerodynamic model of the aircraft. The Craidon geometry description file is created by the program *WINGDES* and is usually named *wavin.final*. The weight file is generated by the program *HSCT* when the option `WEIGHT` is used. This file is usually named *hsct.genesis*. The aerodynamic load file is also generated by the program *HSCT* when the option `LOADS` is used. This file is usually named *loads.all*. Craidon geometry description could be found in Ref. [47]. The other two input files will be described here.

Besides input files a user can also change some parameters of the structural model. This can be accomplished by changing the values of the parameters in the `PARAMETER` statements of the program and recompiling the program. Some important parameters that a user may want to change will also be described here.

E.1 Input Files

hsct.genesis

This file provides information about the weight of nonstructural items of the HSCT. The weights in this file are given for a half of the aircraft, because of the symmetry of the structural model. Here is an example of *hsct.genesis* file. All the lines in it are self-explanatory, except for the first line.

```
121281.2974    84591.1688   232371.2845   438243.7506
    45319.9299      # ENGINES, ENGINE OIL, THRUSTS
     7448.5052      # VERTICAL, HORIZONTAL TAILS
        0.0000      # ENGINE NACELLES
      790.0000      # CREW
      817.7026      # MISCELLANEOUS
     3758.6396      # FUEL SYSTEM, UNUSEFUL FUEL
      712.9916      # AVIONICS
      566.6076      # AUXILIARY POWER UNITS
      509.1678      # INSTRUMENTS
     1329.5083      # NOSE LANDING GEAR
    11235.7601      # MAIN LANDING GEAR
     4744.0326      # SURFACE CONTROL
       77.1745      # HYDRAULIC SYSTEM
     2290.8109      # ELECTRIC SYSTEM
     2130.2727      # AIR CONDITION SYSTEM
      213.0473      # ANTI ICING
     6794.5000      # BAGGAGE, CARGO, CONTAINERS
    32542.6467      # FURNISHING, PASSENGERS, SERVIES
    20633.9424      # WING BENDING MATERIAL WEIGHT
    16164.0301      # WING FLAPS, LAEDING & TRAILING
    29476.4633      # WING NONSTRUCTURAL, ETC
    66274.4359      # WING WEIGHT
```

The first number in the first line (121281.2974) is the sum of the weights given in lines two to nineteen.
The second number in the first line (84591.1688) is 1/2 of the sum of the weights of the wing and the fuselage.
The third number in the first line (232371.2845) is 1/2 of the required fuel weight.
The fourth number in the first line (438243.7506) is 1/2 of the gross weight calculated by FLOPS.

loads.all

This file contains information about aerodynamic forces at aerodynamic panels of the aerodynamic model of the aircraft for four load cases. There are three columns of numbers in this file. The first column is the x-coordinate (chordwise) of the point of application of the force, the second column is the y-coordinate (spanwise) of the point of application of the force, and the third column is the value of the aerodynamic force. Information for each load case is written under the information for the previous load case with the two header lines for each load case. In the first line of the header there is information about the Mach number (`M`) and the load factor (`n`). The Second line of the header consists of two numbers: the first is the number of aerodynamic forces for this load case, the second is the angle of attack that is required to trim the aircraft. Below is an example of *loads.all* file.

```
Load Case:  M=2.40, n=1.00
709    3.754368
 53.21960    0.00000  274.33229
 56.97107    0.00000  234.50104
 61.32847    0.00000  235.50085
 . . .
199.36144   78.88970   27.51675
200.76502   78.88970  288.73514
204.89706   78.88970  212.05286
Load Case:  M=1.20, n=1.00
2231    1.982675
 51.68104    0.00000   89.56923
 53.18033    0.00000   65.66447
 54.50513    0.00000   60.82321
 . . .
204.20725   78.88970  208.90393
205.53205   78.88970  197.84471
206.76650   78.88970  146.83800
Load Case:  M=0.60, n=2.50
105    12.520544
 78.71529    2.66294 20772.48512
105.01443    2.66294 16861.33219
131.31357    2.66294 15852.92888
 . . .
205.16096   77.22536  1399.26781
206.49578   77.22536   979.31316
207.83060   77.22536   589.67318
Load Case:  M=2.40, n=2.50
709    8.789074
 53.21960    0.00000  1060.30968
```

```
 56.97107    0.00000  859.86550
 61.32847    0.00000  825.02968
 . . .
199.36144   78.88970   85.48915
200.76502   78.88970  900.18188
204.89706   78.88970  668.52594
```

E.2 Internal Parameters of the Mesh Generator

All the important parameters that a user may want to change are placed in the special files and these files are automatically included in the code, when it is compiled. There are four files containing parameters *CRAID.DAT, GENINP.DAT, LOCAL.DAT, SCONF.DAT*. Each of the files contains a description of the parameters that are located in it. Here is a brief description of each file and the parameters in it.

CRAID.DAT

This file contains the parameters of the Craidon geometry description. The values used over here are taken from the parameters used to create the aerodynamic model. A detailed description of the parameters is given in Ref. [47]. The names of the parameters used in this file are taken from Ref. [47].

GENINP.DAT

This file contains the parameters that are related to the structural optimization program *GENESIS*. They specify the details of the HSCT finite element model for structural optimization. Here are the most important parameters.

```
NLCASES - Number of load cases used in the structural optimization
DENS1   - Density of the material for the elements included in wing
               bending material weight calculations
DENS2   - Density of the material that is not supposed to affect
               structural optimization
NDVPLT  - Number of design variables associated with plate elements
NDVROD  - Number of design variables associated with rod elements
BAREA   - Area used in buckling constraints
```

```
BTHICK  - Thickness used in buckling constraints
BL1, BL2, BL3 - Lengths used for buckling constraints
```

Description of the parameters that follow could also be found in Ref. [44].

```
TRTHRL  - Truncation threshold level for normalized constraints
NCNSRR  - Number of constraints to be retained per region per load case
MNAOPT  - maximum number of approximate optimizations to be performed.
IPRINT  - Print control for optimizer
DELP    - Fractional change allowed for each design property during
               optimization. This provides move limits
DPMIN   - minimum move limit imposed for properties
CONV2   - Absolute change in the objective function to detect hard
               convergence
GMAX    - maximum constraint violation allowed at the optimum
```

LOCAL.DAT

This file contains mostly the parameters associated with the internal input/output. However, there are also two parameters that affect the structural model:

```
MNCNST - maximum number of nodes that are constrained in their motion at the
              plane of symmetry of the aircraft
NALCAS - total number of load cases
```

SCONF.DAT

This file contains the parameters that define the structural arrangement of the model.

```
NOS     - Number of spars in the outer part of the wing (farther
               spanwise from the plane of symmetry than the line
               connecting leading and trailing edge break points)
NIR     - Number of ribs in the inner part of the wing (closer
               spanwise to the plane of symmetry than the line
               connecting leading and trailing edge break points)
NOR     - Number of ribs in the outer part of the wing
NFFT    - Number of frames in the tail part of the fuselage
NFFN    - Number of frames in the nose part of the fuselage
```

```
RLCS1  - Relative root chord of the leading edge control surface
RLCS2  - Relative tip chord of the leading edge control surface
RLCS3  - Relative root chord of the trailing edge control surface
RLCS4  - Relative tip chord of the trailing edge control surface
NTANKS - Number of fuel tanks
NSITEM - Number of nonstructural items, which weight should be
              considered
NAMX   - maximum number of points were aerodynamic loads are given for
              one load case
```

In the description above the chord-lengths of the leading and trailing edges of the control surfaces are given as a fraction of that wing chord to which the leading and trailing edges of the control surface belong.

Appendix F

Parameters for Calculating Wing Bending Material Weight from FE Model

After the structural optimization is completed the wing bending material weight may be calculated from the FE model using the program *wbm2s*. This program reads in the input file for the structural optimization, the file with the history of the structural optimization, and the file generated by *HSCT* program — *hsct.genesis*. The input file for the structural optimization is created by the program *mesh2* and named *hsctgo.dat*. The file with the history of the structural optimization is generated by the structural optimization code *GENESIS* and is usually named *hsctgo.HIS*. The file *hsct.genesis* is described in Appendix E. The output of the wing bending material weight calculation program *wbm2s* is the file *wbmwg.res* which contains information about the wing bending material weight and the gross weight calculated from the FE model and calculated by FLOPS. To change some parameters in *wbm2s*, the user must change the `PARAMETER` and `DATA` statements and recompile the program. The important parameters are given below.

```
NGRIDM  - maximum number of grid points in the FE model
NDESVM  - Number of structural optimization design variables
```

```
NUMWDVR - Number of design variables for describing portion of
               the wing bending material weight corresponding to
               rod elements
NUMWDVT - Number of design variables for describing portion of
               the wing bending material weight corresponding to
               triangular (plate) elements
NELINDV - maximum number of elements corresponding to one design
               variables
RO      - Density of the material used
```

There are four important `DATA` statements that the user could change while adjusting the calculation of the wing bending material weight.

```
NWEITDVR - Array with ID-numbers of the design variables associated
                with rod elements that are accounted for while
                calculating the wing bending material weight
CWEITDVR - Weighting coefficients for the correspondent ID-numbers from
                NWEITDVR
NWEITDVT - Array with ID-numbers of the design variables associated with
                triangular (plate) elements that are accounted for while
                calculating the wing bending material weight
CWEITDVT - Weighting coefficients for the correspondent ID-numbers from
                NWEITDVT
```

Appendix G

Parallel Code

As described in Chapter 4, parallel computing is used to speed up the process of structural optimization of many HSCT configurations. The program that implements the dynamic data task scheduling by a *master-slave* paradigm is called *g4n29*. Within this program one processor (*the master*) monitors the work of the other processors (*the slaves*). First the master-processor reads in the file with the governing information for N structural optimizations, then it reads in the N by 29 matrix of HSCT configuration design variables from the input file. Each row represents a set of 29 design variables for a particular HSCT configuration. The HSCT configuration design variables are described in Chapter 2. Then the master processor creates as many working directories as there are slave-processors at its disposal. It prepares the input data file for aerodynamic load calculations in each of the working directories. After that the master-processor assigns the particular working directory to each of the slave-processors and the slave-processors start their own calculations. Meanwhile the master processor creates one more working directory and prepares the next consecutive input data file in it for the slave-processor which finishes its task first. When one of the slave-processors finishes its task, the master processor sends to it the name of the new working directory where the slave-processor will now work, and the slave-processor starts the new task in the working directory prepared for it. The master-processor copies the desired results obtained by the slave-processor into a separate directory where files with all the results are collected, cleans up the working

directory where the slave-processor was working, and prepares the next consecutive input data file in it. After that the master-processor waits for the next slave-processor to finish the task. While doing all this, the master processor also keeps track of which slave-processor is doing calculations for which particular row of the matrix with the HSCT configuration design variables. This whole procedure continues until there is nothing more to compute.

Here is the example of the file with governing information that the master-processor reads in the very beginning. This file must have the name *inpgovn.dat*.

```
first and last index numbers of input files for Genesis:
5       100
Name of the input file with design matrix in 29 design variables
design.variables.matr
```

The second line in this file gives the first and the last indices of the rows in the matrix of the HSCT configuration design variables for which structural optimization should be performed. The fourth line gives the name of the file with the matrix of HSCT configuration design variables.

When the slave-processors do their tasks, they call a shell-script program and structural optimization is called from this shell-script along with the aerodynamic loads calculation and the wing bending material weight calculation. Below is an example the code for such a shell script program which must have the name *execn.shell*.

```
#
#=================================================================
#
#       Shell file for running:  mesh generator,
#                                load generator,
#                                structural optimization on Genesis,
#                                wing bending material weight
#                                                    calculation.
#
#       It is assumed that all necessary files are already in
#               the working directory.
#
#=================================================================
#
#       path1 - path to serial code of mesh generator.
```

```
#       path3 - path to Genesis executable (serial version)
#       path5 - path to the program calculating wing bending material
#                                                                 weight
#       path7 - path to shell file of "WINGDES" to calculate aerodynamic
#                                                                  loads
#
#       $1 - name of the working directory (supposed to be passed here)
#
#=====================================================================
#



path1=/home3/vladimir/Genesisnew/Ser_ver/SerLoadg/New/
path3=/home3/vladimir/Genesisnew/Ser_ver/
path5=/home3/vladimir/Genesisnew/Ser_ver/SerLoadg/Wbm/
path7=/home3/vladimir/29NewOpt/WorkDir/



cd $1

#================================================
#       Running Wingdes
#================================================

${path7}GetCamberDes3



#================================================
#       Mesh generator
#================================================
#

${path1}mesh2


#================================================
#       Running Genesis
#================================================

${path3}sg


#================================================
#       Wing bending material weight calculation
#================================================

${path5}wbm2s
```

When the master-processor cleans up the working directory and copies results from the structural optimization into the appropriate place, the shell script program *cpoutn.shell* is used. Below is an example of such a shell script.

```
#
#====================================================================
#
#       Shell file for copying resultant files from working
#               directory into directory with results.
#
#       Also we are "cleaning" the working directory for future usage.
#
#====================================================================
#
#       path4bm - path to directory where the results of structural
#                 optimizations should be stored (BENDING MATERAIL FILES)
#       path4his - path to directory where the results of structural
#                  optimizations should be stored (OPTIMIZATION HISTORY)
#       path4sdat - path to directory where the results of structural
#                   optimizations should be stored (OPTIMIZATION DATA)
#
#       $1 - name of the working directory ( supposed to be passed here )
#       $2 - index number of input files   ( supposed to be passed here )
#
#====================================================================
#


path4bm=/home3/vladimir/pub/576/
path4his=/home3/vladimir/pub/576/
path4sdat=/home3/vladimir/pub/a.d.new/


cd $1

cp     wbmwg.res       ${path4bm}awd.$2.bm
cp     hsctgo.HIS      ${path4his}awd.$2.str.HIS
cp     hsctgo.OUT      ${path4his}awd.$2.str.OUT
cp     hsctgo.dat      ${path4sdat}awd.$2.str.dat


rm     *.*
```

Vita

Vladimir O. Balabanov was born on November 29, 1965, in Zhukovsky, Moscow Region, Russia. In 1989 he earned the M.S. degree in aerospace engineering from the Moscow Institute of Physics and Technology (MFTI). Since 1989 he worked for four years as a research engineer at the Central Aerohydrodynamic Research Institute (TsAGI) in Zhukovsky, Russia. While still working at the Central Aerohydrodynamic Research Institute, he started graduate studies towards Ph.D. degree at the Moscow Institute of Physics and Technology and by August 1993 he completed three years of graduate studies. In August 1993 he continued his education at Virginia Polytechnic Institute and State University in Blacksburg, Virginia. While studying at Virginia Polytechnic Institute and State University he worked for four months as an intern at the Boeing company. In 1995 he earned the M.S. degree in aerospace engineering and in 1997 the Ph.D. degree in aerospace engineering, both from Virginia Polytechnic Institute and State University. In July, 1997 he started working for Vanderplaats Research and Development Inc.